THE UNIVERSITY
of EDINBURGH

Iron and Nickel Complexes as Catalysts in CO_2/Epoxide Coupling, Radical Polymerisation and Hydrocyanation Reactions

Eszter Fazekas

A thesis submitted at the University of Edinburgh for the

Degree of Doctor of Philosophy

2018

Table of contents

Declaration

The work described in this thesis is of my own, unless I have acknowledged help from a named person or referenced a published source. This thesis has not been submitted, in whole or in part, for any other degree.

Signed …….

Date …….

Acknowledgements

I am immensely thankful for all the things I have learned and all the people I have met during my time as a PhD student at the University of Edinburgh. Aside from the usual agony of a PhD journey, it has been particularly challenging for me to switch research groups and start from scratch in my third year, but the incredible help and support of the following people made it all possible.

I would like to thank Prof. Dieter Vogt for giving me the opportunity to join his group and start my first project on hydrocyanation reactions. I would also like to acknowledge our industrial partner, Evonik, for their generous funding and in particular Prof. Robert Franke for his useful advice. During this time, I have thoroughly enjoyed working with wonderful colleagues: Anna, Dani, Laura, Vero, George, Lewis, Viktor, Evert, Nicola, Bachir, Judith, Dani2, Felix and Maria. Thanks for being there through the good times and the bad! I will never forget taking our mascot (The Traveling Peas) on group trips to Amsterdam, Dublin, Berlin, Loch Lomond and Kilconquhar; nor self-counselling in the pub after our lab literally exploded. Special thanks to my talented project student, Rachael, who has contributed to this work.

After my first group left Edinburgh, I was lucky enough to be 'adopted' by Prof. Michael Shaver, for which I am extremely grateful. Thank you for being a truly helpful supervisor and providing me with great project ideas, guidance and encouragement even when I thought I would never complete my degree. I am proud to have worked with some fantastic people in the Green Materials Laboratory: Gerry (thank you for proofreading!), Yaz, Ben, Meng, Vishal, Dan, Fern, Stefan, Jake, Laura, Mo, Joanne, Rebecca, Melanie, Yuechao, Mitch and Utku. Thanks for always being welcoming and ready to help when the GPC broke.

I cannot be grateful enough to Dr Jennifer Garden, who has been an incredible mentor and role model to me on both a professional and a personal level. Thank you, Jenni! You are the most knowledgeable person I know and your kindness, patience and enthusiasm helped me through the toughest times of my PhD. Although I have never officially been a member, I am proud to have infiltrated the Garden Group, which I'm sure has an extremely successful future ahead! Jay, Weronika, Rebecca, Jamie, Euan and everyone in office 209, thank you so much for making the last period of my PhD enjoyable!

I would like to thank everyone at the School of Chemistry for providing an efficient and inspiring environment. I am especially grateful to those who have helped me with technical support including Dr. Gary Nichol (X-ray), Dr Lorna Murray and Mr Juraj Bella (NMR), Dr Logan Mackay and Mr Alan Taylor (mass spectrometry).

Special thanks to the members of the Pokemon Go King's Building group for providing a great company for procrastination. Gotta catch 'em all!

Team Peffer Bank (Jacky, Jurgita, Viktor and Paul): it was a great privilege to live next door to friends for years. Thanks for always being there (literally), whether we needed pet-sitters or an excuse to order takeaway food.

A huge thanks to friends and family both back in Hungary and in the UK for your constant support, especially for visiting us in Edinburgh and maintaining our supply of pálinka.

Finally, I have the most thanks for my amazing husband, Gyuri. You have been my rock for the past 10 years and I would never have been able to do this without you! Thanks for tolerating me when I became insufferable writing this thesis. I would also like to thank our emotional support hedgehog, Rozi, whose cuddles probably saved me thousands of pounds in therapy.

Lay summary

Catalysts are compounds that are able to enhance the efficiency of chemical processes. They are widely used in the chemical industry in the production of plastics, pharmaceuticals and agrochemicals. A large proportion of commonly used catalysts are based on expensive and rare metals such as palladium and platinum. Switching to other, earth-abundant metals would ensure the sustainability of catalysts as well as decreasing their price. However, the development of such alternative catalyst systems is not yet well established, and this development is underpinned by a deeper understanding. The aim of this study was to develop new catalysts based on abundant, inexpensive metals such as nickel or iron and apply them in three different chemical reactions. Firstly, nickel-based catalysts were used in a process called 'hydrocyanation'. This reaction is an important step in the production of nylon, which is a widely-used plastic in textile and fibre industry. Secondly, iron-based catalysts were applied to convert carbon-dioxide to value added chemicals called 'cyclic carbonates'. These compounds are utilised in the production of fuels and batteries. Finally, the iron catalysts were also used to produce plastics, including biodegradable versions. These can be great substitutes of traditional, petrochemical-based analogues that contribute to plastic pollution.

Abstract

Transition metal complexes are essential for a wide range of homogeneously catalysed processes. Along with the constant optimisation of ligand design, the utilisation of cheap and easily available metals has become increasingly important. This work explores the synthesis of novel complexes comprising some of the most abundant first-row transition metals, as well as their application as catalysts in small molecule activation and polymerisation reactions.

The application of novel/underexplored bidentate ligands was investigated the in Ni-catalysed hydrocyanation of alkenes. A tetraphenol-based diphosphite ligand, TP2, and the corresponding Ni^0 complex were synthesised and characterised *via* X-ray crystallography. Contrary to previously reported patents, the complex was shown to isomerise 2-methyl-3-butenenitrile. Another diphosphite ligand, Biphephos, was employed in the hydrocyanation of styrene as a benchmark substrate. This allowed the optimisation of important reaction parameters such as the pre-formation of the Ni complex or the continuous addition of the HCN source. Biphephos was also studied in the hydrocyanations of butadiene and 3-pentenenitrile, but most importantly, it showed remarkably high activity in the isomerisation of 2-methyl-3-butenenitrile.

A series of eight half salen ligands and the corresponding novel Fe^{III} chloride complexes were synthesised. Characterisation *via* X-ray crystallography revealed monometallic structures with trigonal bipyramidal geometries around the metal centre. The air- and moisture-stable complexes were applied as catalysts in the coupling of CO_2 and epoxides which led to the exclusive formation of cyclic carbonates. Remarkably high activities were achieved, moreover, some structure-activity relationships were uncovered. Notably, the catalysts were extremely robust and showed efficiency in the presence of oxygen, water and a large loading of unpurified substrate. The substrate scope of the reaction was extended, including the sterically challenging internal epoxide, cyclohexene oxide.

The activity of the half salen Fe^{III} complexes was further explored investigating polymerisation reactions. The complexes were employed as mediators in the reverse atom transfer radical polymerisation of styrene and methyl methacrylate. Using AIBN or V-70 initiators, the complexes exerted moderate to good control over the molecular weights and dispersities of the obtained polymers. Some structure-reactivity relationships were discovered, along with the presence of competing mechanisms. The complexes were also applied in the ring opening polymerisation of *rac*-lactide using propylene oxide to generate the active Fe-alkoxide species *in situ*. Importantly, high conversions could be achieved with the addition of a low ratio of epoxides. However, GPC and MALDI-ToF mass spectrometry analyses of the obtained polymers revealed poor control over the molecular weights and dispersities, indicating a strong presence of transesterification side-reactions.

Publications

Stable Fe(III) phenoxyimines as selective and robust CO_2/epoxide coupling catalysts

Eszter Fazekas, Gary S. Nichol, Michael P. Shaver, Jennifer A. Garden*

Dalton Transactions, **2018,** *47*, 13106-13112.

Iron^{III} half salen catalysts for atom transfer radical and ring opening polymerizations

Eszter Fazekas, Gary S. Nichol, Jennifer A. Garden*, Michael P. Shaver*

ACS Omega, **2018**, *3*, 16945-16953.

Abbreviations

2M2BN	2-methyl-2-butenenitrile
2M3BN	2-methyl-3-butenenitrile
3PN	3-pentenenitrile
4PN	4-pentenenitrile
ADN	adiponitrile
AIBN	2,2’-azobisisobutyronitrile
ATRP	atom transfer radical polymerisation
BINAP	2,2'-bis(diphenylphosphino)-1,1'-binaphthyl
BIPPP	binaphthyl-isopropylphenyl-diphosphite
BO	butylene oxide
CCT	catalytic chain transfer
CHC	cyclohexene carbonate
CHO	cyclohexene oxide
CRP	controlled radical polymerisation
Đ	molecular weight distribution
DBFphos	1,1'-(4,6-dibenzofurandiyl)bis(1,1-diphenylphosphine)
DCM	dichloromethane
DFT	density functional theory
DIPP	diisoproylphenyl
dippe	1,2-bis(diisopropylphosphino)ethane
DPEphos	bis-(2-(diphenylphosphino)phenyl)ether
dppb	1,4-bis(diphenylphosphino)butane
dppe	1,2-bis(diphenylphosphino)ethane
dppp	1,3-bis(diphenylphosphino)propane
HCN	hydrogen cyanide
^{i}Pr	isopropyl
L	ligand
LDA	lithium diisopropylamide
M	metal
Me	methyl
MMA	methyl methacrylate
M_n	number average molecular weight
$M_{n,th}$	theoretical molecular weight
OMRP	organometallic mediated radical polymerisation
Ph	phenyl
PLA	poly(lactic acid)
PO	propylene oxide
ROP	ring opening polymerisation
Sixantphos	(10,10-dimethyl-10H-phenoxasilin-4,6-diyl)-bis(diphenylphosphine)
TBABr	tetrabutyl ammonium bromide
TBAI	tetrabutyl ammonium iodide

TBAX	tetrabutyl ammonium halide
TBP	trigonal bipyramidal
^{t}Bu	*tert*-butyl
THF	tetrahydrofuran
Thixantphos	1,1'-(2,8-dimethyl-4,6-phenoxathiindiyl)bis(1,1-diphenylphosphine)
TOF	turnover frequency
TON	turnover number
V-70	2,2'-azobis(4-methoxy-2,4-dimethylvaleronitrile)
Xantphos	4,5-bis(diphenylphosphino)-9,9-dimethylxanthene

Chapter 1

General introduction

The work described in this thesis focuses on the development of novel catalyst complexes featuring earth-abundant, first-row transition metals. As the application of these systems was investigated in fundamentally distinct fields of homogeneous catalysis (including polymerisation, hydrocyanation and CO_2 coupling reactions), a more detailed introduction of each topic will be given at the beginning of the corresponding chapters (Chapter 2-4). Nevertheless, a few overarching motifs in terms of catalyst design and substrate choice will be introduced herein.

The history of homogeneous transition metal-catalysed reactions goes back for almost a hundred years.[1, 2] One of the earliest milestones, the Co-catalysed hydroformylation, was discovered by Roelen *et al.* in the 1930s.[3] This process (later improved by the introduction of more efficient Rh-based catalysts) has quickly become the dominant technique in industry for the synthesis of commodity aldehydes. Similarly, the majority of early homogeneous processes were developed for the production of bulk chemicals, as only these large-scale applications could justify the financial requirements of catalyst design and appropriate engineering. Another important example, the Wacker process - involving the Pd-catalysed oxidation of ethylene to acetaldehyde - was commercialised in the 1950s. It was only in the 1990s that homogeneously catalysed processes became ubiquitous in the smaller-scale fine chemicals industry, exploiting the intense academic effort that had been carried out in this field. Since then, many related transformations have become indispensable tools in the repertoire of synthetic chemists, including hydrogenation, hydrofunctionalisation, C-C coupling, metathesis and oxidation reactions.[4] The significant contribution of these developments to society was acknowledged by a series of Nobel Prizes awarded for the discovery of homogeneously catalysed processes at the beginning of the 21st century: Heck, Negishi and Suzuki in 2010; Grubbs, Schrock and Chauvin in 2005; as well as Noyori, Knowles and Sharpless in 2001.

Importantly, the majority of the large-scale homogeneous processes traditionally utilise catalyst complexes based on precious metals including Rh, Pd, Ag, Os, Ir, Pt and Au along with other second- and third-row transition metals. The most relevant examples include Pt-catalysed hydrosilylation, Pd-catalysed hydrogenation and the aforementioned Rh-catalysed hydroformylation reactions.[4] While these systems provided exceptional catalyst efficiencies, the limited supply and high cost of the requisite precious metal precursors imposes a clear financial drawback and a significant risk in maintaining future capacity. To match the high activity and selectivity of these well-established systems, the focus has now shifted towards the development of sustainable and economic catalytic methods using earth-abundant transition metals, such as Ti, Fe, Co and Ni. Notably, these first-row metals have previously been widely employed as heterogeneous catalysts, for example in the Fe-catalysed Haber-Bosch process (synthesis of ammonia from N_2 and H_2) or the Co- or Fe-catalysed Fischer-Tropsch reactions (converting CO and H_2 into hydrocarbons). It is worth mentioning that aside

from the search for earth-abundant homogeneous catalysts, there has been significant interest in developing metal-free, organocatalysed processes.[5, 6]

The work in this thesis concentrated on the development of homogeneous catalysts featuring Ni and Fe, both of which are extremely abundant with Fe being, in fact, the most abundant transition metal in Earth's crust (Figure 1). Consequently, these metals are significantly less expensive than the precious metal counterparts. For example, in 2015 $Pd(OAc)_2$ cost 75 $/g while $Ni(OAc)_2$ cost around 10 $/g.[7] A further advantage of first-row transition metals is that most of them are essential to life (such as Fe) or biocompatible (such as Ti and Ni). Therefore, the application of these metals in catalytic processes and the trace presence of residual metals in chemical products has a reduced impact on health and the environment in comparison to second- or third-row transition metals. Moreover, these metals offer potential as efficient substitutes for toxic elements such as In, Hg, Pb and Bi that have also been commonly used in homogeneous catalysis.[8]

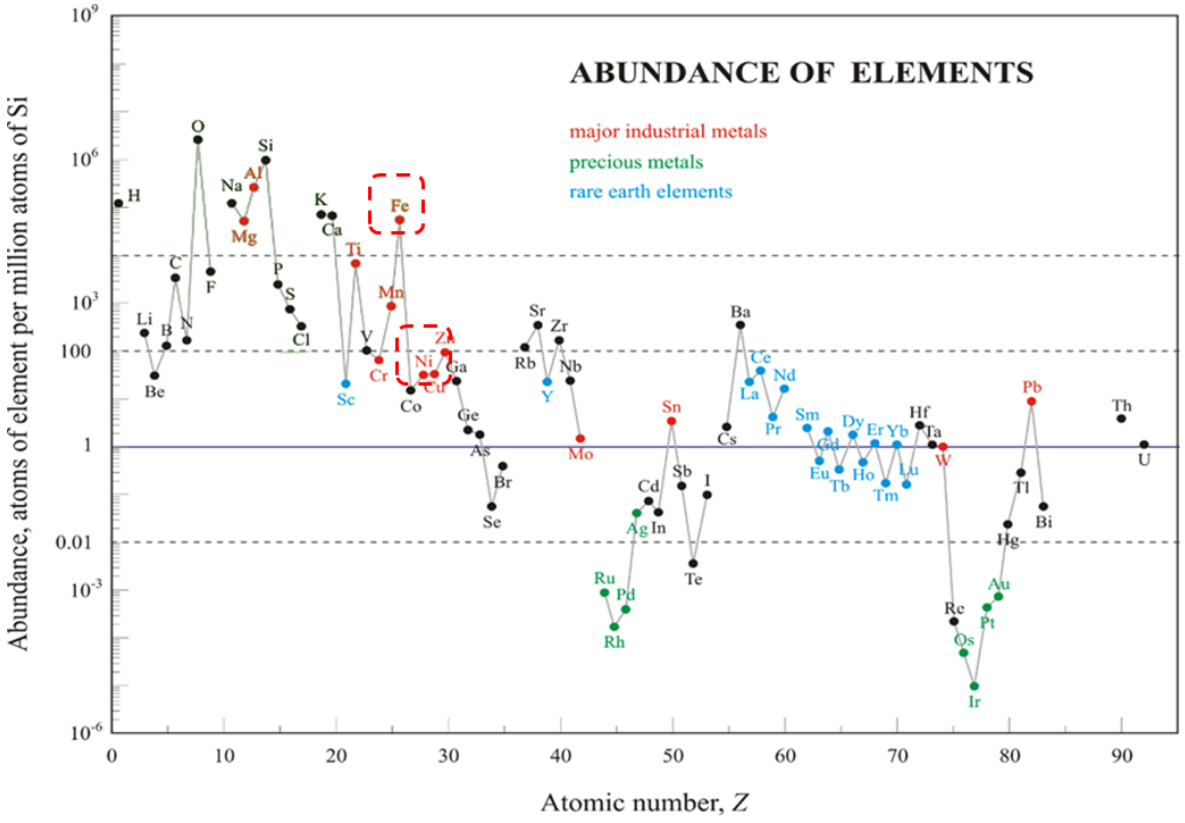

Figure 1: Abundance of the elements in Earth's crust.[9]

First-row transition metals have been shown to undergo facile one-electron oxidation state changes, which have been exploited in a broad range of homogeneous catalytic processes.[4] Examples include polymerisation and C-C coupling, as well as alkene and alkyne hydrofunctionalisation reactions such as hydroboration, hydrocyanation, hydroamination and hydrosilylation. Some of these systems rely on the use of air- and moisture-sensitive complexes, which has led to the development of appropriate industrial procedures (e. g. the *DuPont* process in hydrocyanation). However, the design

of more robust catalysts comprising earth-abundant metals, to enable truly low-cost and easily available processes on an industrial scale, remains a challenge.

Ancillary ligands are known to be of key importance in exploiting base metals in homogeneous catalysis. The relative ease with which the catalyst can be modified by changing the ligand environment has enabled chemists to realise dramatic efficiency improvements in various processes. By tailoring the steric and electronic properties of the ligands, rate enhancements of many orders of magnitude have been obtained.[4, 10] Importantly, increased catalyst activity represents a cost factor, as higher turnover rates allow higher space-time yields of the overall process. Moreover, modulating the electronic properties of the metal, and influencing the steric environment of the coordination sphere can also introduce control over the catalytic process. Consequently, ligand design provides the opportunity to fine-tune the chemo-, regio-, and stereoselectivity of the overall transformation. This has a significant effect on the cost-efficiency, as high selectivity ensures a more effective conversion of the feedstocks, requires simplified work-up equipment and leads to a reduced quantity of waste. Bi- or multidentate ligands have the additional advantage of the 'chelate effect', and can therefore provide increased stability and a higher degree of control over the coordination environment of a metal compared to analogous monodentate ligands. When placed in the appropriate coordination environment, first-row transition metals can often compete with precious metals in terms of activity and selectivity. However, more detailed insight into structure-activity relationships remains vital to develop new catalyst systems and further optimise existing processes.

Alongside exploiting sustainable metals within catalysis, it is also important to investigate the opportunities of using renewable feedstocks. From this point of view, the work in this thesis involved the utilisation of two sustainable starting materials: carbon dioxide (CO_2) was used in coupling reactions, while lactide was chosen as monomer for ring opening polymerisations. Converting waste CO_2 into useful chemicals (carbon capture and utilisation, CCU) has been recently considered to be a more desirable alternative to carbon capture and storage (CCS).[11] The relatively large scale of waste CO_2 production means that CCU will never significantly reduce the anthropogenic CO_2 emission. However, adding value to waste CO_2 by converting it into commercially important products including methanol, cyclic carbonates and polycarbonates is certainly attractive.[12] Other current economic and societal issues include the depletion of fossil fuel feedstocks and the accumulation of traditional (often polyolefinic) plastics in the environment. Consequently, the use of annually renewable resources such as lactide, and the development of degradable polymers such as poly(lactic acid) are of major interest.

References

1. W. R. Moser and D. W. Slocum, *Homogeneous Transition Metal Catalyzed Reactions*, ACS, **1992**.
2. A. Klein, B. Goldfuss, *Inorganics* **2018**, *6*, 1-4.
3. R. Franke, D. Selent and A. Börner, *Chem. Rev.*, **2012**, *112*, 5675-5732.
4. P. W. N. M. van Leeuwen, *Homogeneous Catalysis - Understanding the Art*, Kluwer, **2004**.
5. D. W. Stephan and G. Erker, *Angew. Chem. Int. Ed.*, **2015**, *54*, 6400-6441.
6. A. P. Dove, *ACS Macro Lett.*, **2012**, *1*, 1409-1412.
7. P. Chirik and R. Morris, *Acc. Chem. Res.*, **2015**, *48*, 2495-2495.
8. L. L. Schafer, P. Mountford and W. E. Piers, *Dalton Trans.*, **2015**, *44*, 12027-12028.
9. https://www.periodni.com/rare_earth_elements.html, Accessed 21/11/2018.
10. R. J. Lundgren, M. Stradiotto, *Ligand Design in Metal Chemistry: Reactivity and Catalysis*, John Wiley & Sons Ltd., **2016**.
11. A. Sternberg, C. M. Jens and A. Bardow, *Green Chem.*, **2017**, *19*, 2244-2259.
12. D. P. Schrag, *Science*, **2007**, *315*, 812-813.

Chapter 2

Ligand development for hydrocyanation and isomerisation reactions

Introduction

Hydrocyanation is an elegant method for carbon-carbon bond formation with a great industrial potential, as the obtained nitriles offer a versatile platform for further utilisation. Choosing an appropriate catalyst system for this process is of fundamental importance. The understanding of the reaction mechanism and the design of new, tailored ligands are key approaches to improve catalyst efficiency. In this chapter a brief summary and evaluation will be given on the 'state of the art' in homogeneously catalysed alkene hydrocyanation, focusing on mechanistic studies and ligand properties. Furthermore, the chapter reports on the synthesis and characterisation of bidentate phosphine and phosphite ligands, as well as their use in Ni-catalysed hydrocyanation and isomerisation reactions.

Hydrocyanation

Hydrocyanation is defined as the addition of hydrogen cyanide (HCN) across a multiple bond. This summary is limited to the homogeneous, transition metal-catalysed hydrocyanation of alkenes, where HCN is added across a C=C double bond to form nitriles (Scheme 1).[1, 2]

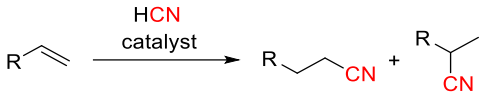

Scheme 1: Hydrocyanation of alkenes.

The obtained products are valuable building blocks in synthetic chemistry as the nitrile group can be readily converted into various functional groups to give for example, amines, carboxylic acids or esters (Scheme 2).[3]

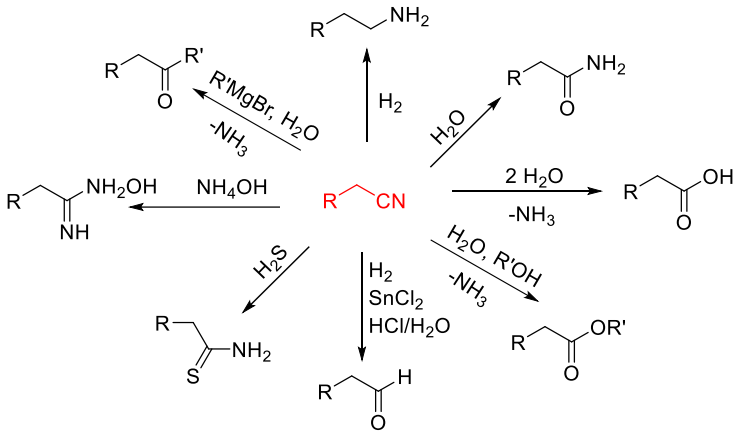

Scheme 2: Several possible conversions of the nitrile group.

Despite the apparent simplicity, atom-efficiency and versatility of the products, the hydrocyanation process still faces major challenges.[4] First of all, the control of regioselectivity is a crucial aspect. The chiral, branched nitriles are mainly used in the synthesis of fine-chemicals (natural products, pharmaceuticals and agrochemicals), whereas the linear *anti*-Markovnikov products are mass-produced on a million-ton scale as polymer or surfactant precursors.[5] Especially in the latter case, the relatively low price of these intermediates requires the hydrocyanation method to be highly efficient and the catalysts to be inexpensive. In addition, the laboratory scale investigation of this reaction is hampered by the difficulties in handling the volatile and extremely toxic HCN. Consequently, the hydrocyanation literature is dominated by industrial patents rather than academic publications.[6]

Industrial relevance

At present, the exclusive industrial application of alkene hydrocyanation is the so called *DuPont* adiponitrile process.[7] Adiponitrile (ADN) serves as precursor of hexamethylenediamine, which is a co-monomer of nylon 66 (Scheme 3). This polyamide is used worldwide in extremely large quantities, manufacturing products such as resins, fibres for textiles, carpets, hoses, airbags and moulded parts. With 71% share of the annual adiponitrile world production (1.2 million tons in 2011) the *DuPont* synthesis (currently conducted by *Invista* and *Rhodia* in the US, France and China) is one of the largest scale homogeneously catalysed processes in the chemical industry.[8] Notably, the remaining 29% of ADN is produced by *Monsanto via* the electrochemical dimerisation of acrylonitrile.[9]

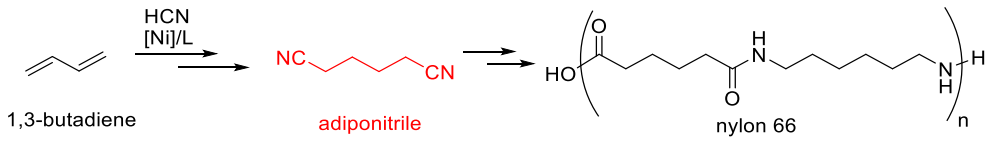

Scheme 3: DuPont adiponitrile process and nylon 66.

The synthesis method involving the Ni-triarylphosphite-catalysed direct addition of HCN to butadiene was pioneered in the late 1960s by Chadwick A. Tolman, William C. Drinkard and co-workers at the *DuPont* laboratories in Wilmington, US. Later on, the growing commercial importance of the large-scale adiponitrile production became a strong driving force to initiate further research into the field. To improve the yield, selectivity and lifetime of the catalyst systems, a deeper understanding of the catalytic cycle and ligand effects became necessary. In fact, these close mechanistic investigations of hydrocyanation reactions have led Tolman to his important concepts of the '16 and 18 electron rule'[10] as well as the ligand electronic (Tolman χ value)[11] and steric (Tolman cone angle θ)[12] effects, which are now fundamental in homogeneous catalysis and transition metal chemistry.

Definition of main ligand parameters

The Tolman χ-value was developed to quantify the ability of a monodentate phosphorus ligand to donate electrons to a transition metal.[11] The concept is based on infrared spectroscopy, comparing the carbonyl (C ≡ O) stretch-vibration frequencies (υ_{CO}) in various $Ni(CO)_3L$ complexes to a reference compound. The weaker π-acceptor phosphines allow a strong π-backbonding to the CO ligands and therefore the vibration moves to lower wavenumbers. On the other hand, the less electron rich phosphites compete with the CO ligands for π-backbonding, leaving the CO stretch vibrations at relatively high wavenumbers (Figure 1). The collected experimental data (converted to χ-values for individual R substituents on PR_3 ligands) allows to estimate the basicity of new ligands without having to synthesise them.

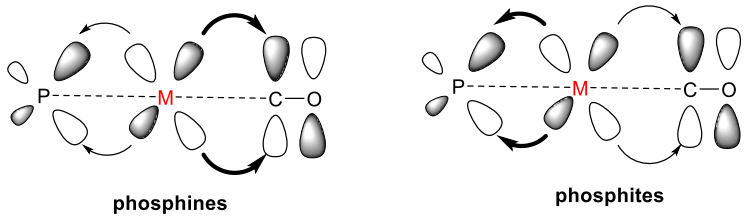

Figure 1: Comparison of π-backbonding in phosphine and phosphite complexes.[13]

The Tolman Cone Angle (θ) is a helpful approach to quantify the 'space filling' ability of ligands, which is an important attribute in terms of coordination and complex-stability.[12] The idea is based on placing a 'cone' around the radii of all ligand substituents (the bond lengths and angles are known from X-ray analysis) and measuring the apex angle of the cone tip, centered 2.28 Å (a typical Ni-P bond length) away from the phosphorus atom (Figure 2). This concept is also suitable to estimate the properties of unknown (even non-symmetrical) ligands, although it has limitations, especially in the case of bidentate ligands.

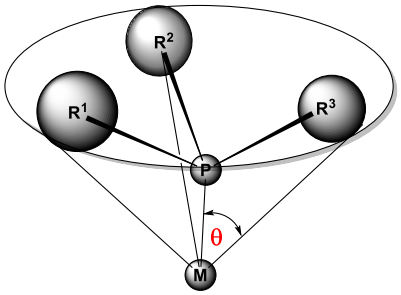

Figure 2: Tolman Cone Angle (θ) of monophosphines.[13]

Later studies found that the Tolman parameters (χ and θ) alone are not necessarily enough to predict a ligands activity in hydrocyanation reactions.[14]

For bidentate chelating ligands it was essential to consider the steric properties in greater detail. The concept of the bite angle (β) (Figure 3) refers to the P-M-P angle formed between the metal and the two phosphorus atoms. It has a major influence on the performance in catalysis by hampering or enhancing the substrate coordination and the reductive elimination of the product. To exclude the dependence on the metal (when comparing two ligands), a standardised version had to be introduced. This natural bite angle (β_n) (calculated with rhodium as dummy metal) allows to consider steric properties determined solely by the ligand backbone.[15] As ligand conformations are dynamic and the bite angle can change consequently, a flexibility range can be defined (in which the conformation energy can go up by 3 kcal/mol from the calculated zero point) to consider slight transformations.

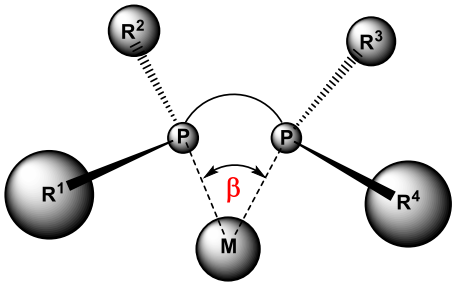

Figure 3: Bite angle (β) of bidentate phosphines.[13]

Mechanistic studies

The intense mechanistic investigation of the *DuPont* process commenced after the discovery that zero-valent Ni, combined with monodentate phosphine or phosphite ligands can be an efficient catalyst for the *anti*-Markovnikov hydrocyanation. In the beginning, several studies focusing on the formation, reactivity and solution behaviour of NiL_4 complexes have been carried out.[16-18] In terms of complex stability, it was found that the electronic properties of the ligand (χ value) are less influential than the steric effects (cone angle and bite angle). Moreover, by isolation and spectroscopic characterisation of some [Ni(alkene)L_2] species, it was shown that they are usually 16-electron complexes.[19] Five-coordinated Ni-hydride [HNi(CN)L_3] intermediates have also been detected, suggesting that during HCN coordination, the protonation occurs before the ligand dissociates (Scheme 4).[20]

$$NiL_4 + HCN \rightleftharpoons HNiL_4^+CN^-$$

$$HNiL_4^+CN^- \rightleftharpoons HNiL_3CN + L$$

Scheme 4: Oxidative addition of HCN.

McKinney *et al.* proposed a catalytic sequence for ethene hydrocyanation that can be divided into a productive and an unproductive subcycle (Scheme 5).[21] The productive process starts with the dissociation of ligands from NiL_4, and the coordination of ethene to the Ni centre. With the oxidative

addition of HCN, followed by the dissociation of a further ligand, a π-alkene nickel-hydride intermediate is formed. Then the insertion of a further substrate molecule into the Ni-H bond affords an intermediate with both a σ- and a π-bound ethene molecule. Experiments using deuterated hydrogen cyanide (DCN) showed that this step is reversible and occurs rapidly compared to the reductive elimination, as deuterium scrambling was detectable between the α and the β positions of the resulting propionitrile. In the next step of the productive cycle, the association of a ligand affords a five-coordinate $L_2Ni(CH_2{=}CH_2)Et(CN)$ complex, which was identified by ^1H NMR spectroscopy as the most stable compound of the process (resting state).[21] These observations led to the conclusion that the reductive elimination of the product determines the rate of the reaction and is the only irreversible step. In the other (unproductive) subcycle NiL_3 is formed *via* ligand dissociation, then the oxidative addition of HCN followed by the dissociation of a further ligand gives the $HNiL_2(CN)$ intermediate, which can return to the productive cycle through the coordination of a substrate molecule.

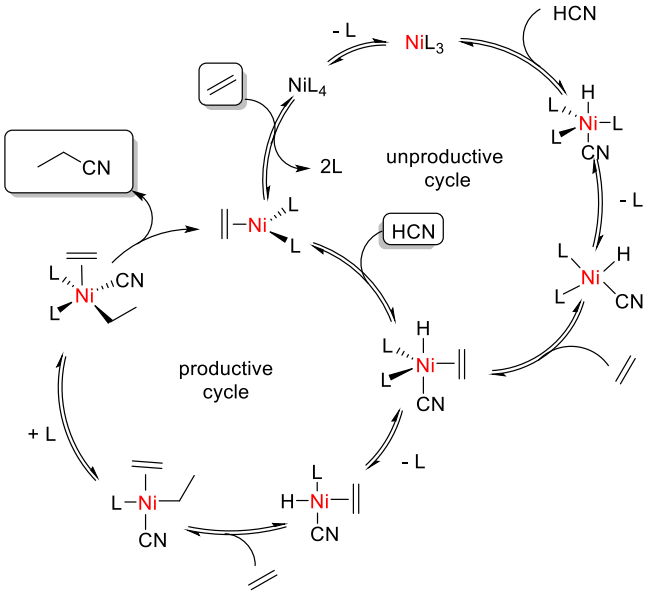

Scheme 5: Proposed catalytic cycle for the Ni-catalysed hydrocyanation of ethene.[21]

Importantly, the presence of a large excess of HCN facilitates the irreversible formation of $Ni(CN)_2$ species, which are catalytically inactive and cause the most prominent problem of the hydrocyanation reaction by shortening the catalyst's lifetime.[22]

A large variety of substrates have been converted using Ni systems with mono- or bidentate P-ligands. In principle, the hydrocyanation of aryl-conjugated olefins always affords the branched nitriles in a higher ratio.[16] This can be explained with the stabilisation of the intermediates through donation of aromatic electrons to the coordinatively unsaturated Ni centre or with the thermodynamic stability of an η^3-benzylallyl intermediate (Scheme 6).[23] However, a dramatic inversion of the regioselectivity can be achieved by the addition of Lewis acids (e. g. $AlCl_3$) to the hydrocyanation of styrene.[24] This

peculiar behaviour was investigated by NMR spectroscopy, deuterium labelling and DFT calculations by Vogt *et al*. On the other hand, with aliphatic alkenes as substrates, usually the linear, *anti*-Markovnikov isomer forms as major product.[25]

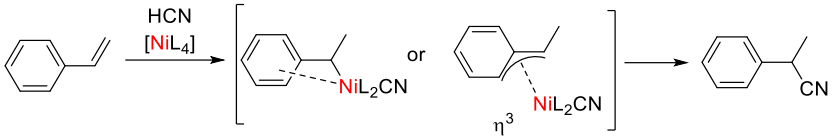

Scheme 6: Stabilising effects in the hydrocyanation of vinylarenes.

In general, the addition of Lewis acids (such as $ZnCl_2$, $AlCl_3$ or BPh_3) accelerates the process of hydrocyanation by increasing the acidity of HCN and enhancing the ionic pathway shown in Scheme 4.[26] Moreover, the regioselectivity towards the linear nitriles can also be maximised *via* addition of Lewis acids, as they increase the steric crowding at the Ni centre, preventing the formation of more congested branched species.[27]

When bidentate ligands are applied, the bite angle can have a fundamental influence on the reaction outcome.[28] It was observed that the key intermediates in the catalytic cycle show coordination geometries close to tetrahedral (β = 109°) or trigonal (β = 120°) P-Ni-P angles.[22] Ligands with wide bite angles (β > 100°) favour the formation of these species and therefore promote the substrate coordination and the rate limiting reductive elimination steps. On the other hand, ligands with a narrower bite angle (100° < β) can make the catalyst more susceptible to deactivation by facilitating the formation of square planar structured (β = 90°), inactive $Ni(CN)_2$ complexes. A series of wide bite angle Xantphos-type diphosphine ligands was applied and compared to regular ligands in the hydrocyanation of styrene to investigate the dependence of the conversion on the bite angle (Scheme 7).[29]

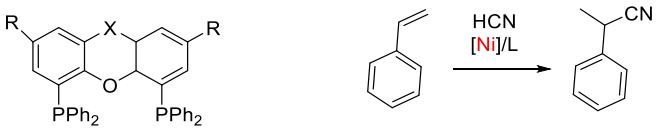

Scheme 7: Backbone of Xantphos type ligands and their application in styrene hydrocyanation.

The striking difference between the performance of wide and narrow bite angle ligands confirmed the hypothesis mentioned above (Figure 4). Moreover, it was observed that an extremely wide bite angles (DBFphos, β = 131°) are also detrimental for the reaction as they can hinder substrate coordination.

Ligand	β	X	R
DBFphos	131°	bond	H
Xantphos	109°	CMe_2	H
Thixantphos	106°	S	CH_3
Sixantphos	105°	$SiMe_2$	H
DPEphos	101°	H, H	H
dppb	98°	-	-
dppp	87°	-	-
BINAP	85°	-	-
dppe	78°	-	-
$P(OPhMe)_3$	-	-	-

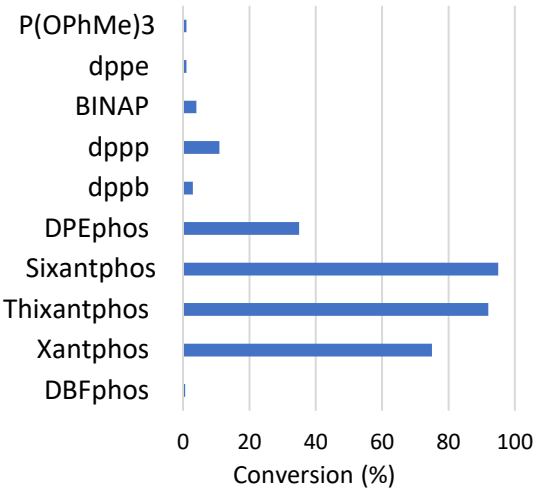

Figure 4: Conversion difference using narrow and wide bite angle ligands.[29]

The steric bulk (Tolman cone angle) of the ligand substituents also has an influence on facilitating the ligand dissociation and preventing the formation of catalytically inactive bis-chelate complexes.[30]

DuPont adiponitrile process

In the *DuPont* process, the hydrocyanation of butadiene to produce adiponitrile consists of three consecutive steps (Scheme 8).[7] Beginning with the mono hydrocyanation of butadiene, a Ni-phosphite catalyst system is used to form a mixture of the linear 3-pentenenitrile (3PN) and the branched 2-methyl-3-butenenitrile (2M3BN). The regioselectivity towards the desired 1,4-adduct peaks around 70%, but strongly depends on the chosen ligand and on other parameters such as catalyst loading, HCN concentration and temperature. After the first reaction, the mononitriles are separated by fractional distillation. In the second step, the undesired 2M3BN is isomerised to 3PN using the same catalyst system in the absence of HCN, affording a linear/branched ratio of about 97/3. A further separation follows, and in the last stage the hydrocyanation of 3PN occurs through an *in situ* isomerisation to the terminal alkene 4-pentenenitrile (4PN). As the internal monoalkene 3PN is not activated as a substrate, the addition of a Lewis acid co-catalyst is necessary for the reaction to proceed quantitatively. In the current industrial procedure, all three reactions are carried out in separate reactors. Moreover, the purification (fractional distillation) of product mixtures add further steps to the process and require additional vessels.

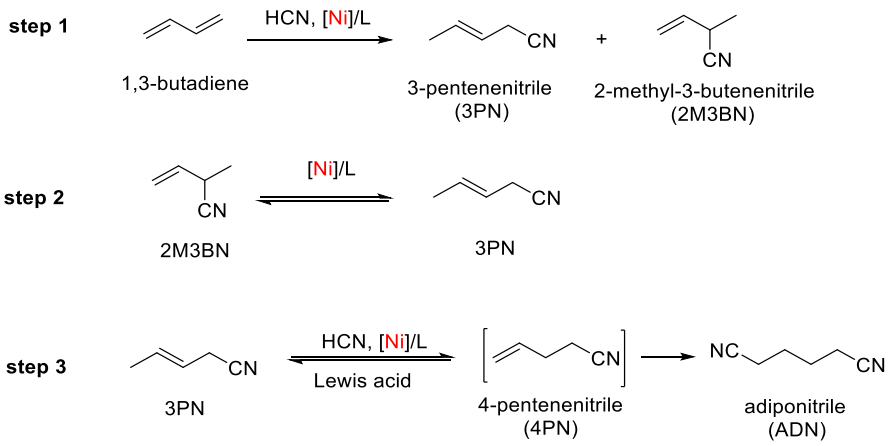

Scheme 8: The three steps of the DuPont adiponitrile process.

When the ADN process was first commercialised in 1971, monodentate $P(OAr)_3$ ligands with cone angles of 120-130° were used (Scheme 9).[25] The susceptibility of these phosphites to hydrolysis necessitated the installation of large, hydrophobic groups to decrease moisture sensitivity. Consequently, in the 1990s bulkier, biphenol-based bidentate diphosphites became prevalent.[31-33] These ligands have been superior in terms of activity and robustness: for the first time, turnover numbers (TON) over 1000 were achieved.[34] Compared to extremely high turnover rates (TON up to millions) achieved in Rh-catalysed hydroformylations, TON-s of a few thousands are considered good performance in Ni-catalysed hydrocyanation reactions to date.

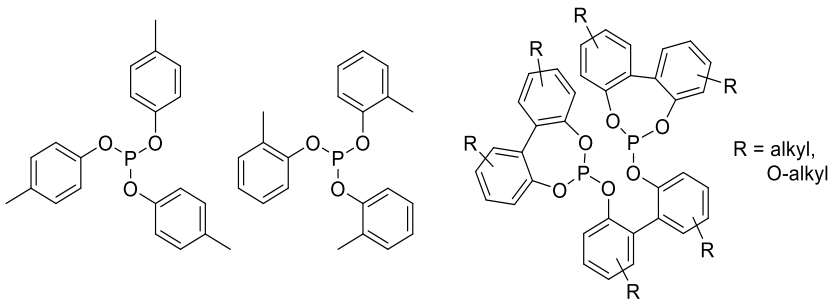

Scheme 9: Monodentate and bidentate ligands in the industrial ADN process.

A general catalytic cycle proposed for the first step of the *DuPont* ADN process with the monodentate L = $P(OEt)_3$ ligand system is shown on Scheme 10.[23] After the dissociation of a ligand the oxidative addition of HCN takes place affording a cyanohydride complex. Subsequently, the dissociation of another ligand promotes the insertion of a substrate molecule into the Ni-H bond, yielding a η^3-crotyl complex. From this step, two different pathways are possible, yielding either the linear or the branched cyanoolefin complexes. The association of ligands then enables the catalyst to re-enter the cycle *via* the reductive elimination of the products. According to Tolman, all the steps are reversible.[23]

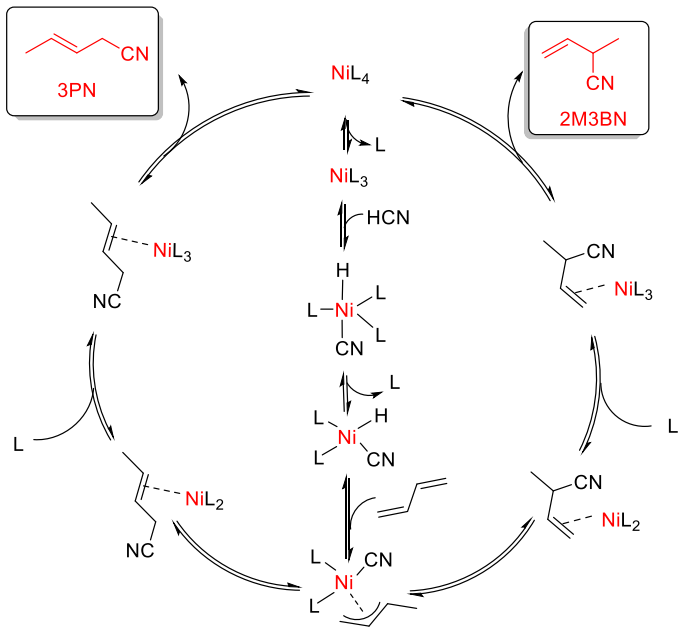

Scheme 10: Proposed catalytic cycle for the hydrocyanation of butadiene.

The second step of the *DuPont* process, the isomerisation of 2M3BN towards the thermodynamically favoured 3PN follows a similar mechanistic pathway. Tolman showed that the coordination of the terminal alkene 2M3BN to the metal centre is faster than the coordination of the internal alkene 3PN.[23] Druliner and co-workers conducted deuterium-labelled isomerisation experiments, in which the D scrambling between the C-2 and C-5 positions of the product suggested that a cascade of de- and re-hydrocyanation might take place (Scheme 11).[35]

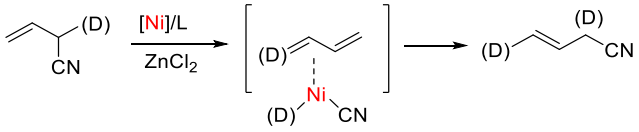

Scheme 11: Deuterium scrambling in the isomerisation of 2M3BN.

In further mechanistic studies Sabo-Etienne and co-workers have been able to isolate and structurally characterise a (dppb)Ni(η^3-C_4H_7)CN complex (Scheme 12, left), which has a fundamental role in the first two steps of the ADN process.[36] Moreover, Jones *et al.* investigated the reaction of a (dippe)η^2-nitrile-Ni^0 complex (Scheme 12, middle), which can undergo oxidative addition both *via* C-CN or C-H cleavage.[37] The effect of solvent polarity on the linear selectivity was also studied by the same group.[38] The Vogt group investigated the isomerisation of 2M3BN using a DPEphos system. The spectroscopic studies proved the reversibility of the reductive elimination step and a [Ni(η^3-crotyl(CN*$ZnCl_2$)(DPEphos)] complex (Scheme 12, right) was isolated and characterised *via* X-ray crystallography.[39]

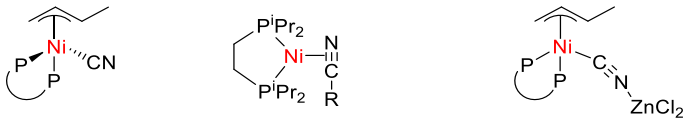

Scheme 12: Structure of three isolated intermediates.

In the last and most challenging step of the *DuPont* ADN synthesis, the *in situ* isomerisation of 3PN to the terminal alkene, 4PN, precedes the hydrocyanation towards adiponitrile. Along with using strong π-acceptor phosphite ligands, the process typically requires the addition of a Lewis acid promotor, which enhances the formation of cationic Ni species. As the kinetic preference for the isomerisation of an internal alkene into a terminal alkene is much stronger than the thermodynamic preference for the conjugated isomer 2-pentenenitrile, the regioselectivity of the reaction towards adiponitrile is typically high. Nevertheless, traces of several by-products depicted in Scheme 13 can occur in the final product mixture.[26]

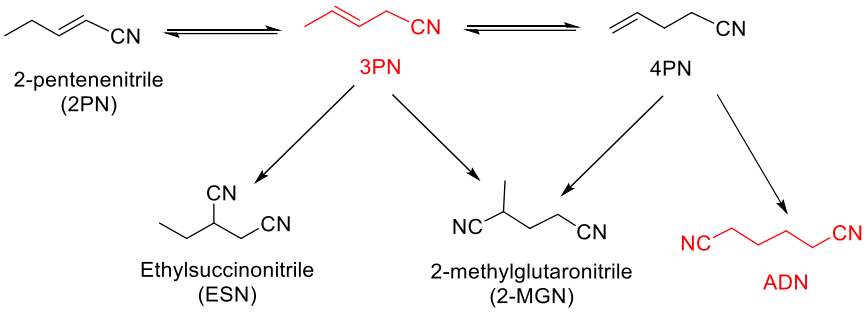

Scheme 13: Formation of possible by-products in the DuPont ADN process.

Recently, Pringle and co-workers introduced a new class of P-ligands bearing a phosphinite cage (Scheme 14). The corresponding Ni complexes were highly active towards the hydrocyanation of 3PN in the presence of Lewis acids.[40, 41] Remarkably, the moisture sensitivity was eliminated due to the methyl groups on the cage providing a hydrophobic environment and steric protection from P-O bond hydrolysis. The same group later reported on the synthesis of similarly structured cage fluorophosphine ligands that were the first ligands without a P-OR group to show activity in the hydrocyanation of 3PN.[42]

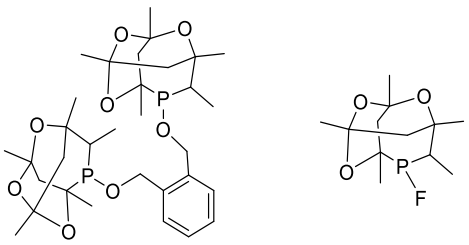

Scheme 14: Structure of cage phosphinite and fluorophosphine ligands. [40,42]

Critical evaluation

To conclude, the Ni-catalysed alkene hydrocyanation has been a major industrial success since the 1970s and will most likely stay relevant as the world demand for nylon 66 is forecast to increase by 2% annually.[8] Indicators of the great interest in this field are the continuously appearing new patents and publications.[43-45] More environmentally friendly alternatives, such as a bio-based synthesis route reported for adiponitrile[46] can only challenge the *DuPont* process if they become feasible on an industrial scale.

The commercialisation of the *DuPont* process initiated a series of investigations resulting in important general concepts in the systematisation of ligand stereoelectronic properties. However, the currently applied catalyst systems, especially the ligands, can be further optimised in terms of activity, selectivity and robustness. Due to the million-ton scale of annual ADN production, even a slight improvement of the process could realise a significant cost-reduction. Moreover, while most research projects focus on the reactions of activated substrates (vinylarenes or dienes), the fewer and less successful examples for monoalkene (3PN) hydrocyanation offer an open challenge to optimise these processes.

The most significant drawback of these systems is the deactivation of the Ni catalysts, which process is yet to be fully understood. To avoid the formation of inactive $Ni(CN)_2$ species (caused by excess cyanide) a slow, continuous addition of HCN is a well-established practice in industry. On the other hand, the safe storage and handling of the extremely toxic HCN gas is a tremendous challenge in academic laboratories. In most countries, pure HCN is not available and must be synthesised locally. A common practice to circumvent this problem is the use of alternative cyanide sources such as acetone cyanohydrin (ACH) or trimethylsilyl cyanide (TMSCN) that can liberate HCN *in situ*. More recently, Morandi *et al.* reported on the transfer hydrocyanation between a large scope of alkyl nitriles and alkenes,[47, 48] while Skrydstrup and co-workers developed double-chamber vessels for the *ex situ* liberation of HCN (Figure 5).[49] Although both of these inventions represent elegant solutions to avoid the use of pure HCN in academic laboratories, the methods are difficult to translate/scale up for the industrial ADN process.

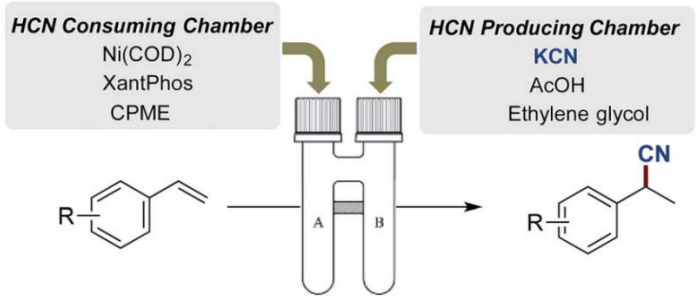

Figure 5: Double-chamber vessel for the ex situ formation of HCN.

Aims

In close collaboration with industrial sponsor, *Evonik*, the goal of this research project was to continue the investigation and development of existing and new catalyst systems for alkene hydrocyanation reactions. From an early stage a large emphasis was placed on finding industrially applicable solutions. This project formed the early part of my doctoral research before the Vogt group left the University of Edinburgh.

The work was focused on the most relevant, large-scale industrial application, the *DuPont* adiponitrile process (Scheme 15). In the current three-stage procedure Ni-phosphite complexes are used to catalyse the double hydrocyanation of butadiene leading to adiponitrile. The efficiency and selectivity of each step are largely dependent on the catalyst system, more specifically on the ligand properties. Therefore, this project targeted the development of potential ligands and ligand combinations to be applied in the *DuPont* process.

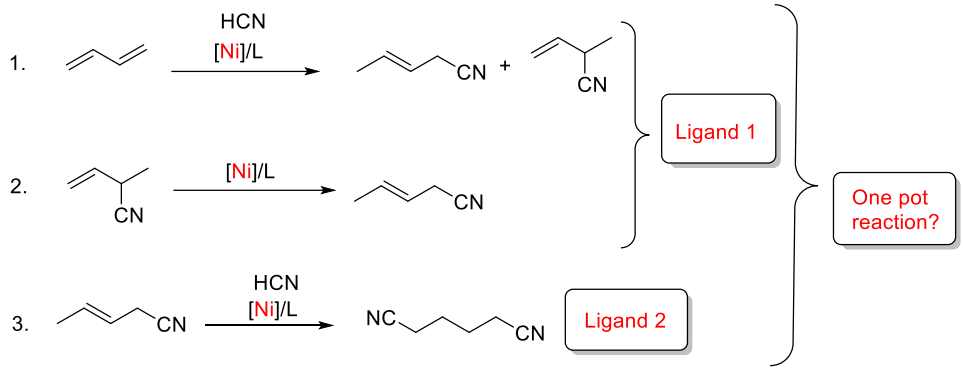

Scheme 15: Possible intensification of the DuPont ADN process.

Previous results in the Vogt group showed that **Ligand 1,** a triptycene-based diphosphine has excellent activity and linear selectivity in the first two steps,[50] while **Ligand 2**, a tetraphenol-backboned diphosphite was believed to be active exclusively in the third step.[51] We aimed to investigate whether this ligand combination can shorten/simplify the procedure and lead to a two pot (or even one-pot) synthesis of adiponitrile. Moreover, a third bidentate diphosphite ligand called **Biphephos** was also selected to be tested in hydrocyanation reactions.

Results and Discussion

Triptycene ligand

Background

Traditionally, the majority of hydrocyanation ligands are taken over from the more extensively investigated and developed field of hydroformylation. The success of Xantphos-type ligands developed by van Leeuven *et al.* in the Rh catalysed hydroformylation inspired several research projects to design similar backbones.[29] Initially, the high performance of these ligands was believed to be caused by the wide bite angle combined with a rigid backbone, but DFT calculations and later experimental observations showed that the xanthene backbone actually has a quite significant conformational flexibility.[52] To avoid this fluxional behaviour, Hofmann *et al.* started to develop even more rigid analogues by introducing a two-carbon bridge on a 9,10-dihydroanthracene backbone.[53] The rigidity of the created ligand family (Scheme 16) decreased the number of possible conformations and greatly simplified the mechanistic analysis of the hydroformylation catalytic cycles.

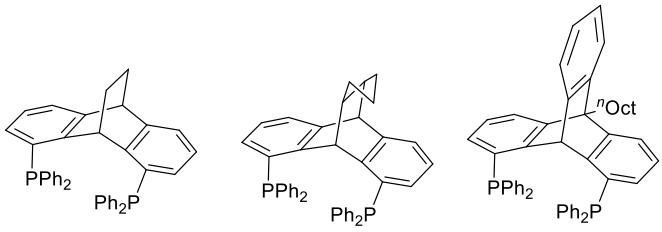

Scheme 16: Rigid diphosphine ligands developed for hydroformylation by Hoffmann et al.

The Vogt group significantly improved the synthetic procedure for one of the triptycene-based diphosphine ligands belonging to the aforementioned family (Scheme 17). The ligand's coordination behaviour to Ni was investigated by NMR spectroscopy and X-ray crystal structure analysis.[50]

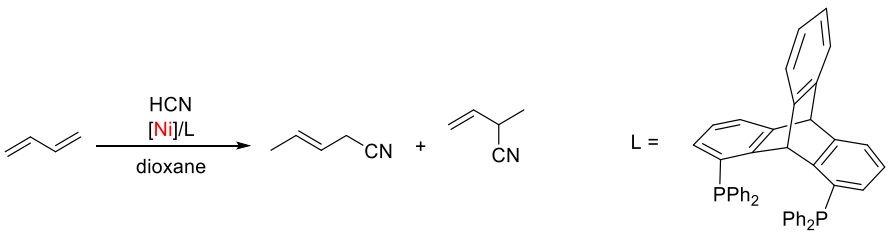

Scheme 17: Triptycene-based ligand used in the hydrocyanation of butadiene.

The triptycene ligand (in combination with $Ni(cod)_2$) was then successfully applied in hydrocyanation reactions for the first time. Remarkably, under optimised conditions it outperformed

three 'state of the art' ligands (Sixantphos, BIPPP and DPPF) in the hydrocyanation of butadiene, both in terms of conversion and linear selectivity (Table 1).

Table 1: Comparison of efficiency using different hydrocyanation ligands.

Ligand	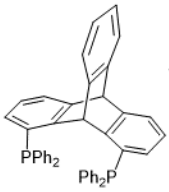 Triptycene	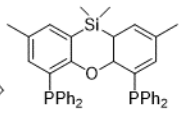 Sixantphos	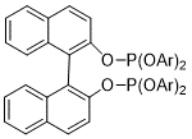 BIPPP	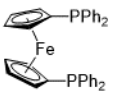 DPPF
Conversion (%)	>99	62.1	78.3	80.2
3PN selectivity (%)	93.3	28	63.2	53.1

Conditions: 90 °C, 3 h, [Ni]:[L]:[butadiene]:[ACH] [1]:[1]:[100]:[150], acetone cyanohydrin (ACH) as HCN source, 2 mL of dioxane.

To explain these excellent results, it was proposed that the Ni(Triptycene) complex can catalyse both the hydrocyanation of butadiene and the isomerisation of 2M3BN to 3PN simultaneously. FTIR spectroscopic studies and DFT calculations were used to postulate a catalytic cycle for concurrent hydrocyanation-isomerisation mechanism (Scheme 18).[54]

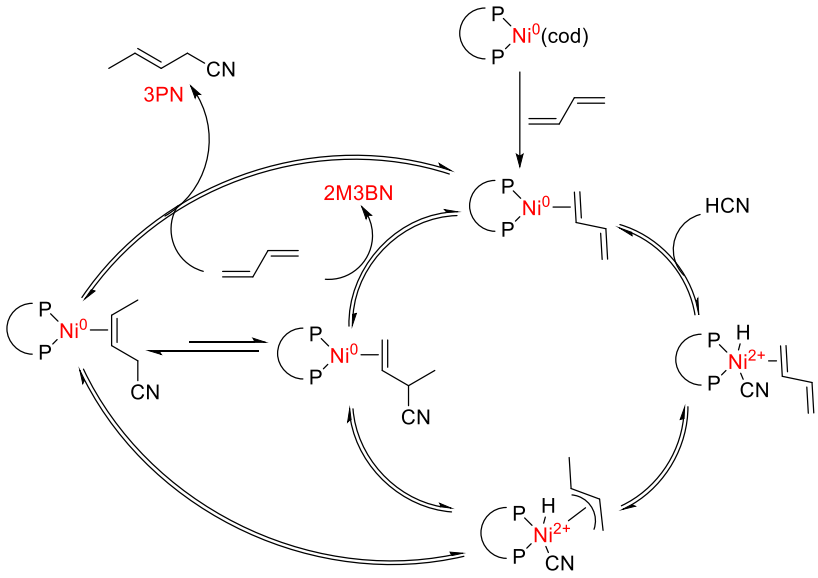

Scheme 18: Proposed catalytic cycle for the concurrent hydrocyanation-isomerisation.

A recent study by Tauchert and co-workers investigated this isomerisation in detail, applying triptycene-based ligands with varying substituents.[55] It was found that electron-donating groups in the para position (methyl or methoxy groups) of the PPh_2 moieties increase the conversion. Moreover, high turnover rates were achieved with 0.05 mol % catalyst loading applying an *n*-octyl modified triptycene ligand. Our goal was to reproduce initial results from Vogt *et al.* and further develop the triptycene-based ligand family *via* fine-tuning the stereoelectronic properties of the substituents.

Synthesis of Triptycene ligand

The triptycene ligand was synthesised *via* a modified procedure originally developed by the Vogt group.[50] The intermediates were identified by ^{1}H, ^{13}C, ^{19}F and ^{31}P NMR spectroscopy as well as with high resolution mass spectrometry.

First 1,8-dichloroanthraquinone and caesium fluoride were refluxed in dry DMSO under an inert atmosphere for 12 hours (Scheme 19). After purification *via* column chromatography the 1,8-difluoroanthraquinone was obtained as a yellow solid in 50% yield.

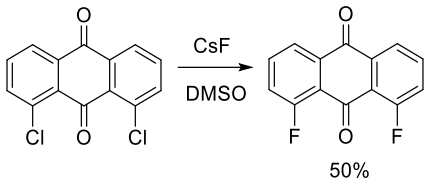

Scheme 19: Synthesis of 1,8-difluoroanthraquinone.

Subsequently, the reduction of the anthraquinone to the corresponding anthracene was carried out using zinc and concentrated aqueous ammonia solution (Scheme 20). The mixture was heated to reflux for 3 hours, extracted with DCM and heated to reflux again with HCl in isopropanol for further 3 hours. The recrystallisation from DCM afforded the pure product in 44% yield as a yellow solid.

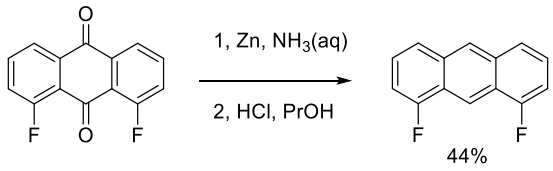

Scheme 20: Synthesis of 1,8-difluoroanthracene.

In the next step, the introduction of the fourth ring was achieved by *in situ* benzyne formation and subsequent Diels-Alder reaction in a one-pot synthesis. The benzyne was produced from anthranilic acid by diazotation with *n*-butyl-nitrite and maleic anhydride, followed by thermal decarboxylation and N_2 liberation (Scheme 21).

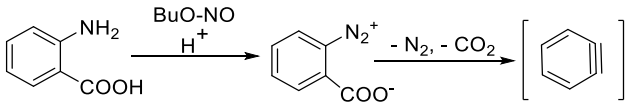

Scheme 21: In situ formation of benzyne.

After heating the 1,8-difluoroanthracene and benzyne mixture to reflux for 8 hours in dichloroethane, the product was precipitated by addition of an ice-cold aqueous solution of potassium-hydroxide. The precipitate was filtered, washed and the 1,8-difluorotriptycene was obtained as a yellow powder in 47% yield (Scheme 22).

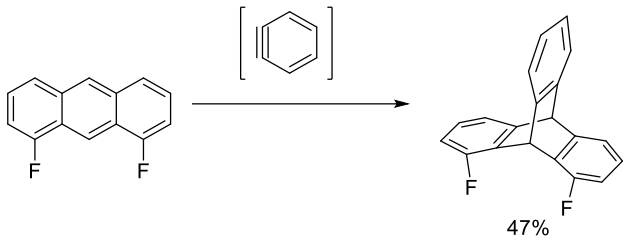

Scheme 22: Synthesis of 1,8-difluorotriptycene.

To introduce the phosphine-moieties in the final step, the formation of $KPPh_2$ from chlorodiphenylphosphine and elemental potassium was attempted. The potassium was suspended in dioxane and PPh_2Cl was added *via* syringe (Scheme 23). After heating the mixture to reflux for 10 hours, the product solution was filtered through a cannula. Although ^{31}P NMR spectrum of the mixture confirmed the formation of the desired product, the subsequent reaction with the 1,8-difluorotriptycene failed on multiple occasions possibly due to the formation of dimeric by-products.

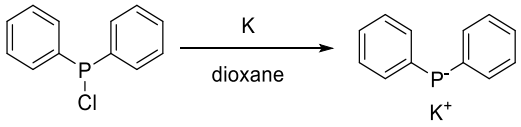

Scheme 23: Attempted synthesis of $KPPh_2$.

Alternatively, the reaction was carried out with a commercial 0.5 M solution of potassium-diphenylphosphide in THF (Scheme 24). After heating the mixture to reflux for 12 hours, the crude product was extracted with DCM, precipitated and washed with methanol to afford the triptycene ligand as white powder with 51% yield.

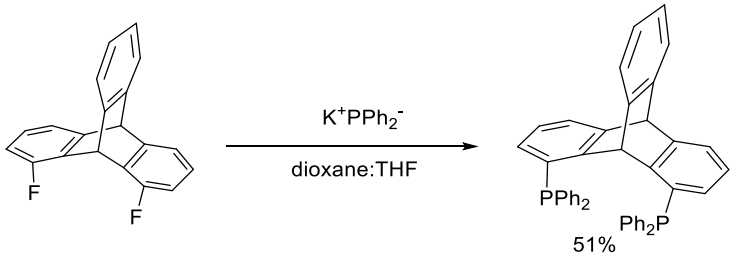

Scheme 24: Synthesis of triptycene ligand.

Due to the Vogt group leaving the University of Edinburgh this project was discontinued and the ligand was not tested in hydrocyanation reactions.

Tetraphenol ligands

Background

A novel ligand family with a rigid tetraphenol (TP) backbone was designed in the Vogt group originally for hydroformylation reactions (Scheme 25).[56] As these bidentate diphosphites featured wide bite angles and bulky substituents, they had high potential to be applied in hydrocyanations.

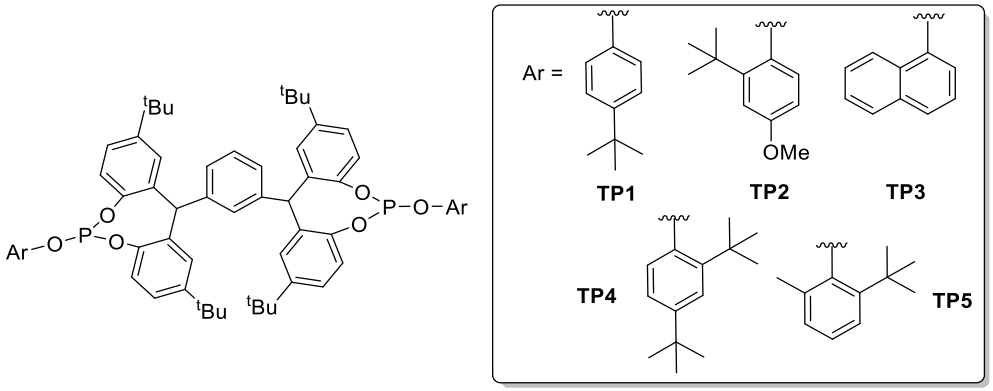

Scheme 25: Ligands with tetraphenol backbone developed by Vogt et al.[56]

In previous studies, investigating the *DuPont* process, surprisingly, TP ligands showed no activity in the hydrocyanation of butadiene or in the isomerisation of 2M3BN.[51] On the other hand, good conversions (up to 39%) and excellent linear selectivities (up to 96%) were achieved in the third step, the hydrocyanation of 3PN. In the presence of $ZnCl_2$ co-catalyst and using acetone cyanohydrin (ACH) as HCN source **TP2** ligand displayed the best performance (entry 2, Table 2). These results were competitive to other high-performing phosphite ligands in patent literature, as the substrate 3PN is an unactivated monoalkene. Our goal was to reproduce these initial results and gain a further mechanistic understanding of the behaviour of this ligand system.

Table 2: Hydrocyanation of 3PN with Ni/TP ligand complexes.

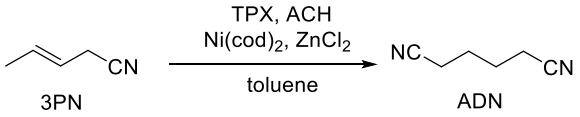

entry	ligand (TPX)	conversion (%)	selectivity (ADN%)
1	TP1	24	83
2	TP2	39	96
3	TP3	15	75
4	TP4	14	59
5	TP5	15	68

Conditions: 90 °C, 3 h, Ni:TPX:3PN:ACH = 1:1:100:150, acetone cyanohydrin (ACH) as HCN source, 2 mL of toluene.

Synthesis of tetraphenol backbones

The tetraphenol backbone (**TP0**) was synthesised following the procedure from the Vogt group.[56] Isophthalaldehyde and an eightfold excess of 4-*tert*-butylphenol were heated and stirred until a homogeneous melt was formed. Concentrated HCl was added dropwise as catalyst and the mixture was heated to reflux for 24 hours (Scheme 26).

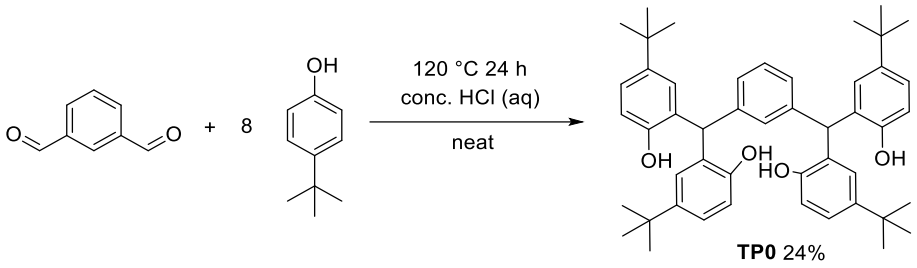

Scheme 26: Synthesis of the tetraphenol backbone.

The literature purification method was slightly modified. After cooling to room temperature, the mixture was neutralised with saturated aqueous $NaHCO_3$ solution and extracted with diethyl-ether. To eliminate the large amount of excess starting material five cycles of steam distillation followed that reduced the amount of phenol in the product mixture from 50% to 5%. After recrystallisation from acetone, **TP0** was isolated as a cream white powder with 24% yield.

Table 3: Syntheses of TP backbone in microwave reactor.

entry	catalyst	heating method	phenol equiv.	T (°C)	t (h)	[product]: [phenol]
1	HCl	Δ (pre melt)	8	120	24	3 : 1
2	HCl	MW (pre melt)	4.4	110	1	1.2 : 1
3	HCl	MW	4.4	110	1	2 : 1
4	$MeSO_3H$	MW (pre melt)	4.4	110	2	1.5 : 1
5	HCl	MW	4	110	2	2 : 1

The backbone synthesis was further optimised on a small scale using a microwave (MW) reactor to shorten the reaction time, reduce the large excess of phenol and consequently simplify the purification. The [product]:[residual phenol] ratio in the crude mixture was monitored *via* ^{1}H NMR spectroscopy. Following the original procedure, the HCl catalyst was added after the formation of a homogeneous melt from the starting materials (entry 2, Table 3), however, higher conversion was achieved by adding the HCl directly to the MW vial. As a loss of HCl was suspected, methanesulfonic acid as a higher boiling catalyst was tested, but the conversion did not increase significantly. It was

found that the reaction time can be shortened from the original 24 hours to 2 hours using MW conditions at 110 °C (entry 5, Table 3). Moreover, the amount of excess phenol could be decreased (from the original 8 equivalents to the stoichiometric 4 equivalents), leading to a simpler purification.

Investigations at *Evonik* reported on the presence of oligomeric by-products in crude **TP0** samples that were suspected to form *via* deprotonation on the tertiary carbon positions.[51] To eliminate this problem, the synthesis of an alternative backbone (**TPA**) was attempted using 1,3-diacetylbenzene to introduce stabilising tertiary methyl groups in the critical positions (Scheme 27). Instead of the desired product, the formation of 2,4-di-*tert*-butylphenol as major product was observed possibly due to Friedel-Crafts and retro-Friedel-Crafts reactions.

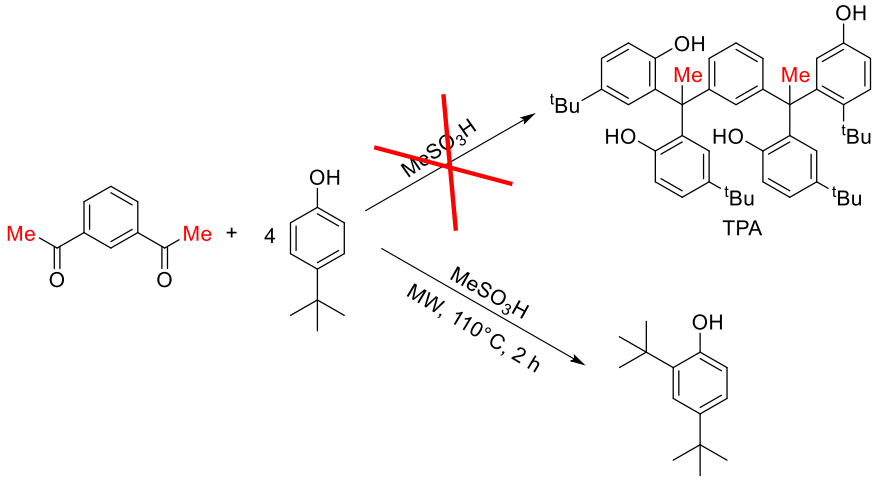

Scheme 27: Synthesis attempt of stabilised tetraphenol backbone TPA.

To increase the stereoelectronic diversity of future TP ligands, a third backbone derivative (**TPB**) was synthesised following a recent publication (Scheme 28).[57] Using *p*-toluenesulfonic acid as catalyst after 2 hours reaction time **TPB** was obtained with 73% yield as a cream white powder after purification *via* simple filtration and washing with acetonitrile. ^{1}H NMR spectrum of the product was in agreement with the literature data.

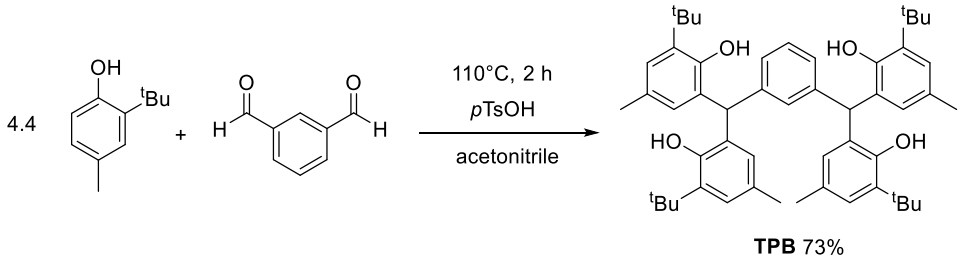

Scheme 28: Synthesis of TPB backbone.

Synthesis of tetraphenol diphosphite ligands

The **TP2** ligand was synthesised in a two-step procedure. First, two equivalents of PCl_3 were reacted with the **TP0** backbone in the presence of Et_3N for 1 hour at 0 °C. Then a THF solution of two equivalents of 2-^{t}Bu-4-methoxyphenol was added dropwise and the mixture was stirred for a further hour at room temperature (Scheme 29). Ammonium salts were filtered off over basic alumina and the solvents were removed *in vacuo*. After recrystallisation from acetone, **TP2** was obtained as a white powder with 9% crystalline yield. The ligand was characterised by ^{31}P, ^{1}H and ^{13}C NMR spectroscopy.

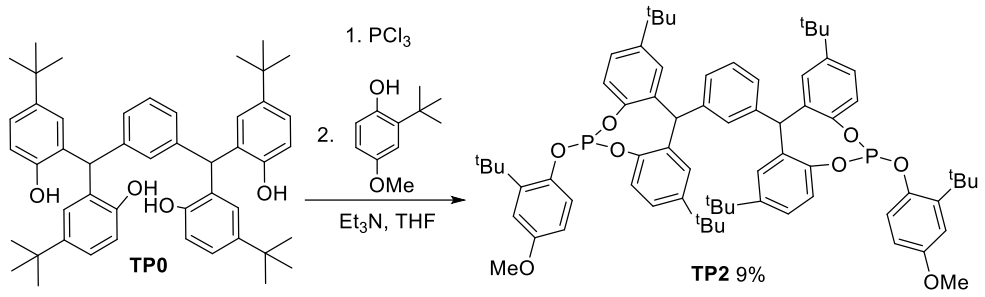

Scheme 29: Synthesis of the TP2 ligand.

Single, colourless, block-shaped crystals of **TP2** were obtained from acetone at -34 °C that enabled the characterisation of the ligand *via* X-ray crystallography. In the resulting molecular structure, P-O bond lengths range from 1.630(3) to 1.639(3) Å which falls in line with other previously reported diphosphite and diphosphonite ligands (Figure 6).[34, 40] One molecule of co-crystallised acetone per asymmetric unit was found in the structure. Notably, in solid state the free ligand took up a 'twisted' conformation allowing maximal distance between the bulky ^{t}Bu groups. This significantly differs from the metal coordinated ligand conformation (*vide infra*).

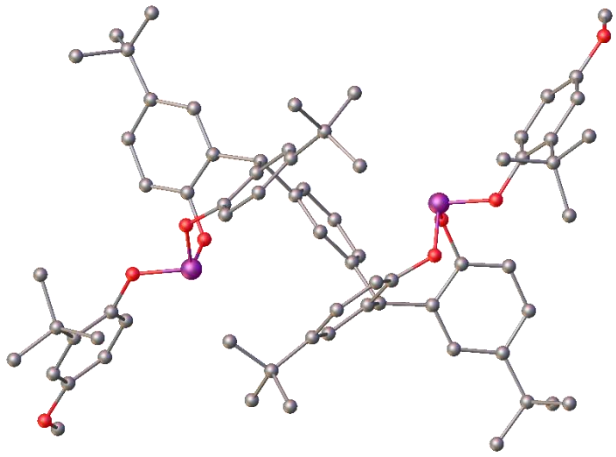

*Figure 6: X-ray molecular structure of the **TP2** solved by Dr Gary Nichol at the University of Edinburgh. Hydrogen atoms and acetone have been omitted for clarity. Selected bond lengths (Å): P1-O1 1.639(3), P1-O2 1.634(3), P1-O1 1.630(3), O1-C1 1.406(5), O2-C22 1.395(5), O3-C12 1.402(5).*

The originally developed TP ligand library (**TP1-TP5,** Scheme 25) featured varying aryl groups with sterically demanding substituents. We aimed to investigate whether the removal of some steric bulk can increase the ligands activity in catalytic hydrocyanations without decreasing the selectivity towards linear nitriles. Consequently, two new TP ligands with unsubstituted phenyl groups on the phosphite moieties were targeted. Following the procedure developed by Vogt *et al.*, the original **TP0** backbone was reacted with two equivalents of PCl_3 and two equivalents of phenol to give **TP6** ligand as a white powder with a low yield of 30% (Scheme 30).

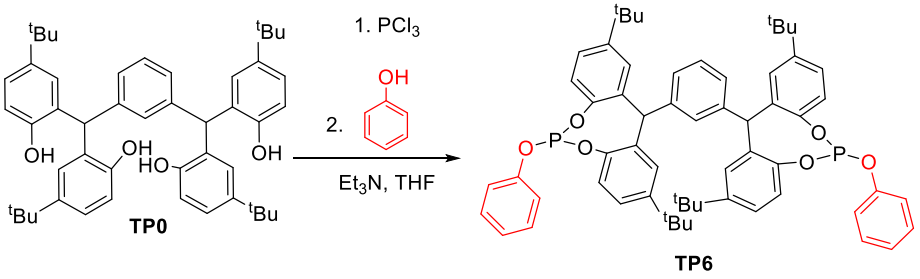

*Scheme 30: synthesis of novel **TP6** ligand.*

The novel **TPB** backbone was also converted into the corresponding diphosphite under identical reaction conditions, affording **TP7** as a cream white powder with a low crude yield of 34% (Scheme 31). The purification of this ligand was attempted *via* column chromatography, however, hydrolysis of some P-O bonds was observed due to the presence of trace water. The moisture-sensitivity of related phosphite ligands is well known in the literature.[58]

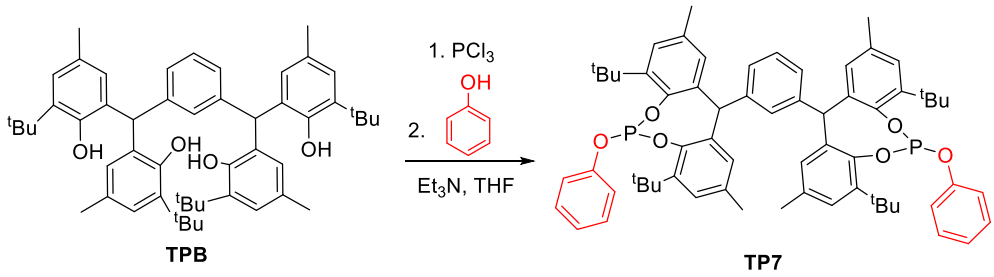

*Scheme 31: Synthesis of novel **TP7** ligand.*

The formation of both **TP6** and **TP7** was confirmed with ^{31}P NMR spectroscopy *via* the appearance of singlet phosphite peaks at 121.3 ppm and 127.8 ppm, respectively. Recrystallisation attempts of these ligands from a wide range of solvents including acetone, acetonitrile, THF, toluene and hexane have been unsuccessful. Consequently, attempts to form the corresponding Ni(cod) complexes have failed, most likely due to the presence of impurities in the ligand bulk materials.

Synthesis and characterisation of a tetraphenol-Ni complex

The extremely air- and moisture-sensitive (TP2)Ni(cod) complex, (**TP2Ni**), was synthesised on a 100 mg scale in the glovebox by stirring **TP2** with 1 equivalent of $Ni(cod)_2$ [cod = 1,5-cyclooctadiene] in toluene for 20 minutes at room temperature (Scheme 32).

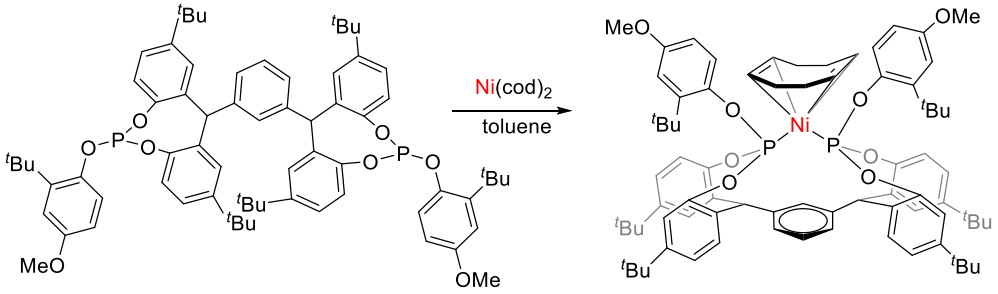

*Scheme 32: Synthesis of the **TP2Ni** complex.*

The resonance shift from 122.5 ppm (free ligand) to 125.4 ppm (complex) in the ^{31}P NMR spectrum indicated the coordination to the Ni centre (Figure 7). Solvents were removed *in vacuo* and the complex was recrystallised from acetone. ^{1}H NMR studies of **TP2Ni** featured significant peak broadening that can be explained with the gradual appearance of paramagnetic Ni^{II} species that are often observed in solution state.[59, 60] Consequently, the ^{1}H spectrum could not be completely assigned, nevertheless, the appearance of free cod signals and the shift of coordinated cod peaks further corroborated the formation of the complex. Additional variable temperature NMR studies were carried out to investigate the coordination of substrates to **TP2Ni** (*vide infra*).

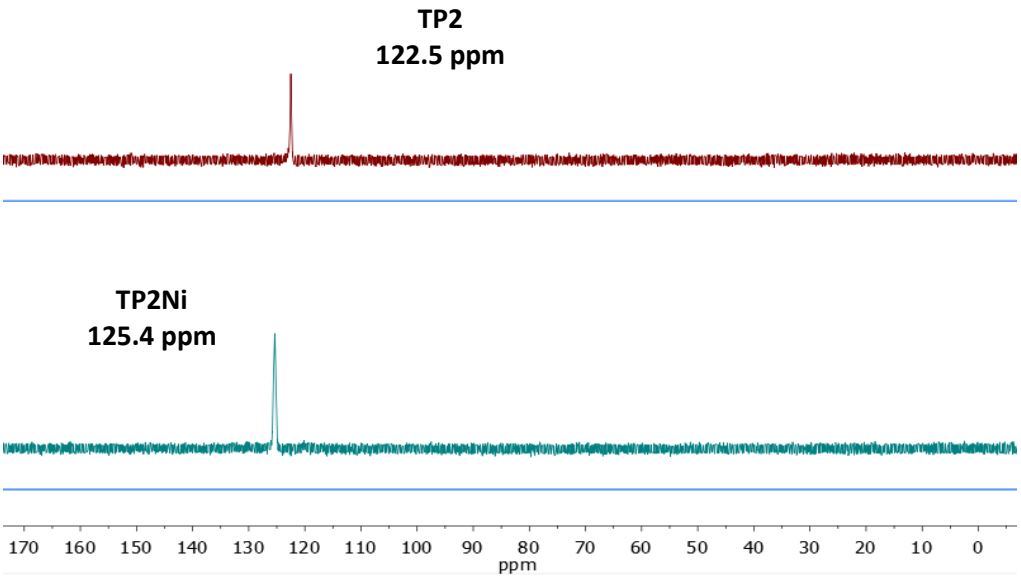

*Figure 7: ^{31}P NMR spectra of **TP2** ligand and **TP2Ni** complex (toluene d_8, 20 °C).*

Single, colourless, rod-shaped crystals of **TP2Ni** were obtained *via* the slow vapour diffusion of heptane into THF. To the best of our knowledge, this is the first example of a Ni^0 diphosphite complex bearing a 1,5-cyclooctadiene ligand characterised by X-ray diffraction (Figure 8). Importantly, **TP2Ni** showed a monomeric configuration in the solid state, suggesting that the **TP2** ligand is sterically demanding enough to prevent the formation of bis-chelate [Ni(P-P)$_2$] species. Ligands that allow the formation of bis(bidentate) complexes were shown to be less effective in hydrocyanation reactions as the accessibility of the metal centre was hindered or completely blocked.[61] The Ni-P bond lengths of 2.099(2)-2.101(2) Å are in agreement with values of other phosphonite and phosphinite Ni(cod) complexes reported in literature.[40, 62] The P-Ni-P bite angle of 106.82(4)° is close to the ideal value for a tetrahedral structure (109.5°) indicating potentially good performance in hydrocyanation and 2M3BN isomerisation reactions.

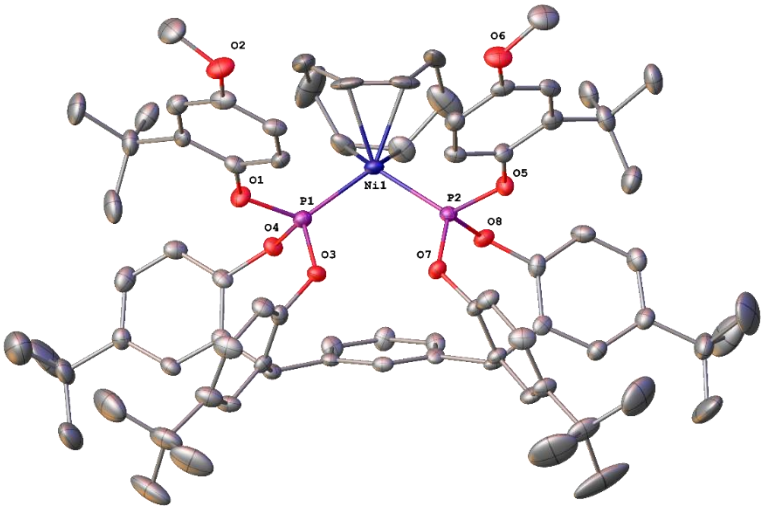

*Figure 8: X-ray molecular structure of **TP2Ni** solved by Dr Gary Nichol at the University of Edinburgh. Hydrogen atoms and THF have been omitted for clarity, thermal ellipsoids are shown at 50% probability level. Selected bond lengths (Å): Ni1-P1 2.101(2), Ni1-P2 2.099(2), Ni1-C1 2.166(6), Ni1-C2 2.152(7), Ni1-C5 2.113(6), Ni1-C6 2.095(6) Selected bond angles (°): P1-Ni1-P2 106.82(4), P1-Ni1-C1 95.1(2), P1-Ni1-C2 124.1(2), P1-Ni1-C5 138.8(2), P2-Ni1-C1 128.9(2), P2-Ni1-C2 95.6(2), P2-Ni1-C5 99.2(2), C2-Ni1-C1 36.6(2), C5-Ni1-C1 92.7(3), C5-Ni1-C2 83.3(3), C6-Ni1-P1 103.6(2), C6-Ni1-P2 130.9(2), C6-Ni1-C1 84.8(3), C6-Ni1-C2 98.3(3), C6-Ni1-C5 37.1(2).*

As catalyst deactivation is an important side-reaction, the synthesis of the deactivated TP2Ni(CN)$_2$ complex was also attempted. **TP2Ni** was stirred with 100 equivalents of acetone cyanohydrin at room temperature for 24 hours in THF. After solvents were removed *in vacuo* ^{1}H and ^{13}C NMR experiments indicated no bis(cyanide) formation and slow diffusion of heptane into the mixture afforded the original **TP2Ni** crystals. These results strengthened our hypothesis that the **TP2** ligand backbone is rigid enough to prevent the formation of square planar (β = 120°) inactive Ni(CN)$_2$ complexes.

Catalytic activity of the TP2Ni complex in the ADN process

As mentioned before, preliminary experiments in the Vogt group with the **TP2Ni** catalyst system showed an absence of activity in the hydrocyanation of butadiene or in the isomerisation of 2M3BN, but good performance was achieved in 3PN hydrocyanations.[51, 63] For a catalyst system to be exclusively active in the most challenging step of the adiponitrile process was quite an unusual finding. As an explanation, it was proposed that the **TP2** ligand sterically hinders the formation of π-allyl intermediates required for the first two steps of the ADN process (Scheme 33).[64] On the other hand, the hydrocyanation of 3PN occurs (after *in situ* isomerisation to 4PN) through a σ-alkyl intermediate.

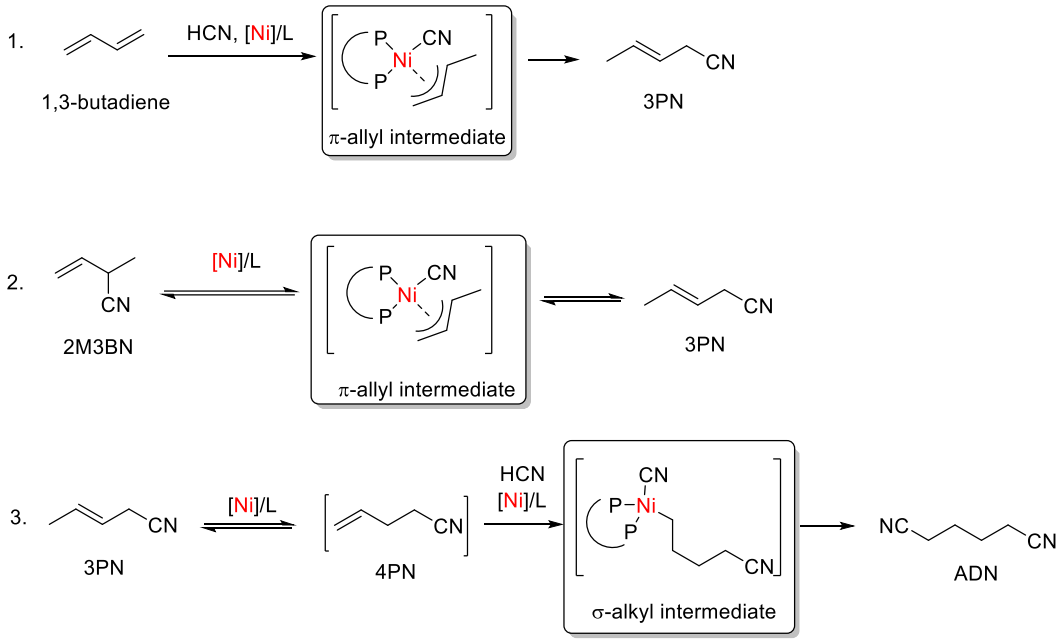

Scheme 33: Occurrence of π-allyl and σ-alkyl intermediates in the ADN process.

In order to confirm the presence of either of the above intermediates in the reaction mixtures, ultra-low temperature and variable temperature ^{1}H NMR spectroscopy experiments were carried out.[22] In an NMR tube 1 to 5 equivalents of substrate were added to the solution of **TP2Ni** in toluene-d_8 at -100 °C and spectra were recorded at 10 °C intervals as the temperature was slowly increased to 80 °C. The optimal temperature to minimise peak broadening (caused by increased viscosity at ultra-low temperatures and too fast reaction at higher temperatures) was at -50 °C (Figure 9). As the freezing point of toluene-d_8 was near -95 °C, an alternative solvent combination (1:1 mixture of THF-d_8 and acetone-d_6) was also tested to allow the examination at lower temperatures, however, no improvement in refinement was achieved.

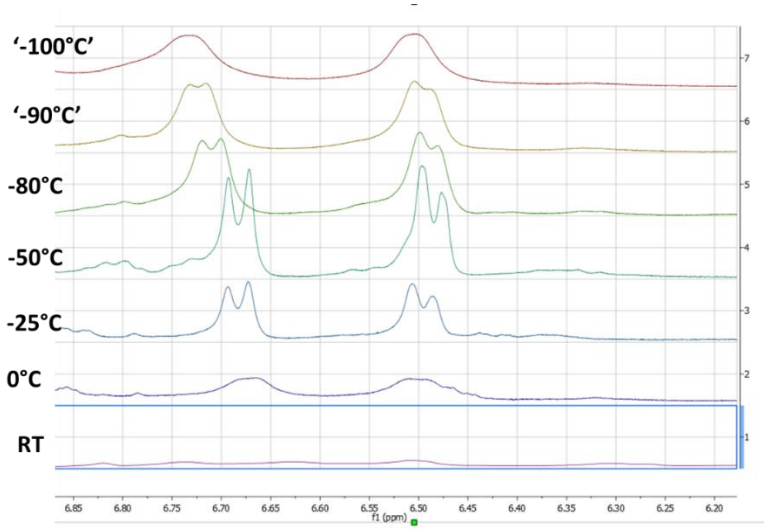

*Figure 9: Peak broadening in variable temperature NMR spectra of **TP2Ni** and 2M3BN.*

Three different substrates (2M3BN, 3PN and allyl bromide as a less sterically encumbered analogue) were investigated. With all three species, a shift in proton resonances compared to the free substrate and the appearance of free cyclooctadiene peaks (at 2.20 and 5.51 ppm) indicated the coordination to the Ni centre. However, signals for the proposed π-allyl and σ-alkyl intermediates could not be unequivocally detected due to the significant peak broadening (possibly caused by the formation of paramagnetic Ni^{II} species). The decomposition of the extremely air- and moisture-sensitive Ni^{0} species was also indicated by a colour change from yellow to black during the ^{1}H NMR experiments.

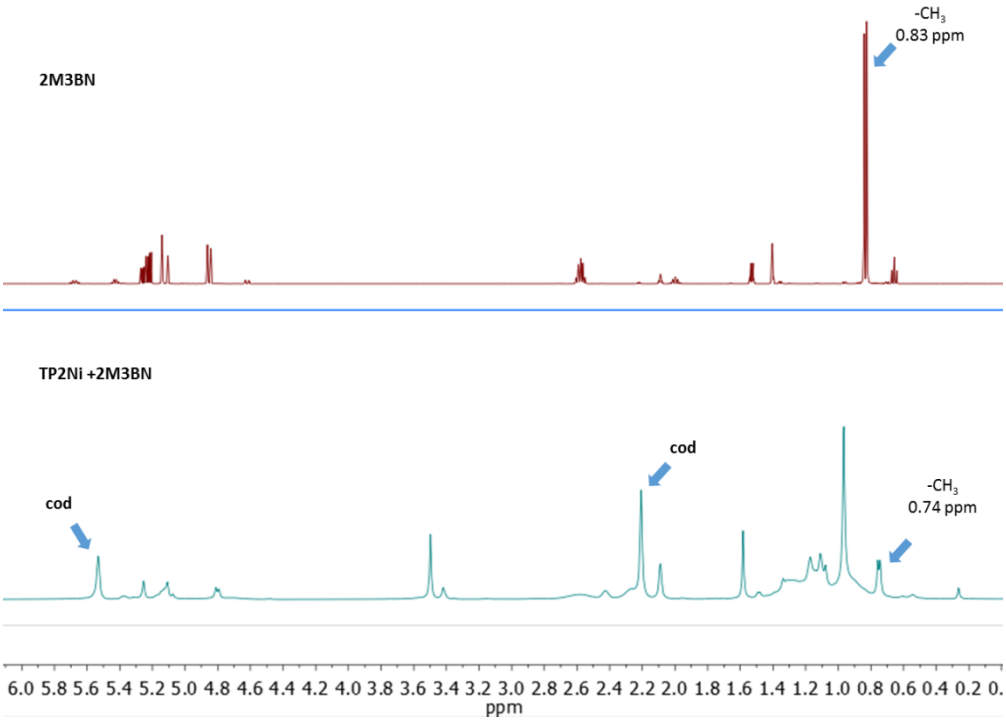

*Figure 10: ^{1}H NMR spectra of 2M3BN and **TP2Ni** complex with 2M3BN.*

Control experiments were carried out with catalyst systems containing three other diphosphorus ligands (**Biphephos, DPEphos** and **BIPPP**) that were known to be active in the isomerisation of 2M3BN and therefore favour the formation of π-allyl intermediates.[22, 65] (Figure 11).

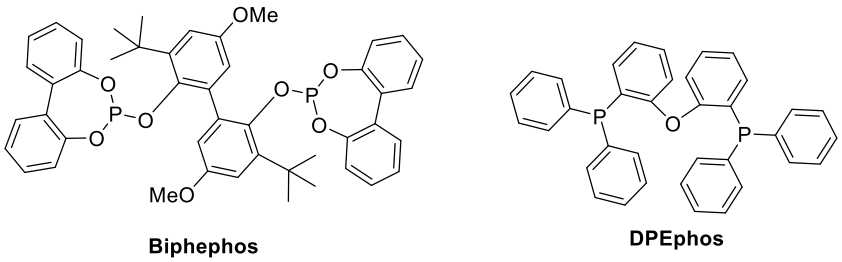

Figure 11: Ligands used as comparison to form π-allyl species.

While **Biphephos** and **DPEphos** were provided by *Evonik*, the BIPPP ligand was synthesised following literature procedures (Scheme 34).[65] 2-Isopropylphenol was reacted with PCl_3 and 1-1'-bi-2-naphthol in the presence of Et_3N to give **BIPPP** as a cream white powder with 66% yield. The ligands were subsequently converted into the corresponding Ni(cod) complexes and following the addition of substrates (2M3BN, 3PN or allyl-bromide) variable temperature ^1H NMR experiments (under identical reaction conditions used with **TP2Ni**) were carried out. Neither of the proposed π-allyl and σ-alkyl intermediates could be detected under the applied reaction conditions.

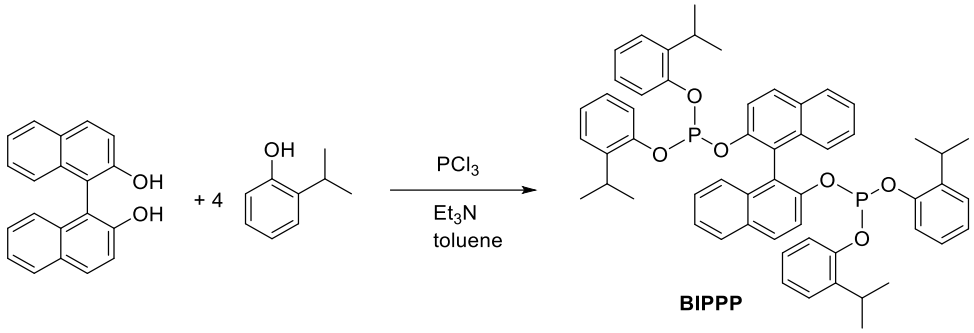

Scheme 34: Synthesis of BIPPP ligand.

Following the ambiguous VT-NMR experiments, the isomerisation of 2M3BN using **TP2Ni** was carried out in toluene at 90 °C and 110 °C. Conversions were determined using gas chromatography (GC) with a flame ionisation detector (FID) calibrated for each of the substrates against *n*-decane as internal standard. Contrary to the previously reported patent, **TP2Ni**, in fact, showed moderate activity in the reaction, reaching conversions of up to 36% after 2 hours (Table 4, entry 1 and 2). These results suggest that the **TP2** catalyst system actually allows the formation of intermediates necessary for the isomerisation of 2M3BN. Under identical conditions, comparative reactions were carried out using **BIPPP** and **DPEphos** ligands. As expected, with these reportedly active systems significantly higher conversions (up to 96%) were achieved (Table 4, entry 3-6).

Table 4: Isomerisation of 2M3BN with different ligands.

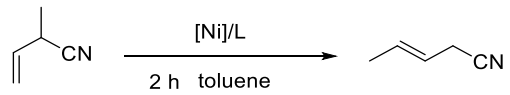

entry	ligand	T (°C)	conversion (%)	3PN yield (%)
1	**TP2**	90	27	26
2	**TP2**	110	36	34
3	**BIPPP**	90	65	62
4	**BIPPP**	110	96	92
5	**DPEphos**	90	95	91
6	**DPEphos**	110	96	87

Conditions: 0.018 mmol Ni, Ni:L:S =1:1:170, t = 2 h, in 2 mL toluene.

The difference in activity of **TP2Ni** compared to **DPEphos-Ni** complex was also investigated *via* DFT calculations carried out by Bernd Hannebauer *et al.* at *Evonik*. In these studies, the free energy levels of the two complexes were compared when coordinating HCN or the substrates. The initial calculations were matching our experimental results, as the more active **DPEphos** system showed transition states of lower energy levels with both substrates (butadiene and 2M3BN) (Figure 12). The further elucidation of the result was cancelled due to the Vogt group leaving the University of Edinburgh.

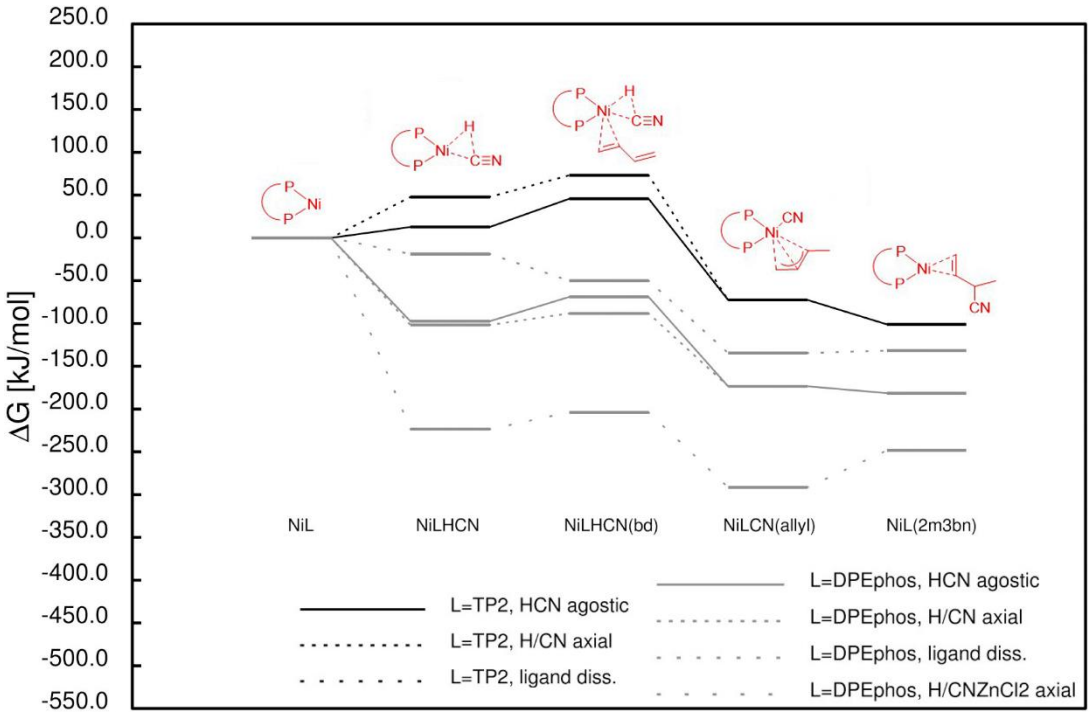

*Figure 12: Comparison of **TP2** and **DPEphos** intermediates using DFT calculations.*

Purity of 2M3BN

During our studies it was found that analytically pure 2M3BN is not commercially available, moreover, in our hands, it was not possible to purify it *via* fractional distillation. Several patents describe that even on industrial scale it can only be enriched in 2M3BN up to 90% *via* fractional distillation on packed columns or adduct formation with bisulphates.[66] Gas chromatography-mass spectrometry (GC-MS) experiments showed that the highest purity we could achieve was 82%, containing double bond isomers such as 2-methyl-2-butenenitrile (2M2BN) and 2-pentenenitrile (2PN) as main impurities (Figure 13). All conversion data from the catalytic reactions was mass-balanced accordingly.

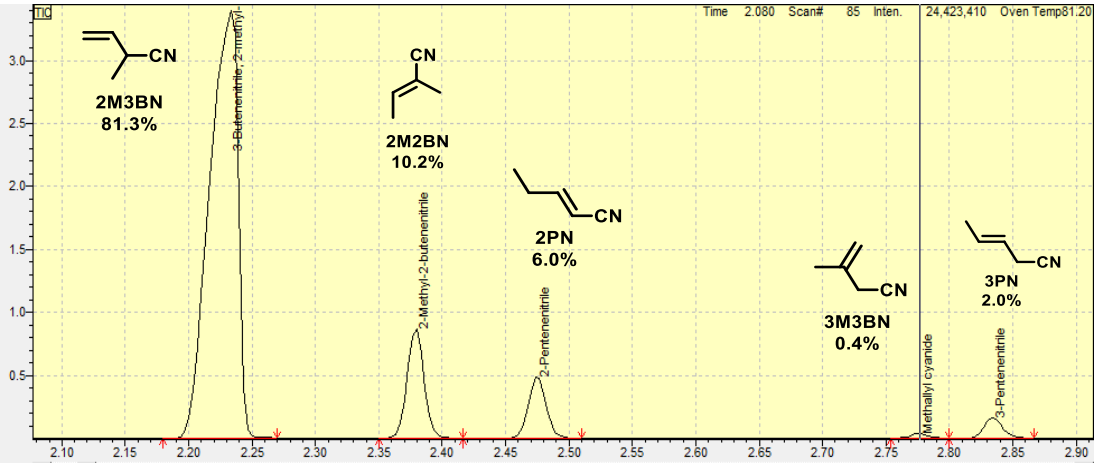

Figure 13: Impurities in the GC-MS chromatogram of commercial 2M3BN.

In attempt to obtain higher purity, the synthesis of 2M3BN was carried out following literature procedures *via* the methylation of allyl cyanide and the allylation of propionitrile (Scheme 35).[67, 68] With both synthetic routes, product mixtures containing less than 50% 2M3BN were achieved, therefore the purification was not carried out. Analytical data from previous co-workers showed that similar (~80% pure) 2M3BN was used earlier in the group without taking the impurities into consideration. This could be a potential explanation for the false negative results achieved with **TP2** ligand in the 2M3BN isomerisation reactions. Another option may be that residual impurities in the bulk of **TP2** ligand caused catalyst deactivation.

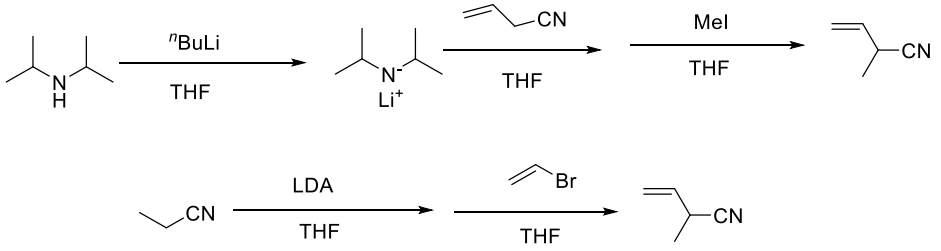

Scheme 35: Attempted synthesis routes for 2M3BN.

Biphephos ligand

Background

Biphephos is a bidentate diphosphite ligand (Figure 14) that was originally patented by *Union Carbide* (now *Dow*) in 1986.[69] In combination with Rh precursors it showed excellent activities and selectivities towards linear aldehydes in the hydroformylation of a wide range of alkenes.[70] Ever since Biphephos has been intensely studied and it became the prototype of all subsequently developed diphosphite ligands for regioselective hydroformylations.[71] Biphephos features a relatively rigid backbone and a wide bite angle (118.98° with Rh) that are promising properties for hydrocyanation catalysis.[72] Surprisingly, it has been underexplored in this field, with only a few patents reported, and a complete absence of examples in the academic literature.

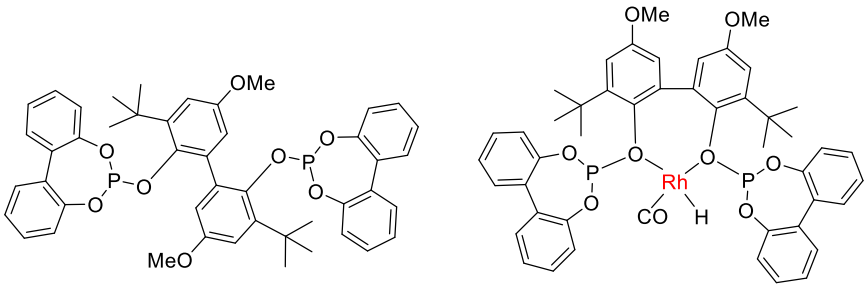

Figure 14: Structure of the Biphephos ligand and a Rh-Biphephos complex.

In a *DuPont* patent, Biphephos was applied in the first two steps of the adiponitrile process: the hydrocyanation of butadiene and the isomerisation of 2M3BN.[73] Separate stock solutions of the Biphephos-Ni complex, HCN and substrates were prepared and combined in small (2 mL), sealed vials. After heating the mixture to 80 °C for one hour, nearly complete conversion was achieved in the hydrocyanation of butadiene, however, the selectivity towards the linear 3PN was very low (around 20 %) (Table 5). Under similar reaction conditions, the isomerisation of 2M3BN was also investigated in the absence of HCN. As Table 6 shows, 3 hours of reaction time was necessary to achieve a relatively high conversion to 3PN.[73]

Table 5: Hydrocyanation of butadiene with Ni/Biphephos catalyst.

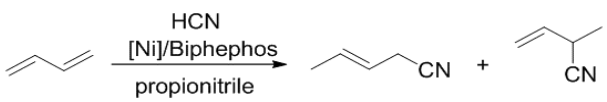

entry	t(h)	conversion (%)	3PN (%)	2M3BN (%)
1	1	94	19	75
2	3	97	21	76

Conditions: 80 °C, Ni:Biphephos:butadiene:HCN = 1:6:2000:excess in 2 ml propionitrile.

Table 6: Isomerisation of 2M3BN using Ni/Biphephos catalyst.

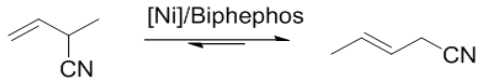

entry	t (h)	ratio 3PN/2M3BN
1	1	1
2	2	3
3	3	13

Conditions: 80 °C, Ni:Biphephos:2M3BN = 1:6:2000 in 2 ml propionitrile.

Biphephos was also tested in the third step, the hydrocyanation of 3PN using a constant flow of HCN gas in the presence of different Lewis acid co-catalysts.[74] Using 6 equivalents of ligand per Ni, after 45 minutes stirring at 70 °C the crude reaction mixtures were analysed *via* gas GC to determine the ratio of the desired adiponitrile (ADN) and a common by-product, 2-methylglutaronitrile (MGN) formed. It was found that $ZnCl_2$ co-catalyst provided the most active catalyst system with a high selectivity (77%) towards ADN (entry 2, Table 7).

Table 7: Hydrocyanation of 3PN with Ni/Biphephos catalyst.

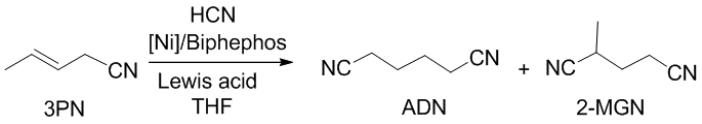

entry	Lewis acid	amount ADN (%)	amount MGN (%)
1	-	1.5	0.2
2	$ZnCl_2$	77	21
3	$SnCl_2$	16	4
4	BPh_3	39	2
5	Ph_3SnOTf	48	2

Conditions: 70°C, 45 min, Ni:L:co-cat:3PN = 1:6:1:1000, constant flow of HCN (30 ml/min), neat.

Further patents mainly describe heterogeneous processes, including the vapour phase hydrocyanation of butadiene using the Biphephos-Ni complex dispersed on a stationary solid phase.[75] The paucity of academic publications with homogeneous conditions prompted us to investigate this promising ligand within our reaction setup. Consequently, the efficiency of Biphephos was tested in hydrocyanation reactions with different substrates. Moreover, to optimise catalyst activity and selectivity, different parameters such as complex pre-formation, solvent, temperature, reaction time, HCN addition speed and HCN source were systematically screened. Parts of the investigation of Biphephos ligand were carried out with the assistance of Rachael Shedden undergraduate project student.

Hydrocyanation of styrene with Biphephos ligand

First, the hydrocyanation of styrene as a model substrate was investigated using the Biphephos ligand. In agreement with previous reports, the regioselectivity towards the branched product, 2-phenylpropionitrile (2PPN), was greater than 99% in all reactions, only traces of the linear nitrile were observed.[24] This allowed us to focus solely on the activity of the catalyst system, not considering regioselectivity issues.

Due to the low solubility of Biphephos in apolar solvents, we studied whether the pre-formation of the Biphephos-Ni complex prior to the reactions was necessary. To form the complex, a 1:1 ratio of the ligand and $Ni(cod)_2$ were stirred in THF at room temperature for 30 minutes, then all volatiles were removed *in vacuo*. Hydrocyanations were carried out neat or in different solvents, with and without complex pre-formation at 70 °C for one hour (Table 8). Without solvent, no conversion was achieved in the hydrocyanation suggesting that the ligand was not soluble in the substrate under these reaction conditions (entry 1, Table 8). On the other hand, 53% of styrene was converted to 2PPN after pre-forming the Ni complex. As expected, slightly lower conversions were achieved when the reactions were carried out in a solvent. Complementarily to the standard toluene and THF, 2-methyltetrahydrofuran (Me-THF) was also considered as an alternative renewable industrial solvent, due to its high boiling point (80 °C) and more hydrophobic nature.[76] Although the difference with and without pre-formation was not significant in the reactions performed in solvents, it was decided to carry out the pre-formation in all future experiments to ensure comparability to the neat reactions.

Table 8: Hydrocyanation of styrene with and without pre-formation of the catalyst complex.

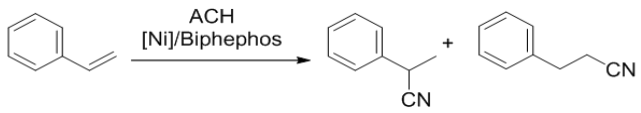

entry	solvent	conversion (%)	
		with pre-formation	without pre-formation
1	neat	53	0
2	toluene	47	34
3	THF	43	40
4	Me-THF	39	43

Conditions: 1 h, 70 °C, 0.018 mmol Ni, Ni:Biphephos:styrene:ACH =1:1:170:250, neat or in 2 mL solvent. Continuous addition of ACH via syringe pump 0.3 ml/h. Reactions were carried out in duplo.

Next, the hydrocyanation of styrene was screened in a wider range of solvents (Table 9). As expected, the conversions were lower compared to the neat reaction. In carbonyl group containing solvents, such as acetone and DMF, a significant decrease in conversion was observed. This may be

attributed to the coordination of these solvents to the Ni centre (entry 8 and 10, Table 9). The best performances were achieved with toluene, hexane, THF and methanol. For the initial optimisation, it was important to identify a diverse range of solvents that are suitable for laboratory scale hydrocyanations. As the use of gaseous HCN is prohibited by safety regulations, the application of a solvent is essential to aid the continuous addition of the HCN source *via* a syringe pump.

Table 9: Hydrocyanation of styrene in different solvents.

entry	solvent	conversion (%)
1	neat	53
2	toluene	47
3	THF	43
4	Me-THF	39
5	MeOH	52
6	1,4-dioxane	40
7	diglyme	40
8	DMF	23
9	hexane	48
10	acetone	34

Conditions: 0.018 mmol Ni, Ni:L:S:ACH =1:1:170:250, t = 1 h, T=70 °C, neat or in 2 mL solvent. Continuous addition of ACH via syringe pump 0.3 ml/h.

Subsequently, the role of the reaction temperature was studied. At ambient temperature no conversion was observed when the hydrocyanation of styrene was carried out in toluene (entry 1, Table 10). Unsurprisingly, increasing the temperature led to gradually higher conversations both in solvents and under neat conditions (entry 2-4, Table 10). When using solvents above the boiling point of acetone cyanohydrin (95 °C) the results became unreproducible, possibly due to homogeneity problems/leaks in the setup consisting of the syringe pump and a septum-covered Schlenk-flask. It was observed that droplets of the ACH evaporated before reaching the reaction mixture.

Table 10: Hydrocyanation of styrene at different temperatures.

entry	T (°C)	conversion (%)	
		neat	in toluene
1	r. t.	5	0
2	70	53	47
3	100	84	26*
4	120	93	87*

*Conditions: 0.018 mmol Ni, Ni:L:S:ACH =1:1:170:250, t = 1h, neat or in 2 mL solvent. Continuous addition of ACH via syringe pump 0.3 ml/h. *Reactions carried out in duplo had error >10% in conversion.*

To summarise these initial optimisation studies using Biphephos ligand, it was shown that with 0.5 mol % catalyst loading the hydrocyanation of styrene reached TONs of up to 158 without solvent, at 120 °C and with slow syringe pump addition of acetone cyanohydrin.

Hydrocyanation of 1,3-butadiene with Biphephos ligand

To test Biphephos in the hydrocyanation of the substrates of the *DuPont* process, preliminary studies with butadiene were carried out. The original reaction setup (a septum-capped Schlenk flask and syringe pump) was found to be unsuitable to use with pure gaseous butadiene, therefore a 40 wt% solution of butadiene in toluene was applied. After stirring for 2 hours at 70 °C, GC analysis of the crude product showed a mixture of mono- and dinitriles (Scheme 36).

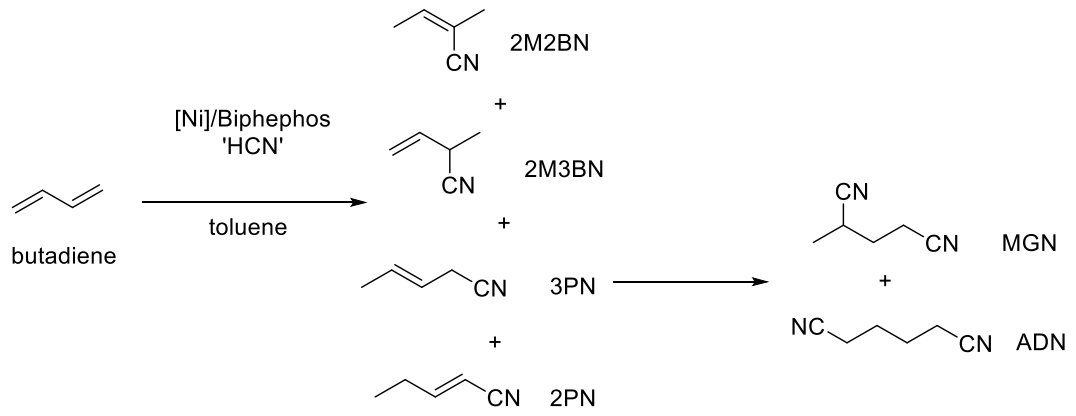

Scheme 36: Products forming in the hydrocyanation of butadiene.

The reactions were originally carried out by adding the HCN source as one aliquot in a closed system (closed Schlenk flask) to prevent the possible loss of butadiene. However, to avoid the aforementioned catalyst deactivation due to the presence of excess HCN, it may be beneficial to

ensure a constant low level of available HCN by gradually dosing the HCN source during the reactions. Surprisingly, when the reactions were repeated using a syringe pump (slow addition of HCN source through a septum), no significant difference was observed (Table 11). Interestingly, the use of acetone cyanohydrin afforded a product mixture with the undesired 2-methyl-2-butenenitrile (2M2BN) and 2-methylglutaronitrile (MGN) as major products. Alternatively, trimethylsilyl cyanide (TMSCN) was applied that pushed the reaction towards the formation of 2M2BN over MGN. Notably, these side-reactions are less observed in the patent literature, where almost exclusively pure HCN is applied. Consequently, the formation of the undesired double-bond isomers may be tentatively attributed to the use of the alternative HCN sources, that are now indispensable in academic research due to safety regulations. Along with the HCN, these compounds also release by-products (e. g. acetone from ACH) that may coordinate to the Ni centre and stereoelectronically influence the substrate coordination. It was concluded that a design of a different reactor setup would be necessary that can simultaneously allow the slow continuous addition of HCN source and optimise reaction conditions to synthesise the desired products, 2M3BN and 3PN.

Table 11: Yield of main and by-products in hydrocyanation of 1,3-butadiene.

entry	HCN source	2M3BN (%)	2M2BN (%)	2PN yield (%)	3PN (%)	MGN (%)	ADN (%)
1	TMSCN	0	13	0	3	3	0
2	TMSCN*	0	12	1	2	3	0
3	ACH	2	11	1	4	8	0
4	ACH*	0	11	1	3	10	1

*Conditions: 0.018 mmol Ni, Ni:L:S:'HCN' =1:1:170:250, T =70 °C, t = 2 h, in toluene. Yields were mass balanced against the internal standard (n-decane) as the volatile butadiene starting material could not be detected in the GC setup used. * Continuous addition of HCN source via syringe pump (0.3 mL/h).*

Isomerisation of 2-methyl-3-butenenitrile with Biphephos ligand

The isomerisation of 2M3BN with Biphephos as a ligand was extensively studied *via* the systematic screening of reaction conditions. As the isomerisations were performed in the absence of HCN, the reaction temperature was not limited by the boiling point of the HCN source. As the first step of the optimisation, the isomerisation was carried out using a variety of solvents at 120°C for 1 hour (Table 12). Similar to the styrene hydrocyanations (Table 9), reactions in acetonitrile and acetone gave the lowest conversions, possibly due to the polar carbonyl and nitrile groups coordinating to the Ni centre. Almost complete conversions were achieved in toluene, hexane and THF. The reaction carried out in 1,4-dioxane led to the highest conversion, but due to this solvent's high toxicity, greener alternatives with similar properties had to be considered. Both 2-methyl-tetrahydrofuran (Me-THF) and cyclopentyl-methyl ether (CPME) provided excellent conversions. Consequently, CPME was chosen to

carry out further experiments due to its higher boiling point, hydrophobicity and lower susceptibility to form peroxides upon storage.[76]

Table 12: Isomerisation of 2M3BN in different solvents.

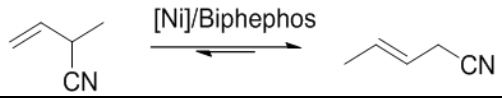

entry	solvent	conversion (%)
1	neat	95
2	Toluene	96
3	Hexane	90
4	Acetonitrile	82
5	Acetone	60
6	1,4-dioxane	98
7	Me-THF	97
8	THF	95
9	CPME	95

Conditions: 0.018 mmol Ni, Ni:L:S =1:1:170, T= 120 °C, t = 1 h, neat or in 2 mL solvent.

Next, the isomerisation was performed at different temperatures. No reaction was observed at room temperature, while the conversion only reached 19% at 70 °C. At 100 °C and 120 °C, good to excellent conversions were achieved. Although the conversion has not dropped by increasing the temperature to 150 °C, after a few minutes, a change of colour from yellow to black was observed, indicating the possible thermal decomposition of the Ni catalyst. Consequently, 100 °C was chosen to carry out further experiments as it allowed a window to investigate the effect of other parameters.

Table 13: Isomerisation of 2M3BN at different temperatures.

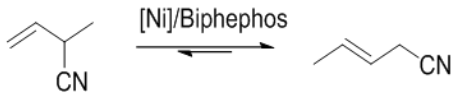

entry	T (°C)	solvent	conversion (%)
1	r.t.	neat	0
2	70	neat	19
3	100	neat	49
4	120	neat	95
5	150	neat	94
6	100	1,4-dioxane	72
7	120	1,4-dioxane	98
8	100	CPME	71
9	120	CPME	95

Conditions: 0.018 mmol Ni, Ni:L:S =1:1:170, t = 1 h, neat or in 2 mL solvent.

Several patents report on the use of an excess of phosphite or diphosphite ligands in hydrocyanation and 2M3BN isomerisation reactions to exert a stabilising effect on the catalyst and reduce the possibility of Ni bis-cyanide [$Ni(CN)_2$] formation.[5] Different metal to ligand ratios (M:L) were screened to investigate whether an excess of Biphephos stabilises the catalyst complex or leads to the formation of inactive species. These experiments were carried out without the pre-formation of the Biphephos-Ni complex. As Table 14 shows, no significant difference was observed between the 1:1 and 1:2 ratios when performing the reaction without solvent or in dioxane. Using CPME, the conversion dropped from 71 to 52% when doubling the ligand ratio. The neat reaction using five equivalents of ligand was unsuccessful, possibly due to the low solubility of the Biphephos in the substrate that prevented efficient stirring (entry 3, Table 14). A substantial decrease of conversion was observed using five equivalents of Biphephos in dioxane or CPME, indicating the possible formation of less active (bis-chelate) Ni species (entry 6 and 9, Table 14).

Table 14: Isomerisation of 2M3BN with different metal:ligand ratios.

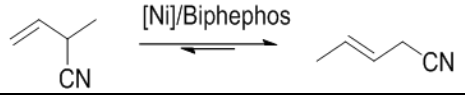

entry	M:L	solvent	conversion (%)
1	1:1	neat	49
2	1:2	neat	51
3	1:5	neat	-
4	1:1	1,4-dioxane	72
5	1:2	1,4-dioxane	78
6	1:5	1,4-dioxane	55
7	1:1	CPME	71
8	1:2	CPME	52
9	1:5	CPME	18

Conditions: 0.018 mmol Ni, Ni:L:S =1:1 to 5:170, T = 100 °C, t = 1 h, neat or in 2 mL solvent.

To further examine the effect of ligand excess, complexation experiments were carried out in the absence of 2M3BN, stirring $Ni(cod)_2$ with five equivalents of Biphephos at 100 °C for one hour (identical conditions to the isomerisation reactions). ^{31}P NMR spectroscopy of the crude mixture revealed that besides the free ligand (146.2 ppm) and the catalyst complex (178.6 ppm), a bis-chelated [$(P\text{-}P)_2Ni$] complex was also formed (162.5 ppm) (Figure 15). Consequently, the reduced activity was attributed to the formation of these extremely stable complexes. Similar species (with other diphosphite ligands) were reported to be catalytically inactive due to the prohibited ligand dissociation.[22] Bis-chelated Biphephos species were previously reported in vapour phase hydrocyanation patents.[77]

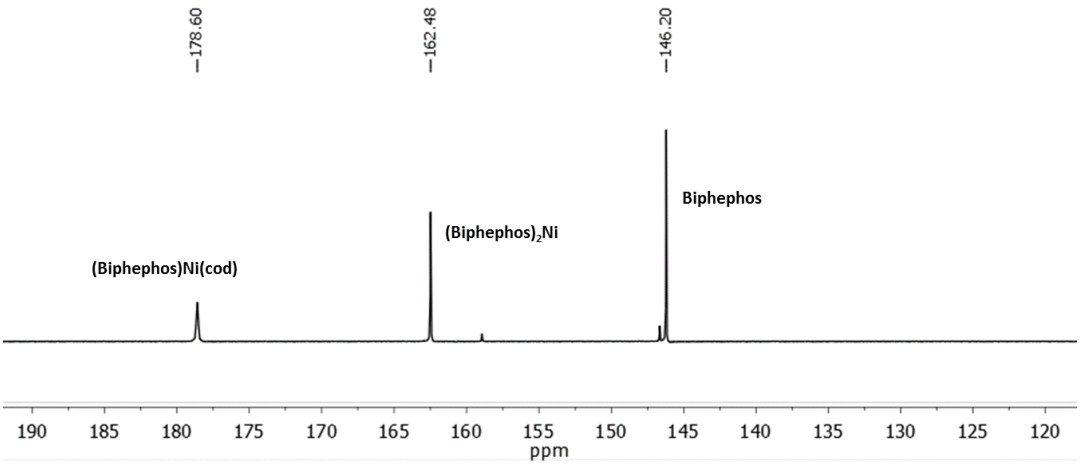

Figure 15: ^{31}P NMR spectrum of catalyst complex, bis-chelate complex and free ligand.

To investigate the catalysts robustness towards a larger ratio of substrate, the isomerisations were performed with an increased loading of up to 2000 equivalents of 2M3BN *versus* Ni. As Table 15 shows, the catalyst loading could be decreased to 0.1 mol % (1:1000 Ni:2M3BN) while maintaining decent activity. The obtained relatively high turnover numbers (up to 326 in neat reactions and up to 343 in CPME) fall in line with other diphosphite-based catalyst systems in the literature.[43, 73] The significant drop in activity using 2000 equivalents of 2M3BN (0.05 mol %) was attributed to the presence of proportionally large amount of impurities in the substrate, leading to catalyst deactivation (entry 4 and 8, Table 15).

Table 15: Isomerisation of 2M3BN with increasing substrate loading.

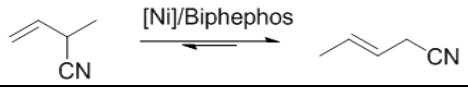

entry	2M3BN:Ni	solvent	conversion (%)	TON
1	170	neat	82	110
2	500	neat	50	228
3	1000	neat	42	326
4	2000	neat	8	23
5	170	CPME	90	129
6	500	CPME	48	177
7	1000	CPME	45	343
8	2000	CPME	5	20

Conditions: 0.018 mmol Ni, Ni:L:S =1:1:170/500/1000/2000, t = 100 °C, t = 1 h, neat or in 2 mL CPME.

To study the kinetic behaviour of the Ni-Biphephos catalyst, experiments were carried out in CPME with 170 equivalents of 2M3BN. A significant deviation from the linear, first-order relationship

between substrate conversion and time was observed (Figure 16). As the GC analysis of crude product mixtures showed the absence of any alternative by-products, the slowing rate was more likely caused by catalyst deactivation.

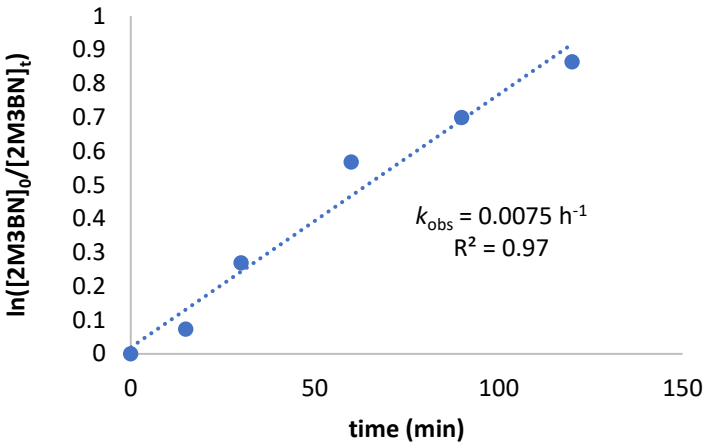

Figure 16: Reaction profile of the isomerisation reaction. Conditions: 0.018 mmol Ni, Ni:L:S =1:1:170, t = 100 °C, in 2 mL CPME.

Finally, the reversibility of the isomerisation was investigated *via* a control reaction using 3PN as substrate under the optimised conditions (Scheme 37). After 24 hours of stirring, GC analysis of the crude reaction mixture showed only traces of 2M3BN, indicating the absence of reverse isomerisation under the reaction conditions applied. This finding is important, as a significant presence of reverse isomerisation would decrease the accuracy of conversions calculated during the optimisation process.

Scheme 37: Isomerisation of 3PN with Biphephos-Ni complex. Conditions: 0.018 mmol Ni, Ni:L:S =1:1:170, 24 h, T = 100 °C, in 2 mL CPME.

Hydrocyanation of 3-pentenenitrile with Biphephos ligand

The last step of the *DuPont* process, the hydrocyanation of 3PN, was also investigated using $ZnCl_2$ as Lewis acid co-catalyst and reaction conditions optimised for other diphosphite ligands in the Vogt group.[51] To test the catalyst system's sensitivity towards an excess of HCN, the direct addition of different HCN sources was compared to the continuous addition *via* syringe pump (s. p.). Notably, the slow administration (entry 3-6) did not provide a significant advantage over the direct addition (entry 1-2), suggesting that the catalyst deactivation is not yet significant under these reaction conditions. As expected, the reactions performed without solvent led to significantly higher conversions than the reactions carried out in THF (entry 1, 3 and 5, Table 16). In all neat reactions, excellent conversions up

to 93% (TON up to 143) were achieved with selectivities towards the desired ADN product up to 80%. These results are comparable to some of the most active diphosphite complexes reported for the hydrocyanation of internal alkenes,[5] showing that the Biphephos ligand can be considered as a good ligand candidate for applications in this step of the *DuPont* process.

Table 16: Hydrocyanation of 3PN in different solvents.

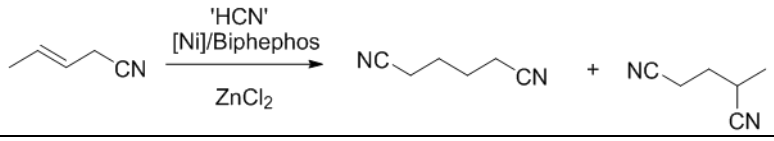

entry	solvent	HCN source and addition	conversion (%)	ADN selectivity (%)
1	neat	ACH direct	91	79
2	THF	ACH direct	60	81
3	neat	ACH s. p.	92	76
4	THF	ACH s. p.	50	78
5	neat	TMSCN s. p.	93	80
6	THF	TMSCN s. p.	55	76

Conditions: 0.018 mmol Ni, Ni:L:$ZnCl_2$:S:ACH =1:1:1:170:250, T =70 °C, t = 2 h, neat or 2 ml THF. Direct or continuous addition of ACH or TMSCN via syringe pump.

Summary and future work

To conclude, the application of three bidentate phosphorus ligand families (Figure 17) was investigated in Ni-catalysed hydrocyanation reactions. The catalytic studies were focused on the three-stage *DuPont* adiponitrile process (hydrocyanation of butadiene, isomerisation of 2M3BN and hydrocyanation of 3PN), which is of great industrial relevance in the production of nylon 66.

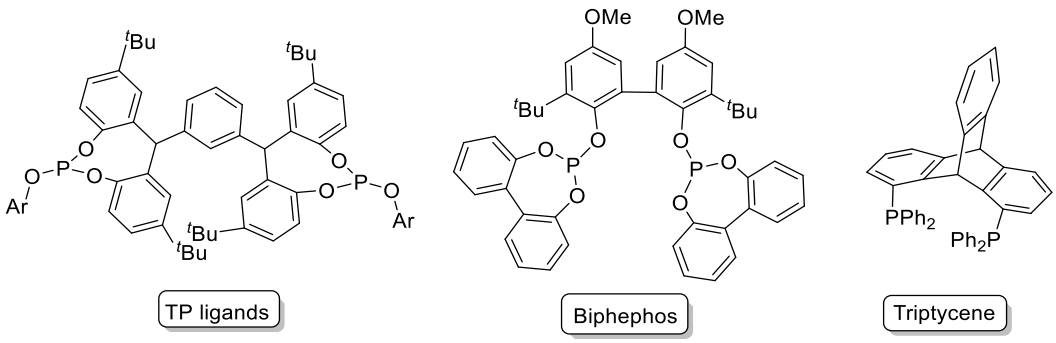

Figure 17: Structure of the investigated ligand families.

A tetraphenol-based diphosphite ligand, **TP2** (Figure 17, left), and the corresponding Ni complex, **TP2Ni**, were synthesised and characterised *via* ^{1}H NMR as well as X-ray crystallography. Contrary to

previous reports, the **TP2Ni** catalyst was shown to be capable of isomerising 2M3BN, albeit with a relatively low activity in comparison to other diphosphite systems. These observations were further confirmed *via* DFT calculations. GC-MS studies revealed that the presence of impurities in the commercial 2M3BN substrate likely contributed to previous negative results in the isomerisation reactions. Variable temperature ^{1}H NMR experiments were attempted to examine the coordination of different substrates (2M3BN, 3PN and allyl bromide) to complex **TP2Ni**, however, solubility issues and significant peak broadening were observed. To enable simpler mechanistic investigations, a novel tetraphenol backbone (**TPB**) and two novel TP ligands (**TP6** and **TP7**) featuring unsubstituted phenyl moieties were designed and synthesised. Potential avenues for future research include the purification of these ligands and their application in hydrocyanation or hydroformylation reactions.

The **Biphephos** ligand (Figure 17, middle) was also tested in hydrocyanation reactions as it featured promising stereoelectronic properties. Initial studies were carried out with styrene as the substrate to optimise the reaction protocols, including the addition method of the HCN source and the pre-formation of the Ni complex. Then focusing on the *DuPont* process, in combination with $Ni(cod)_2$, the system showed moderate activity and linear selectivity in the hydrocyanation of butadiene and 3PN. The **Biphephos** complex was particularly active in the isomerisation of 2M3BN, achieving conversions that are competitive with the best diphosphite systems reported in the literature. Consequently, a systematic optimisation of the reaction parameters was carried out, reaching high turnover rates after 1 h (TON up to 343) in CPME as solvent at 100 °C using 0.1 mol % catalyst loading. Due to safety regulations, only alternative HCN sources, such as ACH and TMSCN were used, however, to truly examine the industrial applicability of this ligand, further studies with pure HCN need to be carried out. Moreover, the design of a reaction setup that enables the continuous slow addition of HCN gas (to prevent catalyst deactivation due to the formation of $Ni(CN)_2$ species) on a laboratory scale remains a challenge.

A previously known **Triptycene**-based diphosphine ligand (Figure 17, right) was also synthesised with the aim of applying it as part of multi-ligand systems in the *DuPont* process. Due to the termination of this project, these catalytic studies have not been carried out. As the triptycene ligand was previously shown to provide high activity and linear selectivity in the hydrocyanation of butadiene, it would be worthwhile employing it simultaneously with another ligand (a diphosphite, for example **TP2**) that exerts a high activity and linear selectivity in the hydrocyanation of 3PN. This combined system - after appropriate optimisation of the reaction conditions - would have the potential to shorten the three-stage *DuPont* process to a one- or two-pot reaction.

Experimental

General considerations

Chemicals were purchased from *Sigma Aldrich, Merck, Acros, Romil* and *Alfa Aesar* and used as received if not mentioned otherwise. Acetonitrile, dichloromethane, THF, toluene and hexane were dried over Al_2O_3 columns in a solvent purification system. Reagents (PCl_3, Et_3N, 2M3BN, 3PN, styrene) and solvents (dioxane, DMSO, Me-THF, CPME) were dried, distilled under Ar, degassed and stored over molecular sieves prior to use. Air- and moisture-sensitive reactions were carried out in an MBraun glove box with Ar atmosphere or using standard Schlenk-techniques. NMR spectra were recorded on Bruker Avance III 500 MHz and Bruker Avance III 400 MHz spectrometers. ^{1}H spectra were measured at 500 MHz (chemical shifts were referenced to residual solvent peaks). ^{13}C spectra were measured at 126 MHz (referenced to TMS). ^{31}P spectra were measured at 202 MHz (referenced to 85% H_3PO_4), ^{19}F spectra were measured at 471 MHz (referenced to $CFCl_3$). In hydrocyanation and 2M3BN isomerisation reactions the sample composition was determined using a Shimadzu GC-2010 gas chromatograph with an Ultra-19091B-102 column (25.0 m, 0.20 mm ID) and flame ionisation detector (FID). Response factors were calculated *via* calibration for each substrate and product. Conversions were calculated against *n*-decane as internal standard. X-ray diffractograms were taken in Paratone oil on a Bruker SMART APEXII diffractometer. Using Olex2, the structure was solved with the ShelXT structure solution program, using the Direct Methods solution method. The model was refined with version of ShelXL using Least Squares minimisation.[78, 79]

Synthesis of 1,8-difluoroanthraquinone

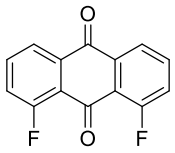

A mixture of vacuum dried 1,8-dichloroanthraquinone (8.0 g, 28.8 mmol) and anhydrous caesium fluoride (16.0 g, 105.2 mmol) in 30 mL thoroughly dried DMSO was stirred for 10 h at 135 °C under an argon atmosphere. After being cooled, the mixture was poured into ice water. The precipitate was filtered, washed with water (4 X 250 mL) and methanol (50 mL), and dried in vacuum. The crude material was purified by column chromatography on a tall basic alumina column with dichloromethane-hexane (1:1) as eluent, affording 1,8-difluoroanthraquinone as yellow crystals. Yield: 3.5 g (14.5 mmol, 50%). ^{1}H NMR (500 MHz, $CDCl_3$) δ 8.13 (dd, *J* = 7.7, 0.9 Hz, 2H), 7.79 – 7.73 (m, 2H), 7.50 (ddd, *J* = 10.8, 8.3, 1.2 Hz, 2H).

Synthesis of 1,8-difluoroanthracene

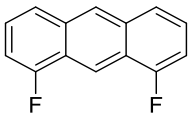

1,8-Difluoroanthraquinone (2.8 g, 11.3 mmol) was mixed with Zn dust (15.0 g, 226.0 mmol) and 60 mL of aqueous 28% NH_3 was added dropwise. The mixture was slowly heated to reflux and stirred for 3 h. After cooling, the aqueous solution was extracted with CH_2Cl_2, dried over $MgSO_4$ and concentrated. The residual crude yellow solid was dissolved in a mixture of 150 mL of ^{i}PrOH and 15 mL of aqueous 37% HCl. After the resulting solution had been heated to reflux for 3 h, it was concentrated and partitioned between CH_2Cl_2 and aqueous $NaHCO_3$. The organic layer was dried and concentrated. The crude product was recrystallised from CH_2Cl_2 to give the anthracene as pale-yellow needles. Yield: 1.1 g (5.0 mmol, 44%). ^{1}H NMR (500 MHz, $CDCl_3$) δ 8.94 (s, 1H), 8.45 (s, 1H), 7.78 (d, *J* = 8.6 Hz, 2H), 7.44 – 7.38 (m, 2H), 7.15 (dd, *J* = 10.8, 7.4 Hz, 2H). ^{13}C NMR (126 MHz, $CDCl_3$) δ 160.2, 158.2, 133.3, 126.2, 125.6, 124.1, 123.0, 113.4, 108.4.

Synthesis of 1,8-difuorotriptycene

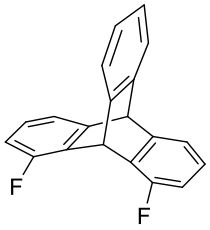

1,8-Difluoroanthracene (3.3 g 15.4 mmol) was suspended in dichloroethane (40 mL) and the mixture was heated to reflux. *N*-butyl nitrite (17.7 mmol, 2.1 mL) was added to the yellow solution, followed by anthranilic acid (17.7 mmol, 2.4 g) in 2-ethoxyethyl ether (15 mL). The latter was added dropwise over a period of 20-30 minutes. After 1 hour the solvent was removed from the dark red solution. A solution of maleic anhydride (7.7 mmol, 0.8 g) in *p*-xylene (15 mL) was added and the mixture was heated to reflux for 12 hours. The solution was cooled by an ice bath and the product was precipitated with a cold solution of KOH in methanol/H_2O (4 g in 33/17 mL). After filtration, the solid was washed with the same solution to give yellow crystals. Yield: 2.1 g (7.2 mmol, 47%). ^{19}F NMR (471 MHz, $CDCl_3$) δ -123.10 (ddd, *J* = 8.6, 5.2, 1.9 Hz). ^{1}H NMR (500 MHz, $CDCl_3$) δ 7.47 – 7.38 (m, 2H), 7.18 (d, *J* = 7.3 Hz, 2H), 7.05 – 7.02 (m, 2H), 6.96 (ddd, *J* = 8.3, 7.3, 5.2 Hz, 2H), 6.75 (td, *J* = 8.7, 0.9 Hz, 2H), 6.20 (s, 1H), 5.48 (t, *J* = 1.8 Hz, 1H). ^{13}C NMR (126 MHz, $CDCl_3$) δ 148.9, 126.9, 125.7, 124.4, 124.1, 119.6, 113.1, 53.9, 39.5.

Synthesis of 1,8-diphenylphosphinotriptycene

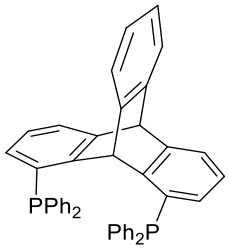

1,8-Difluorotriptycene (0.7 g 2.4 mmol) was dissolved in 10.0 mL of THF. $KPPh_2$ (5.0 mmol, 10.0 mL of 0.5 M solution in THF) was slowly added and the mixture was heated to reflux for 12 hours. The excess of potassium phosphide was quenched by adding brine (10 mL). The product was extracted with CH_2Cl_2, dried over $MgSO_4$, concentrated and washed with methanol to give the final product as a white powder. Yield: 0.8 g (1.2 mmol, 51%). ^{31}P NMR (162 MHz, $CDCl_3$) δ -14.96. ^{1}H NMR (500 MHz, $CDCl_3$) δ 7.37 – 7.25 (m, 22H), 6.92 (t, *J* = 7.5 Hz, 4H), 6.68 – 6.63 (m, 2H), 6.54 (d, *J* = 7.4 Hz, 2H), 5.95 (d, *J* = 7.3 Hz, 1H), 5.46 (s, 1H). ^{13}C NMR (126 MHz, $CDCl_3$) δ 145.7, 143.7, 137.2, 136.8, 136.7, 134.5, 134.6, 134.3, 133.1, 129.2, 128.7, 128.6, 128.4, 125.3, 124.8, 124.7, 124.6, 124.05, 122.9.

Synthesis of TP0 backbone

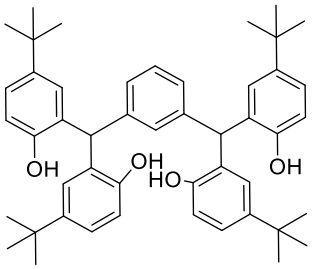

The backbone was synthesised following literature procedures.[56] A mixture of 4-tert-butylphenol (72.0 g, 480.0 mmol) and isophthalic dicarboxaldehyde (8.1 g, 60.0 mmol) was heated with stirring until a homogeneous melt had formed (110 °C). Concentrated HCl (10.0 mL, 37%) was added dropwise and the reaction was continued for a further 12 h at 110 °C. The excess phenol was removed by steam distillation and the residue was recrystallised from acetone and purified by flash column chromatography to yield the product as light yellow powder. Yield: 10.3 g (14.7 mmol, 24%). ^{1}H NMR (500 MHz, $CDCl_3$) δ 7.28 – 7.24 (m, 1H), 7.14 (s, 1H), 7.10 (dd, *J* = 8.4, 2.4 Hz, 4H), 7.07 (dd, *J* = 7.8, 1.4 Hz, 2H), 6.98 (d, *J* = 2.4 Hz, 4H), 6.71 (d, *J* = 8.4 Hz, 4H), 5.90 (s, 2H), 5.72 (s, 4H), 1.16 (s, 36H). ^{13}C NMR (126 MHz, $CDCl_3$) δ 151.2, 143.6, 142.3, 128.5, 127.4, 124.6, 115.8, 44.9, 34.2, 31.5.

Synthesis of TPB backbone

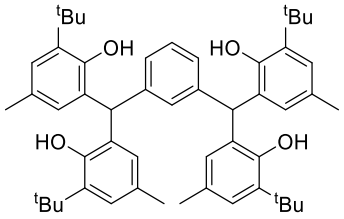

The backbone was synthesised following literature procedures.[57] A mixture of 2-tert-butyl-4-methylphenol (27.0 g, 171 mmol), isophthalaldehyde (5.0 g, 37 mmol) and *p*-toluenesulfonic acid (0.71 g, 3.8 mmol) was heated to 110 °C and stirred for 2 hours. After cooling to room temperature, acetonitrile (50 ml) was added to the dark solution and the formed suspension was filtered. The product was obtained as a cream white powder. Yield: 20.40 g (14.7 mmol, 73%). ^{1}H NMR (500 MHz, $CDCl_3$) δ 7.10 (ArH, s, 4H), 7.06–6.98 (ArH, m, 4H), 6.68 (ArH, s, 4H), 5.47(ArH, s, 2H), 4.90 (ArH, s, 4H), 2.05 (CH_3, s, 12H), 1.44 (^{t}BuH, s, 36H).

Synthesis of TP2 ligand

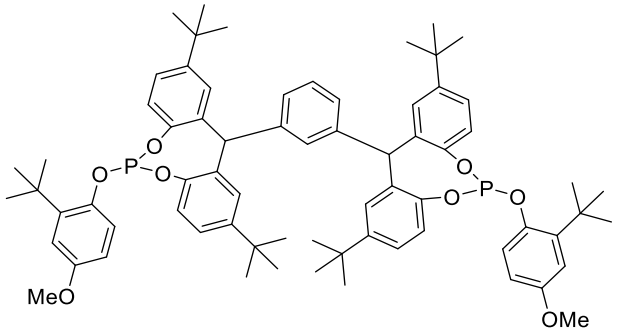

TP2 ligand was synthesised following literature procedures.[56] The tetraphenol backbone (TP0) (2.1 g, 3.0 mmol) and Et_3N (5.4 mL, 36.0 mmol) were added dropwise to a solution of PCl_3 (0.6 mL, 6.5 mmol) in 20 mL of THF at -10 °C, and the mixture was stirred for 40 minutes. 2-*Tert*-butyl-4-methoxyphenol (1.1 g, 6.1 mmol), dissolved in 10 mL of THF was added dropwise at -10 °C. The mixture was stirred for 1 h at room temperature. Salts were filtered off over a short (5 cm) pad of basic alumina and volatiles were removed *in vacuo*. The residue was recrystallised from acetone to yield the desired product as a white powder. Yield: 0.30 g (0.3 mmol, 9%). ^{31}P NMR (202 MHz, C_6D_6) δ 122.6 (s). ^{1}H NMR (500 MHz, C_6D_6) δ 7.45 (d, *J* = 8.8 Hz, 2H), 7.38 (d, *J* = 2.3 Hz, 4H), 7.12 – 6.99 (m, 14H), 6.51 (dd, *J* = 8.7, 3.1 Hz, 2H), 5.78 (s, 2H), 3.36 (s, 6H), 1.41 (s, 18H), 1.15 (s, 36H). ^{13}C NMR (126 MHz, $CDCl_3$) δ 155.6, 147.8, 146.8, 145.4, 143.2, 142.1, 134.6, 128.6, 128.1, 127.3, 126.5, 125.9, 125.2, 123.1, 120.5, 114.6, 110.2, 55.7, 45.6, 35.0, 34.5, 31.6, 30.1.

Synthesis of TP6 ligand

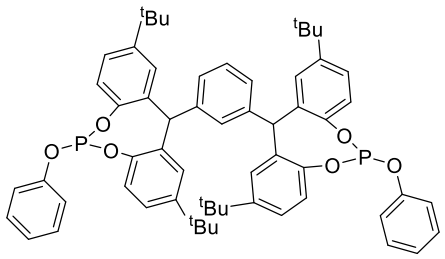

Tetraphenol backbone (TP0) (2.1 g, 3.0 mmol) and Et_3N (5.4 mL, 36.0 mmol) were added dropwise to a solution of PCl_3 (0.6 mL, 6.5 mmol) in 20 mL of THF at -10 °C, and the mixture was stirred for 40 minutes. A solution of phenol (0.61 g, 6.1 mmol) in 10 mL of THF was added dropwise at -10 °C. The mixture was stirred for 1 h at room temperature. Salts were filtered off over a short (5 cm) pad of basic alumina and all the volatiles were removed *in vacuo.* Crude yield (calculated from ^{31}P NMR integration): 0.85 g (0.9 mmol, 30%). ^{31}P NMR (202 MHz, C_6D_6) δ 121.3 (s).

Synthesis of TP7 ligand

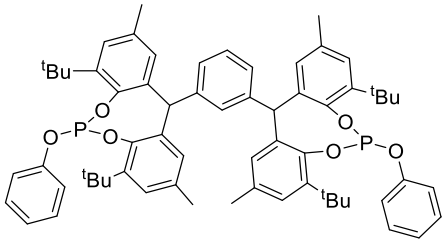

Tetraphenol backbone (TPB) (2.6 g, 3.0 mmol) and Et_3N (5.4 mL, 36.0 mmol) were added dropwise to a solution of PCl_3 (0.6 mL, 6.5 mmol) in 20 mL of THF at -10 °C, and the mixture was stirred for 40 minutes. A solution of phenol (0.61 g, 6.1 mmol) in 10 mL of THF was added dropwise at -10 °C. The mixture was stirred for 1 h at room temperature. Salts were filtered off over a short (5 cm) pad of basic alumina and all the volatiles were removed *in vacuo.* Crude yield (calculated from ^{31}P NMR integration): 1.02 g (1.0 mmol, 34%). ^{31}P NMR (202 MHz, C_6D_6) δ 127.8(s).

Synthesis of TP2Ni complex

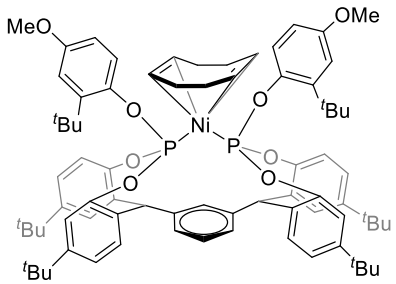

A solution of TP2 (23.0 mg, 0.018 mmol) in 1.0 mL of benzene-d_6 was added to $Ni(cod)_2$ (5.0 mg, 0.018 mmol) in a Schlenk-tube and stirred for 10 minutes. ^{31}P NMR (202 MHz, toluene-d_8) δ 125.3 (s). Due to peak broadening the ^{1}H NMR spectrum could not be unambiguously assigned.

Synthesis of BIPPP ligand

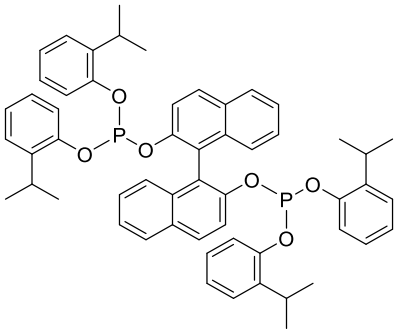

BIPPP ligand was synthesised following literature procedures.[65] 2-Isopropylphenol (1.9 g, 14.0 mmol) and Et_3N (6 mL, 43.00 mmol) were added dropwise at -10 °C to a solution of PCl_3 (0.95 g, 6.99 mmol) in 100 mL of toluene and the mixture was stirred for 30 min. Binaphthol (1.00 g, 3.50 mmol) dissolved in 10 mL of THF was added dropwise to the mixture at -10˚C. The mixture was stirred for 1 h at room temperature. Salts were filtered off over a short pad of basic alumina and all volatiles were removed *in vacuo*. The product was recrystallised from hexane. Yield: 2.04 g (2.3 mmol, 66%). ^{31}P NMR (202 MHz, C_6D_6) δ 131.5 (s).

General procedure for hydrocyanation experiments

The appropriate ligand (0.018 mmol) and $Ni(cod)_2$ (0.018 mmol) were dissolved in 1.0 mL of THF and stirred for 30 min in a 15 mL Schlenk tube. Volatiles were removed *in vacuo*. Substrate (1,3-butadiene, 3-pentenenitrile or styrene, 170-2000 equiv.) was added by an Eppendorf pipette, followed by 50 µL of *n*-decane as internal standard. Acetone cyanohydrin (400 µL, 250 equiv.) or trimethylsilyl cyanide (500 µL, 250 equiv.) was added *via* Eppendorf pipette or slow addition with a syringe pump (0.3 mL/h) and the mixture was warmed to the appropriate reaction temperature in an oil bath and stirred for the appropriate reaction time. The mixture was cooled to 0 °C and flushed with a gentle stream of argon for one minute to remove traces of HCN. Samples were filtered through a short silica column and analysed by GC and GC-MS, using the *n*-decane as internal standard.

General procedure for 2M3BN isomerisation experiments

Ligand (0.018 mmol) and $Ni(cod)_2$ (0.018 mmol) were dissolved and stirred for 30 min in 1.0 mL of THF in a 15 mL Schlenk tube. Then volatiles were removed *in vacuo*. 2-Methyl-3-butyronitrile (170- 2000 equiv.) was added by an Eppendorf pipette, followed by 50 µL of *n*-decane as internal standard and

solvent. The mixture was warmed to the appropriate reaction temperature in an oil bath and stirred for the appropriate reaction time. The reaction product was cooled to room temperature. Samples were filtered through a short silica column and analysed by GC and GC-MS, using *n*-decane as internal standard.

References

1. K. Huthmacher and S. Krill, *Applied Homogeneous Catalysis with Organometallic Compounds 2nd ed.*, Wiley, Weinheim, Germany, **2002**, 465-486.
2. T. V. Rajanbabu, in *Organic Reactions*, Wiley Hoboken, United States, **2011**, 1-74.
3. P. Pollak, G. Romeder, F. Hagedorn and H. Gelbke, *Ullman's encyclopedia of industrial chemistry*, Wiley, Weinheim, Germany, **1985**, 363-376.
4. W. Keim, *Angew. Chem.*, **1990**, *102*, 251-260.
5. L. Bini, C. Müller and D. Vogt, *ChemCatChem*, **2010**, *2*, 590-608.
6. M. Beller, J. Seayad, A. Tillack and H. Jiao, *Angew. Chem. Int. Ed.*, **2004**, *43*, 3368-3398.
7. P. W. N. M. van Leeuwen, *Homogeneous Catalysis: Understanding the Art*, Kluwer, Dordrecht, The Netherlands, **2004**, 229-233.
8. *Adiponitrile Market: Global Industry Analysis and Forecast to 2015 to 2021*, **2018**.
9. D. E. Danly, *J. Electrochem. Soc.*, **1984**, *131*, 435-442.
10. C. A. Tolman, *Chem. Soc. Rev.*, **1972**, *1*, 337-353.
11. C. A. Tolman, *J. Am. Chem. Soc.*, **1970**, *92*, 2953-2956.
12. C. A. Tolman, *Chem. Rev.*, **1977**, *77*, 313-348.
13. A. Behr and P. Neubert, in *Applied Homogeneous Catalysis*, Wiley VCH, Weinheim, Germany, **2012**, 82-91.
14. N. Fey, A. G. Orpen and J. N. Harvey, *Coord. Chem. Rev.*, **2009**, *253*, 704-722.
15. C. P. Casey and G. T. Whiteker, *Isr. J. Chem.*, **1990**, *30*, 299-304.
16. W. C. Drinkard and R. W. J. Lindsey, *DuPont Patent,* US3496215, **1970**.
17. W. P. Giering, A. Prock, K. Eriks, M. N. Rahaman and H.-Y. Liu, *Organometallics*, **1989**, *8*, 1-7.
18. L. W. Gosser and C. A. Tolman, *Inorg. Chem.*, **1970**, *9*, 2350-2353.
19. W. C. Seidel and C. A. Tolman, *Inorg. Chem.*, **1970**, *9*, 2354-2357.
20. C. A. Tolman, *J. Am. Chem. Soc.*, **1970**, *92*, 4217-4222.
21. R. J. McKinney and D. C. Roe, *J. Am. Chem. Soc.*, **1986**, *108*, 5167-5173.

22. W. Goertz, W. Keim, D. Vogt, U. Englert, M. Boele, L. van der Veen, P. Kamer and P. W. N. M. van Leeuwen, *Dalton Trans.*, **1998**, 2981-2988.
23. C. A. Tolman, R. J. McKinney, W. C. Seidel, J. D. Druliner and W. R. Stevens, *Homogeneous nickel-catalyzed olefin hydrocyanation*, Elsevier, US, **1985**, 11-46.
24. L. Bini, E. A. Pidko, C. Müller, R. A. van Santen and D. Vogt, *Chem. – Eur. J.*, **2009**, *15*, 8768-8778.
25. C. A. Tolman, *J. Am. Chem. Edu.*, **1986**, *63*, 199.
26. C. A. Tolman, W. C. Seidel, J. D. Druliner and P. J. Domaille, *Organometallics*, **1984**, *3*, 33-38.
27. B. W. Taylor and H. E. Swift, *J. Catal.*, **1972**, *26*, 254-260.
28. M.-N. Birkholz, Z. Freixa and P. W. N. M. van Leeuwen, *Chem. Soc. Rev.*, **2009**, *38*, 1099-1118.
29. M. Kranenburg, P. C. J. Kamer, P. W. N. M. van Leeuwen, D. Vogt and W. Keim, *Chem. Comm.*, **1995**, 2177-2178.
30. W. Keim, A. Behr, H. O. Lühr and J. Weisser, *J. Catal.*, **1982**, *78*, 209-216.
31. T. Foo, J. M. Garner and W. Tam, *DuPont Patent,* WO9906357, **1999**.
32. M. Bartsch, R. Baumann, D. P. Kunsmann-Keitel, G. Harderlein, T. Jungkamp, M. Altmayer, W. Siegel and F. Molnar, *BASF Patent,* WO03033142 **2003**.
33. C. P. Lenges, *DuPont Patent,* WO03076394, **2003**.
34. M. J. Baker, K. N. Harrison, A. G. Orpen, P. G. Pringle and G. Shaw, *Chem. Comm.*, **1991**, 803-804.
35. J. D. Druliner, *Organometallics*, **1984**, *3*, 205-208.
36. A. Chaumonnot, F. Lamy, S. Sabo-Etienne, B. Donnadieu, B. Chaudret, J.-C. Barthelat and J.-C. Galland, *Organometallics*, **2004**, *23*, 3363-3365.
37. J. J. Garcia and W. D. Jones, *Organometallics*, **2000**, *19*, 5544-5545.
38. B. D. Swartz, N. M. Reinartz, W. W. Brennessel, J. J. García and W. D. Jones, *J. Am. Chem. Soc.*, **2008**, *130*, 8548-8554.
39. J. Wilting, C. Müller, A. C. Hewat, D. D. Ellis, D. M. Tooke, A. L. Spek and D. Vogt, *Organometallics*, **2005**, *24*, 13-15.
40. I. S. Mikhel, M. Garland, J. Hopewell, S. Mastroianni, C. L. McMullin, A. G. Orpen and P. G. Pringle, *Organometallics*, **2011**, *30*, 974-985.
41. S. Mastroianni, I. Mikhel and P. Pringle, *Rhodia Patent,* WO2010102962, **2010**.
42. N. Fey, M. Garland, J. P. Hopewell, C. L. McMullin, S. Mastroianni, A. G. Orpen and P. G. Pringle, *Angew. Chem. Int. Ed.*, **2012**, *51*, 118-122.

43. C. Ni and J. J. Ostermaier, *Invista Patent,* CN106975519, **2017**.
44. W. J. I. Tenn, *Invista Patent,* WO2013181096, **2013**.
45. R.-H. Fischer, R. Baumann, V. Wloka and H. Luyken, *BASF Patent,* WO2016041930, **2014**.
46. D. Jian-Jun, H. Yao-Bing, F. Chi, G. Qing-Xiang and F. Yao, *ChemSusChem*, **2012**, *5*, 617-620.
47. X. Fang, P. Yu and B. Morandi, *Science*, **2016**, *351*, 832-836.
48. B. Morandi, X. Fang and Y. Peng, *K. MBH Patent,* WO2017093149 **2017**.
49. S. K. Kristensen, E. Z. Eikeland, E. Taarning, A. T. Lindhardt and T. Skrydstrup, *Chem. Sci.*, **2017**, *8*, 8094-8105.
50. L. Bini, C. Müller, J. Wilting, L. von Chrzanowski, A. L. Spek and D. Vogt, *J. Am. Chem. Soc.*, **2007**, *129*, 12622-12623.
51. A. Christiansen, R. Franke, D. Fridag , D. Hess, B. Kreidler, D. Vogt, L. Bini, M. Janssen and B. Hamers, *Evonik Patent,* WO2011023756, **2011**.
52. C. R. Landis and J. Uddin, *Dalton Trans.*, **2002**, 729-742.
53. W. Ahlers, R. Paciello, D. Vogt and P. Hofmann, *BASF Patent,* WO02083695, **2002**.
54. L. Bini, E. J. E. Houben, E. A. Pidko, C. Müller and D. Vogt, *Catal. Today*, **2010**, *155*, 271-278.
55. M. E. Tauchert, D. C. M. Warth, S. M. Braun, I. Gruber, A. Ziesak, F. Rominger and P. Hofmann, *Organometallics*, **2011**, *30*, 2790-2809.
56. M. Janssen, L. Bini, B. Hamers, C. Müller, D. Hess, A. Christiansen, R. Franke and D. Vogt, *Tetrahedron Lett.*, **2010**, *51*, 1971-1975.
57. J. A. L. Wells, M. L. Seymour, M. Suvova and P. L. Arnold, *Dalton Trans.*, **2016**, *45*, 16026-16032.
58. P. W. N. M. v. Leeuwen, P. C. J. Kamer, C. Claver, O. Pàmies and M. Diéguez, *Chem. Rev.*, **2011**, *111*, 2077-2118.
59. N. Benetis, J. Kowalewski, L. Nordenskiöld and U. Edlund, *J. Magnet. Res.*, **1984**, *58*, 282-293.
60. A. J. Bridgeman, *Dalton Trans.*, **2008**, 1989-1992.
61. M. E. Tauchert, T. R. Kaiser, A. P. V. Göthlich, F. Rominger, D. C. M. Warth and P. Hofmann, *ChemCatChem*, **2010**, *2*, 674-682.
62. A. P. V. Göthlich, M. Tensfeldt, H. Rothfuss, M. E. Tauchert, D. Haap, F. Rominger and P. Hofmann, *Organometallics*, **2008**, *27*, 2189-2200.
63. L. Bini, PhD thesis, Eindhoven University of Technology, **2009**.
64. C. A. Tolman, *J. Am. Chem. Soc.*, **1974**, *96*, 2780-2789.
65. J. Wilting, M. Janssen, C. Müller, M. Lutz, A. L. Spek and t. D. Vog, *Adv. Synth. Catal.*, **2007**, *349*, 350-356.

66. T. Jungkamp, R. Baumann, M. Bartsch, G. Haderlein, H. Luyken and J. Scheidel, *BASF Patent,* WO2005073179, **2005**.
67. C. P. Casey, N. W. Vollendorf and K. J. Haller, *J. Am. Chem. Soc.*, **1984**, *106*, 3754-3764.
68. D. V. Gribkov, K. C. Hultzsch and F. Hampel, *Chem. – Eur. J.*, **2003**, *9*, 4796-4810.
69. E. Billig, A. G. Aabatjoglou and D. R. Bryant, *U. Carbide Patent,* US4668651, **1987**.
70. R. Franke, D. Selent and A. Börner, *Chem. Rev.*, **2012**, *112*, 5675-5732.
71. J. R. Johnson, G. D. Cuny and S. L. Buchwald, *Angew. Chem. Int. Ed.*, **1995**, *34*, 1760-1761.
72. B. Moasser, C. Gross and W. L. Gladfelter, *J. Organomet. Chem.*, **1994**, *471*, 201-209.
73. T. Foo, J. M. Garner, R. Shapiro and W. Tam, *DuPont Patent,* WO9622968, **1996**.
74. W. Tam, K. A. Kreutzer and R. J. Mckinney, *DuPont Patent,* WO9514659, **1995**.
75. J. D. Druliner, *DuPont Patent,* WO9616022, **1996**.
76. C. J. Clarke, W.-C. Tu, O. Levers, A. Bröhl and J. P. Hallett, *Chemical Reviews*, **2018**, *118*, 747-800.
77. J. D. Druliner and N. Herron, *DuPont Patent,* WO9736856, **1997**.
78. G. Sheldrick, *Acta Crystallogr. C*, **2015**, *71*, 3-8.
79. O. V. Dolomanov, L. J. Bourhis, R. J. Gildea, J. A. K. Howard and H. Puschmann, *J. Appl. Crystallogr.*, **2009**, *42*, 339-341.

Chapter 3

Iron half salen complexes: synthesis, characterisation and application in CO_2/epoxide coupling

Introduction

Half salen ligands and complexes

Schiff base ligands are attractive due to their versatility and simple, inexpensive synthesis through the condensation of aldehydes and primary amines.[1] Most prominently, the tetradentate (bis-Schiff base) salen-type ligands have become ubiquitous in homogeneous catalysis as they are suitable for stabilising almost all metal ions in various oxidation states (Figure 1).[2] Some salen complexes also show stability towards air, moisture and high temperatures. While typically featuring a four coordinate scaffold in the plane of the metal centre, these complexes can also accommodate one or two additional ancillary ligands/substrates/reactants in the axial positions.[1] The facile steric and electronic modulation of the ligand (by varying the substituents on the phenol rings or on the diimine-bridge) enables fine-tuning of the complexes' catalytic activity and solubility. Consequently, active and selective salen-type catalysts have been employed in a wide range of homogeneous reactions including alkylations, oxidations and polymerisations.[3-5] Salen ligands containing chiral moieties achieved remarkable success in asymmetric homogeneous catalysis.[6]

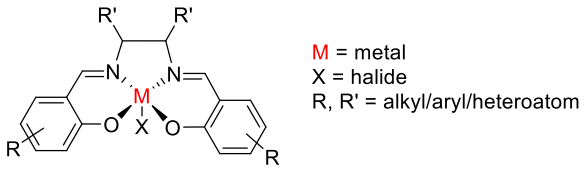

Figure 1: General structure of salen complexes.

The 'half salen' analogues (bidentate phenoxyimines) have also been studied since the 1930s, yet they have received significantly less attention.[7, 8] This may be due to their more complicated coordination chemistry, as multiple bidentate ligands are required to achieve the double chelating effect that a single tetradentate salen ligand can provide. Typically, the half salen ligands support a single metal centre with an $(N,O)_2$ tetracoordinate framework (Figure 2).

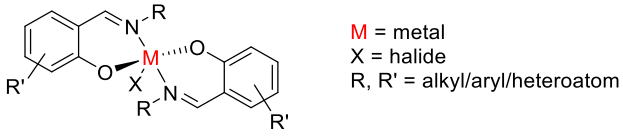

Figure 2: General structure of half salen complexes.

Although half salen complexes have predominantly been investigated as catalysts for homogeneous polymerisation reactions (*vide infra*, Chapter 4), they have also been applied for small molecule transformations. Half salen catalysts featuring a range of metals have been developed, with

the complexes most commonly featuring a bis(bidentate) (L_2M) coordination mode. In one of the earliest examples, Noyori and co-workers used N-α-phenylethyl substituted half salen Cu complexes (Figure 3, left) in the synthesis of optically active carboxylate derivatives achieving high enantioselectivities.[9] Similarly, Zhu *et al.* developed Mg complexes with bulky, ^{t}Bu substituted half salen ligands (Figure 3, middle) for the catalytic hydrosilylation of ketones, resulting excellent conversions.[10] Moreover, chiral Al half salen complexes were efficient in the silylcyanation of aldehydes,[11] while Mn based bis-chelated derivatives showed high activity in phosphate hydrolysis.[12] Compared to the standard salen scaffold, half salen ligands offer the advantage of being more applicable in mixed ligand systems. Piers *et al.* investigated the insertion of acrylonitrile into the Pd-Me bond of complexes that were supported by a single half salen and an additional phosphine ligand (Figure 3, right).[8] Similar complexes from Ojwach *et al.* showed excellent activity in the hydrogenation of alkenes.[13]

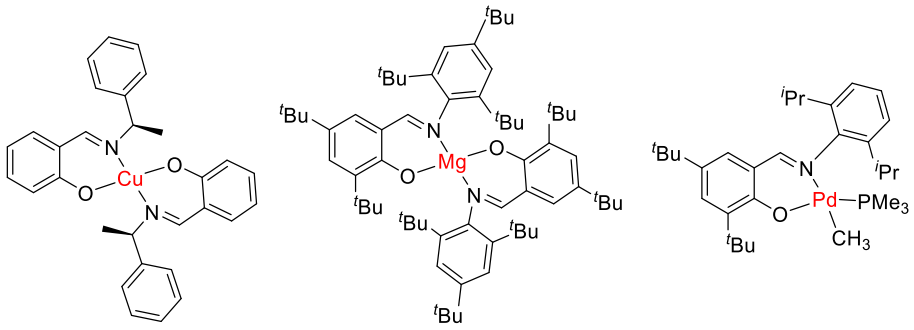

Figure 3: Examples of half salen complexes used in small molecule activation. Cu complex by Noyori et al.,[9] Mg complex by Zhu et al.[10] and mixed ligand Pd complex by Piers et al.[14]

As discussed in Chapter 1, iron catalysts are currently in high demand due to the abundance, low cost and versatility of this non-toxic metal. The most common oxidation states of iron (Fe^{II} and Fe^{III}) are suitable to catalyse a broad scope of homogeneous reactions. Fe^{III} compounds are especially attractive, due to their air- and moisture-stability that enables user friendly synthesis and handling. While complexes with tetradentate salen-type ligands have been well researched,[15] studies investigating bidentate half salen Fe complexes are relatively scarce.[16, 17,18]

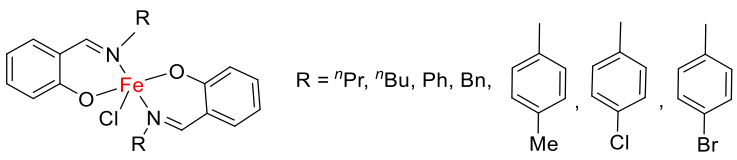

Figure 4: First Fe^{III} half salen complexes by Murray et al.[17, 19]

In the late 1960s, Murray *et al.* described the synthesis of the first $L_2Fe^{III}X$-type half salen complexes including a thorough characterisation *via* IR spectroscopy and mass spectrometry (Figure 4).[17, 19] Since then, a series of related Fe^{II} and Fe^{III} complexes have been reported, including the most recent

examples with extremely bulky [C_6H_2-2,6-($CHPh_2$)$_2$-4-OMe] groups on the ligand (Figure 5, left).[20, 21] Despite their simple synthesis and versatility, the catalytic activity of these complexes has not yet been thoroughly explored. Oxazoline substituted Fe half salen complexes were used as catalysts in sulphide oxidation,[22] while related complexes with azobenzene groups on the imine (Figure 5, right) were shown to undergo photocatalysed isomerisation reactions in UV light.[23] Oruari *et al*. reported half salen ligands as sensors to selectively detect metals including Fe^{II} and Fe^{III} ions *via* visible colour change upon complexation,[24] while the groups of Repo[18] and Saleh[25] have developed a series of half salen Fe^{III} halide catalysts for CO_2/epoxide coupling reactions (*vide infra*).[18, 25]

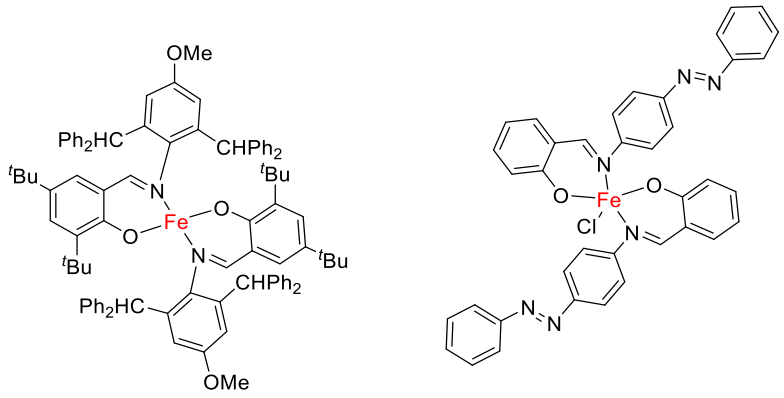

Figure 5: Bulky Fe^{II} complex and azobenzene substituted Fe^{III} complex.[20, 21, 23]

Synthesis of cyclic carbonates *via* CO_2/epoxide coupling

Catalytic transformations of carbon dioxide (CO_2) are an important strategy to valorise this waste gas and potentially reduce the environmental impact of its accumulation in the atmosphere.[26] Thus, using this non-toxic, non-flammable, inexpensive and renewable C1 building block as a feedstock has received considerable interest within both academia and industry.[27] As well as reductive processes transforming the thermodynamically stable CO_2 to methanol, formic acid or methane, coupling reactions of CO_2 with more complex, highly reactive compounds have also been intensively studied over the past 40 years.[28]

The addition of CO_2 to epoxides (also known as oxiranes) is a practical and atom efficient method to produce value-added polycarbonates and/or cyclic organic carbonates (Scheme 1).[29] While the formation of cyclic carbonates (1,3-dioxolan-2-ones) is thermodynamically favoured, the selectivity of the reaction is also determined by various parameters including the choice of catalyst, co-catalyst, epoxide, solvent and temperature.[30]

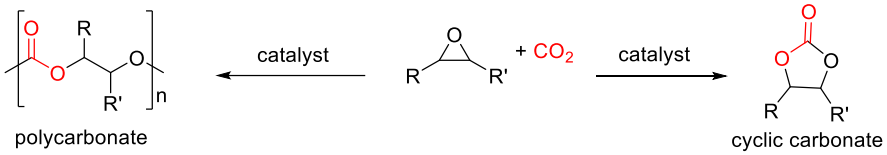

Scheme 1: Possible products of CO_2/epoxide coupling reactions.

The non-toxic cyclic carbonates (Figure 6) have various applications including use as high-boiling solvents, lubricants, electrolytes for batteries, intermediates in the synthesis of fine chemicals and as precursors in polymer synthesis.[30-35] Ethylene and propylene carbonates have been commercially synthesised since the 1950s.[36] Recently, the utilisation of cyclic carbonates as co-monomers (alongside diamines or polyamines) in polyurethane production is gaining momentum, significantly reducing the toxicity and moisture sensitivity issues attributed to the traditional isocyanate route.[37] Due to its sustainability and atom efficiency, CO_2/epoxide coupling has become the predominant approach for the synthesis of cyclic carbonates, replacing conventional methods such as the addition of the extremely toxic phosgene to diols.[31]

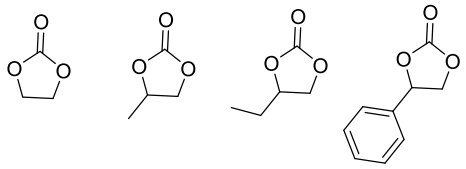

Figure 6: Most frequently produced cyclic carbonates.[31]

As CO_2 is a remarkably inert and kinetically stabile compound, catalysts are required to overcome the significant activation energy barrier of its conversion.[30, 38, 39] Homogeneous metal catalysts are most widely employed, as they exert the highest activity in the synthesis of cyclic carbonates.[30] Nevertheless, heterogeneous counterparts can also offer some technical advantages such as stability and reusability.[40] In addition (and outside the scope of this summary), metal halides, organocatalysts and ionic liquids are also frequently studied as catalyst systems for CO_2/epoxide coupling.[31]

The first reports on cyclic carbonate synthesis from the 1940s described the reaction of ethylene oxide with CO_2 in the presence of activated charcoal and NaOH under harsh conditions (high pressure, 200°C).[41] The addition of nucleophilic salts as catalysts was introduced in the following decade: a patent by Lichtenwalter *et al.* describes the screening of a wide range of ammonium chloride and bromide salts.[42] Quaternary ammonium and phosphonium halides have since been widely studied as catalysts for CO_2/epoxide coupling reactions,[31] along with recyclable, polymer supported onium salts that were developed in the 1990s.[43] Some of the most commonly applied examples are shown in Figure 7, including tetrabutylammonium halides (TBAX), phosphonium halides and bis(triphenylphosphine) iminium chloride (PPNCl).

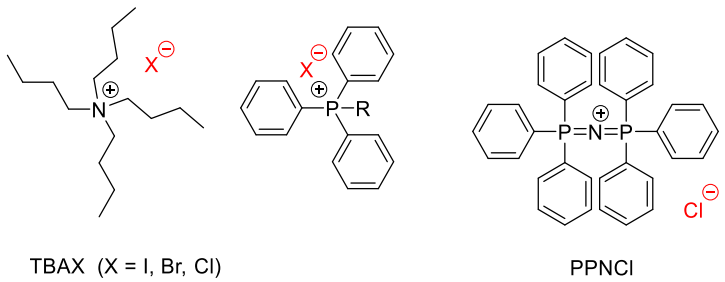

Figure 7: Commonly used (co-)catalysts in cyclic carbonate synthesis.

A reaction mechanism for the TBAX-catalysed coupling of CO_2 with an epoxide was proposed in 2002 by Caló *et al.* [44] In the first step, the halide nucleophilically attacks and ring-opens the epoxide. The obtained alkoxide anion subsequently attacks the CO_2 carbon and finally the cyclic carbonate is formed *via* intramolecular ring closure (Scheme 2).

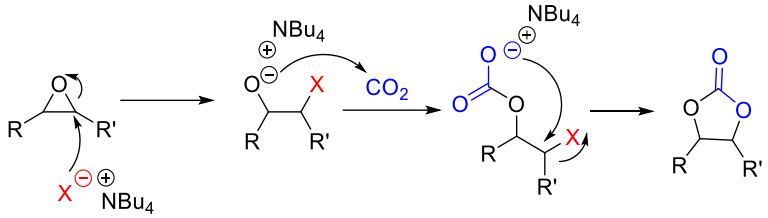

Scheme 2: Proposed mechanism of cyclic carbonate formation catalysed by ammonium halides.[44]

When nucleophilic salts are employed alone as catalysts - which is still a predominant industrial approach - large catalyst loadings (nearly stoichiometric amounts) are typically required to achieve high conversions, and the turnover frequencies (TOF) usually do not exceed 1000 h^{-1}.[45, 46] In academia, recent developments have typically exploited the onium salts as co-catalysts in binary/bifunctional systems in combination with a Lewis acidic metal that can significantly increase the turnover rates. The catalyst/co-catalyst ratio in these binary systems was shown to have a dramatic influence on both the activity and selectivity towards cyclic carbonate versus polycarbonate formation.[31]

Inoue *et al.* reported on the first metal catalysed system to synthesise cyclic propylene carbonate in 1978, using porphyrin-based Al methoxide complexes at room temperature (Figure 8, left).[28] In the following decades, analogous Mg, Co, Cr and Sn porphyrin complexes were developed which, in combination with nucleophilic co-catalysts, achieved high conversions in the coupling of CO_2 and terminal epoxides.[31] Ema and co-workers incorporated the co-catalyst into the porphyrin backbone (Figure 8, right): by varying the number of integrated onium groups, extremely high activities (TOFs up to 46 000 h^{-1}) were realised.[47] More recently, the same group also described tuning capabilities *via* the introduction of electronically diverse ligand substituents near the metal centre of bifunctional Zn-porphyrin complexes.[48] It was shown that electron donating groups decreased the activity, whereas electron withdrawing groups gave a significant activity increase. These findings correspond with previous reports describing a direct correlation between the catalytic activity and the Lewis acidity of the metal centre.[49]

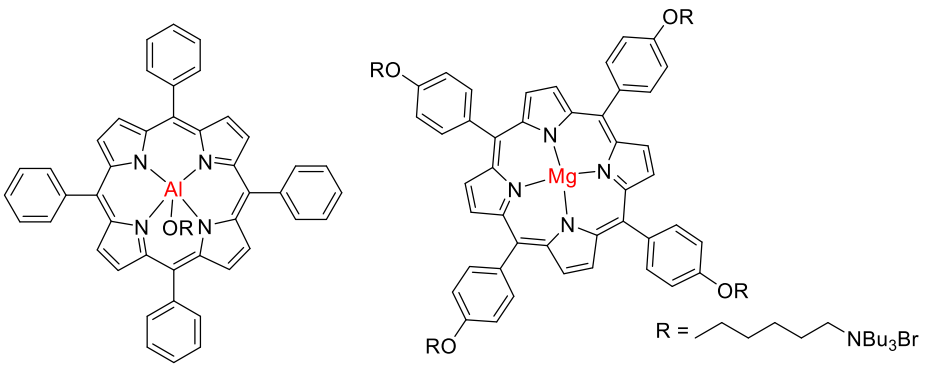

Figure 8: Al-porphyrin complex catalyst by Inoue et al. [28] and Mg analogue with incorporated co-catalyst on the ligand by Ema et al.[47]

The proposed mechanism for bi-component catalysts in the coupling of CO_2 and an epoxide is depicted in Scheme 3. Upon coordination to the Lewis acidic metal centre, the epoxide C-O bonds become increasingly polarised, which facilitates the nucleophilic attack and subsequent ring opening. Studies by Kleij and co-workers have shown that while the attack on a methylene carbon (of a terminal epoxide) is predominantly controlled by steric factors (i.e. the bulk of the substrate R substituent), the attack on a methine carbon is more influenced by electronic factors. The next step is the insertion of CO_2 into the metal-alkoxide bond. The obtained metal carbonate can either serve as an initiator to ring open further epoxide units (followed by CO_2 insertion) to form a polymer chain, or 'backbite' to form a cyclic carbonate through intramolecular ring closure. As a side-reaction, the homopolymerisation of the epoxide can also occur.

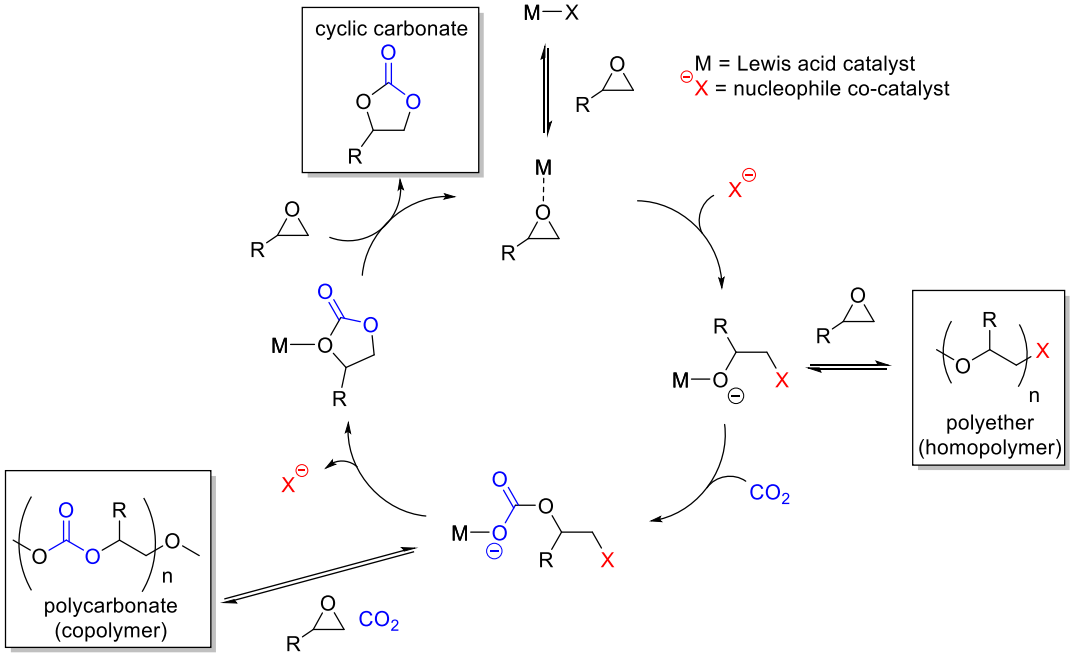

Scheme 3: Proposed catalytic cycle of CO_2/epoxide coupling towards cyclic carbonates with possible polymerisation side reactions.

Darensbourg *et al.* have shown that cyclic carbonates can also form *via* the catalytic depolymerisation of polycarbonates.[50] The rate determining step of the catalytic cycle largely depends on the reaction conditions, but most commonly the insertion of CO_2 is the slowest step.[31] Retention of the configuration after the cycloaddition of CO_2 to enantiopure styrene oxide suggested that the reaction proceeds *via* double inversion (2x S_N2) mechanism.[51] An alternative S_N1 pathway has also been proposed, based on examples where a small amount of racemisation was observed in the synthesis of chiral cyclic carbonates, especially at elevated reaction temperatures (Scheme 4).[52, 53]

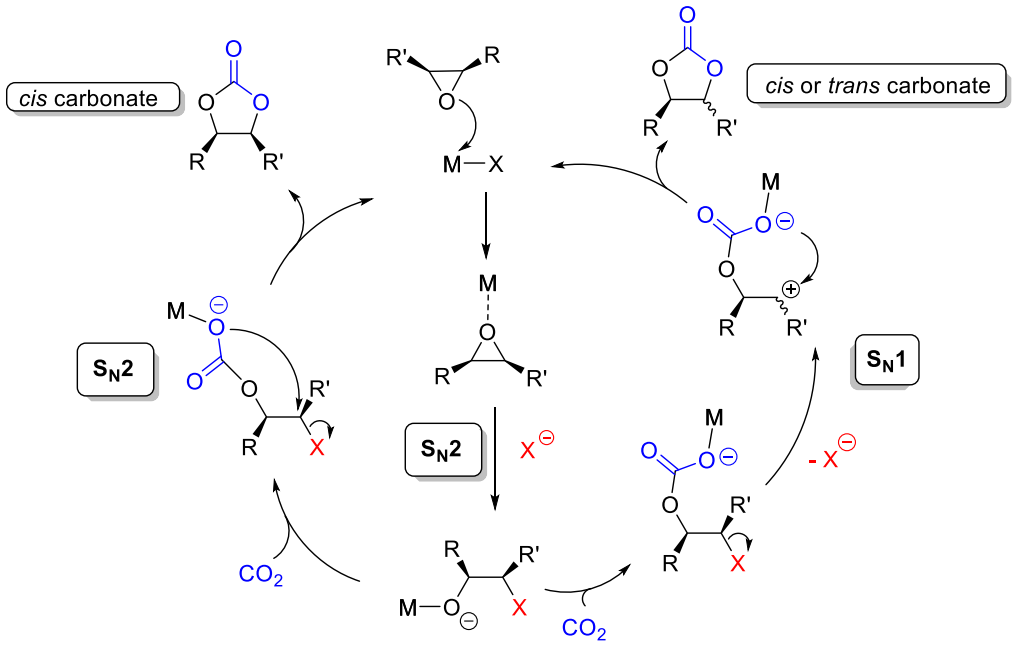

Scheme 4: Proposed mechanisms of S_N2 and S_N1 pathways in cyclic carbonate formation.[53]

Complexes of the 'privileged' salen-type ligands have been widely employed as catalysts in CO_2/epoxide coupling reactions. Binary catalyst systems containing a nucleophilic salt and a Lewis acidic Cr, Co, Zn or Al salen/salphen complex were shown to be highly active in this process.[54] In combination with a TBABr co-catalyst, Cr salphen complexes synthesised by North *et al*. (Figure 9, left) gave excellent conversion of terminal epoxides at ambient temperature and only 1 bar of CO_2 pressure.[55] Inspired by the developments with porphyrin-based systems, Cr salen complexes with a nucleophilic co-catalyst embedded into the ligand were also developed, providing excellent turnover rates (TOF up to 2000 h^{-1}) in the synthesis of propylene carbonate.[56] Kleij and co-workers successfully used Zn salphen complexes (Figure 9, right) with TBAI as a nucleophile source in the coupling of CO_2 and propylene oxide, however, relatively high catalyst loadings (2.5 mol %) were required to achieve high conversions. Moreover, the substrate scope of this catalyst system was limited to the sterically more accessible terminal epoxides. Investigating the effect of solvents revealed that the catalysis is highly efficient under mild conditions (25 °C at 2 bars) when the reactions are performed in polar solvents (such as methyl ethyl ketone) that offer a relatively high CO_2 dissolution potential.

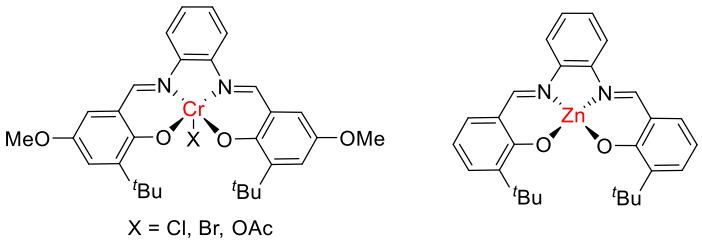

Figure 9: Structure of Cr-salphen complexes by North et al.[55] and Zn salphen complex by Kleij et al.[57]

Al salen and related complexes have also been extensively studied in CO_2/epoxide coupling reactions.[58] In 2004, Lu *et al*. reported the use of a monometallic Al complex (Figure 10, left) that, in the presence of a co-catalyst, converted propylene oxide to cyclic propylene carbonate at room temperature.[59] Dimeric, μ-oxo bridged derivatives (Figure 10, right) generally displayed enhanced activity towards the synthesis of cyclic carbonates in comparison to the monometallic counterparts, albeit under different reaction conditions.[51, 60, 61] North and co-workers proposed that this advantageous activity was due to the close proximity of the two metal centres, which can simultaneously activate both the epoxide and the CO_2. While this bimetallic complex was an extremely efficient catalyst for terminal epoxides even at 0°C and atmospheric pressure, it showed limited success for the conversion of internal epoxides.

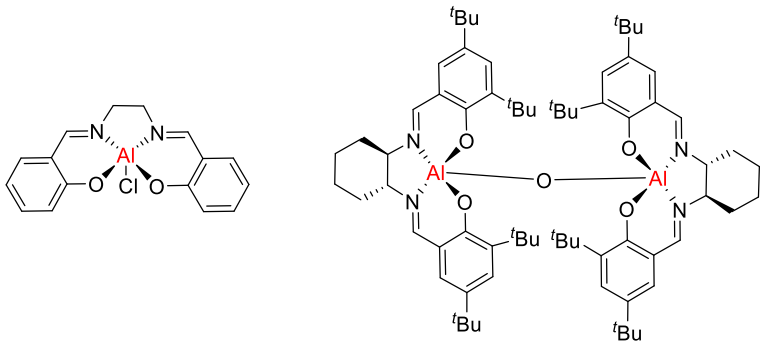

Figure 10: Monometallic Al salen complex investigated by Lu et al. [59] and bimetallic oxo-bridged Al salen by North et al.[51]

Due to the steric hindrance of the substituents and the stabilisation of reaction intermediates, the reactivity of internal (typically disubstituted) and terminal (monosubstituted) epoxides differs significantly. The nucleophile typically attacks the less substituted carbon of a terminal epoxide, while electronic factors become more dominant in the attack of internal epoxides with both sides being sterically 'blocked'. As a benchmark substrate, cyclohexene oxide (CHO) is often used to assess the activity of a catalyst system towards the cycloaddition of internal epoxides and CO_2. Moreover, CHO is also suitable to investigate the catalysts' selectivity towards cyclic carbonate versus polycarbonate synthesis (Scheme 5). The formation of cyclohexene carbonate (CHC) is in fact less likely, as the conformational requirements of the cyclohexyl ring place a ring strain onto the adjoined five-

membered carbonate ring. Consequently, catalyst systems for the efficient production of polyCHC are well known, but optimisation towards the selective formation of CHC is more challenging.[30]

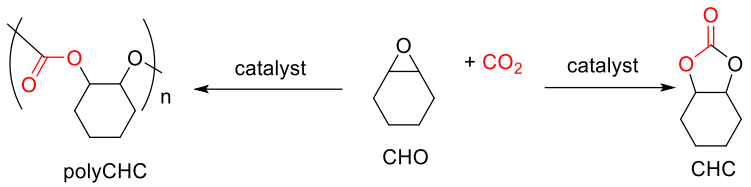

Scheme 5: Synthesis of cyclic cyclohexene carbonate versus poly(cyclohexene carbonate).

The widely researched tetradentate porphyrin- and salen-based catalysts often feature a distorted square pyramidal geometry, with a rigid, planar coordination around the metal centre and the halide in the apical position. A more flexible ligand framework was introduced by Kleij and co-workers, who employed catalysts based on tetradentate amino triphenolate ligands (Figure 11, left).[62] The corresponding Al complexes (in combination with TBAX co-catalysts) were extremely active towards the coupling of CO_2 and propylene oxide, reaching TOFs up to 36 000 h^{-1}. Remarkably, these catalysts were also efficient in the conversion of a broad scope of epoxides, including internal epoxides such as CHO and terpene oxides.[30] The increased activity was attributed to the near trigonal bipyramidal geometry featuring fewer donor atoms in the plane of the metal centre and therefore enabling the coordination of bulky internal epoxides, and facilitating the attack of the nucleophile co-catalyst. Complexes of Y, Yb, Sm and Nd with a similar bis[amino(diphenolate)] ligand (Figure 11, right) also showed high activity (TOFs up to 4000 h^{-1}) in cyclic carbonate synthesis under mild reaction conditions.[63]

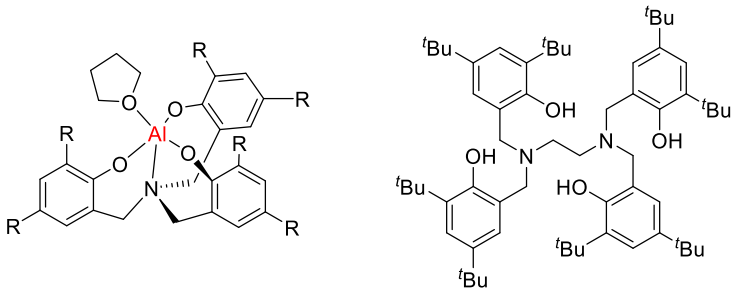

Figure 11: Structure of amino triphenolate complex by Kleij et al. [62] and bis[amino(diphenolate)] pro-ligands by Yao et al.[63]

To avoid the toxicity issues associated with the commonly used Co, Cr and Zn containing catalysts, a search for non-toxic alternatives, such as Fe, is ongoing. In comparison to some of the previously mentioned examples, iron-based catalysts have so far achieved relatively low turnover rates in CO_2/epoxide coupling reactions. Döring and co-workers tested Fe^{II} and Fe^{III} complexes carrying identical tetradentate Schiff-base ligands in the coupling of CO_2 and terminal epoxides and found higher activity using the Fe^{III} species.[64] In 2011, Williams *et al.* reported on a bimetallic macrocyclic Fe^{III} complex (Figure 12, left) that could selectively switch between the formation of CHC or poly(CHC)

depending on the catalyst:co-catalyst ratio.[65] Rieger, Capacchione and co-workers developed dithioether triphenolate type ligands with the softer Lewis donor, sulphur, to coordinate the Fe centre.[66] Dimeric Fe^{III} complexes of these ligands (Figure 12, right) with TBAX co-catalysts were effective in the synthesis of cyclic carbonates from CO_2 and terminal epoxides as well as CHO, reaching TOF up to 580 h^{-1} for propylene oxide (100 °C, 20 bar, neat). In 2016 the same group reported a new generation of related homodinuclear complexes that provided the highest reported TOF values for Fe catalysed propylene carbonate synthesis to date (TOF up to 5200 h^{-1}, 120 °C, 20 bar, neat).[67] To achieve these excellent results, the addition of 10 equivalents of TBABr co-catalyst was required. Interestingly, DFT calculations suggested that only one of the two Fe centres participates in the catalysis, therefore the exceptionally high activity was attributed to the hemilabile sulphur atom in the ligand that can reversibly decoordinate to facilitate the substrate coordination.[67] Most recently, monometallic analogues were also trialled, enabling similarly good conversions under mild conditions, which further corroborates the suggestion that only one Fe centre is involved in the catalysis.[68]

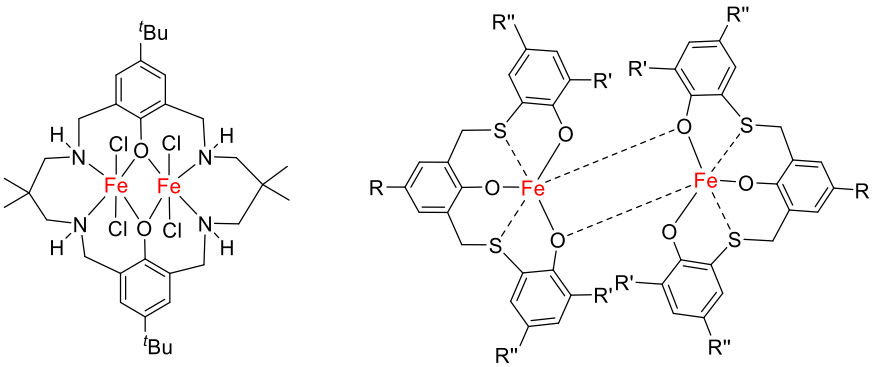

Figure 12: Structure of bimetallic Fe catalyst by Williams et al. [65] and dithioether triphenolate complex by Capacchione et al.[66]

The previously mentioned amino triphenolate ligands developed by Kleij *et al.* were also used to support Fe^{III} as the Lewis acidic metal centre.[69] Depending on the nature of the *ortho* substituent on the phenolate moieties, monomeric or dimeric complexes were formed (Figure 13). The former showed higher activity in CO_2/epoxide coupling, which was attributed to the greater accessibility of the metal. A particular focus was therefore placed on the application of these catalysts in the cycloaddition of CO_2 to internal epoxides, investigating the stereocontrol towards *cis* versus *trans* cyclic carbonate formation.[70, 71] Kerton *et al*. developed tetradentate, amino biphenolate supported Fe^{III} complexes featuring a square pyramidal geometry (Figure 13, right).[72] These catalysts were also active in the coupling of CO_2 with propylene oxide reaching TOFs up to 180 h^{-1} at 100 °C and 20 bars of CO_2 pressure and could provide a limited conversion of the internal CHO.

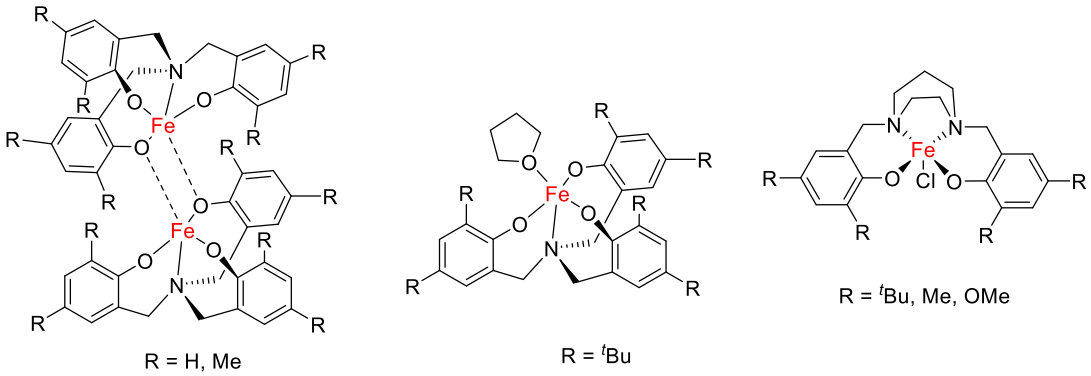

Figure 13: Structures of dimeric or monomeric Fe amino triphenolate complexes by Kleij et al.[69] and amino biphenolate complex by Kerton et al.[72]

Fe^{III} complexes stabilised by salen-type ligands have also been investigated as catalysts for cyclic carbonate synthesis. Al-Ramahi and co-workers used NEt_2 substituted salphen complexes (Figure 14, left) in the coupling of CO_2 and styrene oxide reaching TOFs up to 289 h^{-1}.[73] Most recently, Lamberti *et al.* successfully applied Fe^{III} salen, salan and salalen complexes (in binary systems with TBABr) in CO_2/epoxide coupling, showing high activities for a broad substrate scope. Remarkably, CHO could be converted with TOF up to 35 h^{-1} after 22 hours at 100 °C and 20 bars of CO_2 pressure using either of the catalysts.[74] The study focused on establishing an order of reactivity of these different classes of ligands, surprisingly finding the most square pyramidal salan complex to be the most active, while the most trigonal bipyramidal salalen complex the least active. The aforementioned half salen analogues reported by Repo *et al.* (Figure 14, right) were applied in the synthesis of cyclic carbonates.[18] Optimisation of the solvent medium revealed that the most polar solvent tested, DMF, gave the highest catalyst activity attributed to its capacity to support polar transition states formed during the ring opening and ring closing reaction steps. Under optimised conditions (10 bar, 145 °C, 3 h), high TOFs up to 343 h^{-1} were achieved. Saleh and co-workers compared Cr^{III}, Co^{III} and Fe^{III} half salen catalysts in the cycloaddition of CO_2 to styrene oxide. Under the conditions tested (5 bars of CO_2 pressure at 130 °C for 48 hours) the Fe^{III} complexes were the most active, reaching TOFs up to 208 h^{-1} in the presence of TBABr co-catalyst.[25]

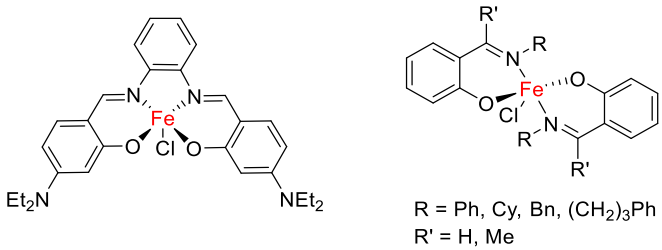

Figure 14: Structure of Fe salen complexes by Al-Ramahi et al. [73] and half salen complexes by Repo et al.[18]

Critical evaluation

To conclude, the homogeneously catalysed coupling of CO_2 and epoxides is a relatively environmentally friendly and an industrially relevant process. It has been increasingly studied in the past two decades (Figure 15) by both academic and industrial laboratories as it is the most attractive route for the synthesis of cyclic carbonates.

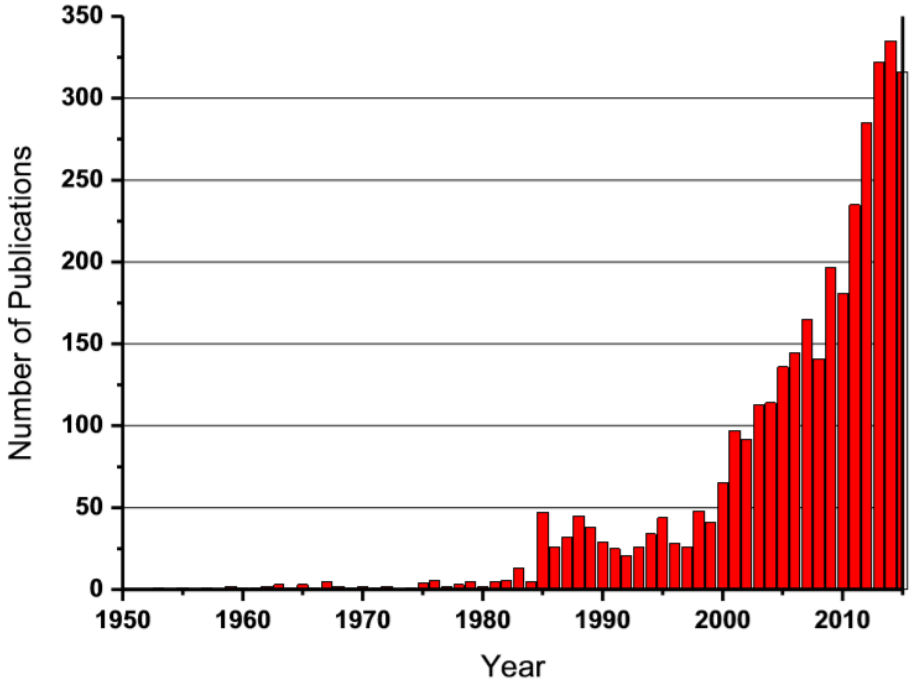

Figure 15: Number of publications for a structural search (synthesis of a 1,3-dioxolan-2-one substructure) in Scifinder.[31]

To improve upon the commercialised method of using onium salts as catalysts, the focus has now shifted towards the application of more active metal complexes. While the abundant and non-toxic Fe is an ideal candidate, only a limited number of Fe catalysts have been developed to date and their general activity falls significantly below to that of other metals such as Mg, Al, Cr or Co.[31]

The majority of research into cyclic carbonate synthesis concentrates on terminal epoxide conversion, as these substrates are more easily ring-opened by nucleophilic attack than internal epoxides. To achieve a truly sustainable method, however, the conversion of bio-derived substrates is necessary. These are most commonly internal epoxides prepared *via* the oxidation of renewable olefinic compounds such as unsaturated fatty acids and terpenes. The development of tandem (oxidation and subsequent CO_2 coupling) systems is a recently emerging topic.[75] The design of novel catalyst complexes with an appropriate coordination environment to allow the conversion of these more challenging internal substrates presents an exciting opportunity.

The choice of substrate also influences the required reaction conditions. Due to the low solubility of CO_2 in epoxides or conventional solvents, high pressure is usually necessary. As CO_2 also offers the opportunity to be both reagent and solvent, coupling reactions working under supercritical conditions have been widely investigated, eliminating the need for environmentally less friendly solvents.[71]

Many reported catalyst systems offer the advantage of converting CO_2 and epoxides under mild conditions, even at room temperature. However, as these cycloadditions are highly exothermic, a significant amount of heat is always produced in industrial scale applications. The effective heat removal (by generating steam) requires reaction temperatures around 150 °C. Moreover, as a green alternative, the temperature of CO_2 waste gas (coming from a power station or production plant) would be also relatively high (60 - 100 °C).[76] From this practical point of view, the thermal stability of the catalyst system can have a greater importance than its reactivity at lower temperatures.

The tolerance of the catalyst towards air, moisture and other impurities is also paramount, especially when considering the use of flue gas as the CO_2 source to further increase the environmental advantages of this reaction.[77] Moreover, a large energy cost reduction could be achieved if the catalyst can convert substrates that did not require rigorous drying and purification prior to the reaction. To summarise, catalyst systems that can combine robustness, recyclability, cost-effectiveness and high reactivity/selectivity would be desirable systems within the area of cyclic carbonate production.

Aims

Exploiting the combined advantages of abundant and non-toxic iron as well as the modular and simple half salen ligands, this research project aimed to design and synthesise novel Fe^{III} half salen complexes. Through the use of X-ray crystallography, we also planned to uncover the coordination behaviour of half salen ligands. Our goal was to apply the Fe^{III} half salen complexes as catalysts in CO_2/epoxide coupling reactions and investigate the structure-activity relationships (Scheme 6).

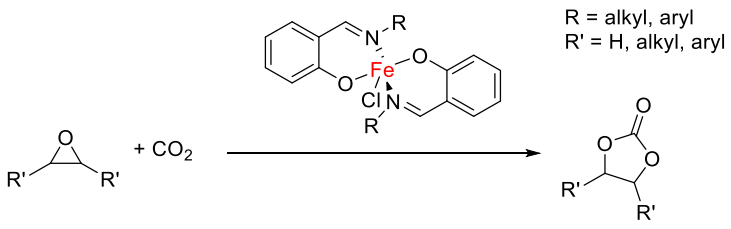

Scheme 6: Study of CO_2/epoxide coupling catalysed by Fe^{III} half salen complexes.

A screening of reaction parameters such as co-catalyst type and ratio, reaction time and catalyst loading was planned to optimise the turnover frequencies. The expansion of the substrate scope of the catalysts was also envisaged.

Finally, we aimed to compare the influence of this ligand system to the standard salen analogues, especially in the conversion of challenging internal epoxides. An important factor was the design of robust Fe^{III} systems that would withstand the presence of air and moisture, with potential in large-scale applications.

Results and discussion

Synthesis of half salen pro-ligands

A series of eight bidentate phenoxyimine (half salen) pro-ligands (**L1**-**L8**) were synthesised according to modified literature procedures *via* the condensation of commercially available primary amines and salicylaldehydes (Table 1).[78, 79] Targeting a stereoelectronically diverse library, substituents with varying steric bulk [methyl or 2,6-diisopropylphenyl (DIPP)] were introduced on the imine, while electron withdrawing (Cl) or electron donating (^{t}Bu) groups were incorporated on the *ortho* and/or *para* positions of the phenol moiety.

*Table 1: Synthesis of pro-ligands **L1-L8**.*

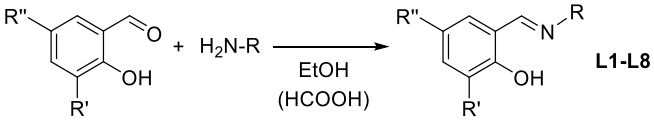

	L1	L2	L3	L4	L5	L6	L7	L8
R	Me	DIPP	Me	DIPP	Me	DIPP	Me	Me
R'	H	H	^{t}Bu	^{t}Bu	^{t}Bu	^{t}Bu	Cl	Cl
R''	H	H	H	H	^{t}Bu	^{t}Bu	H	Cl
Yield (%)	95	92	97	98	98	82	99	91

Syntheses using diisopropylaniline (for **L2**, **L4** and **L6**) were carried out in the presence of formic acid as a catalyst to promote the condensation of the more sterically encumbered amine.[80] After stirring for 16 hours at ambient temperature, the formation of the desired Schiff base products was confirmed by a colour change from colourless to yellow and the appearance of imine proton resonances at 8.2-8.4 ppm ($CDCl_3$) in the ^{1}H NMR spectra of the crude reaction mixtures. Following the purification *via* filtration and (with the exception of the liquid product **L1**) recrystallisation from ethanol, excellent yields (82 – 99 %) were achieved. **L1** was obtained as an orange oil, **L3** yielded green crystals and all other products (**L2**, **L4**-**L8**) were obtained as yellow crystals. While all eight half salen

pro-ligands have been reported in the literature;[78, 80-82] **L3**, **L7** and **L8** were previously not fully characterised. Consequently, these pro-ligands were characterised by ^{1}H and ^{13}C NMR spectroscopy, high resolution mass spectrometry (HRMS) and elemental analysis.

Synthesis of Fe^{III} half salen complexes

The Fe^{III} half salen complexes (**C1**-**C8**) were synthesised through the deprotonation of pro-ligands **L1-L8** using NaH. Subsequent reaction with 0.5 equivalents of anhydrous $FeCl_3$ in THF at room temperature gave an immediate colour change from yellow to dark purple, which indicated the formation of the bis-chelated Fe^{III} chloride complexes (Table 2). The NaCl by-product was removed *via* cannula filtration and the complexes were isolated in moderate to high yields (45-98%) as dark purple-brown solids. As the paramagnetically shifted ^{1}H NMR spectra of complexes **C1**-**C8** provided only limited information, the stoichiometry was confirmed *via* HRMS and elemental analysis. As an alternative synthesis route, the pro-ligands could be directly metalated with anhydrous $FeCl_3$ in the presence of Et_3N (to neutralise the formed HCl).[18] However, this method afforded lower yields after purification.

*Table 2: Synthesis of Fe^{III} half salen complexes **C1**-**C8**.*

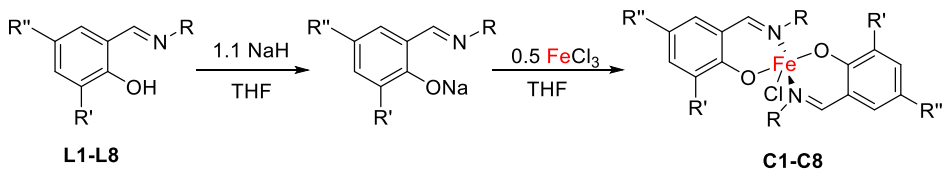

	C1	C2	C3	C4	C5	C6	C7	C8
R	Me	DIPP	Me	DIPP	Me	DIPP	Me	Me
R'	H	H	^{t}Bu	^{t}Bu	^{t}Bu	^{t}Bu	Cl	Cl
R''	H	H	H	H	^{t}Bu	^{t}Bu	H	Cl
Yield (%)	81	52	98	49	89	49	74	45

With the metal in its higher oxidation state (Fe^{III}), the complexes proved to be oxygen- and moisture-stable, which allowed the preparation of single crystals of six compounds under air. Typically, complexes featuring the N-DIPP group on the ligand (**C2**, **C4** and **C6**) were more difficult to crystallise, possibly due to their very high solubility in common laboratory solvents arising from the apolar DIPP substituent. From this sub-group of complexes, only **C6** could be successfully crystallised using DCM as solvent (Figure 19). Single crystals of the N-methyl substituted complexes **C1**, **C5**, **C7** and **C8** were obtained *via* the slow evaporation of DCM. (Figures 16, 18, 20, 21). Single crystals of **C3** (Figure 17) were grown from toluene with one equivalent of the solvent co-crystallising in the unit cell. The

X-ray crystallographic data was collected by Dr Gary Nichol and the structures were elucidated with the help of Dr Jennifer Garden (University of Edinburgh).

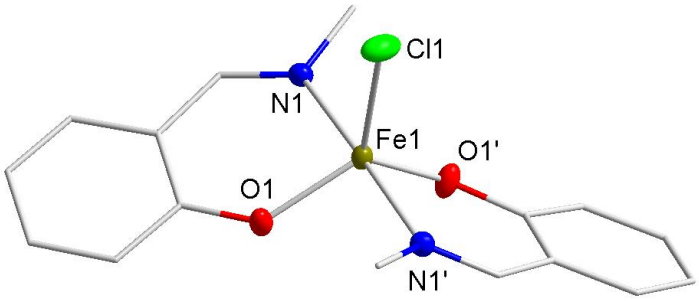

*Figure 16: Molecular structure of **C1** with ellipsoids set at the 50% probability level. Hydrogen atoms have been omitted for clarity. Selected bond lengths (Å): Fe1-Cl1 2.2713(5), Fe1-O1 1.8758(9), Fe1-N1 2.111(1). Selected bond angles (°): O1-Fe1-Cl1 119.50(3), O1'-Fe1-O1 121.00(6), O1-Fe1-N1' 88.46(4), O1-Fe1-N1 90.28(4), N1-Fe1-Cl1 91.28(3), N1-Fe1-N1' 177.44(5).*

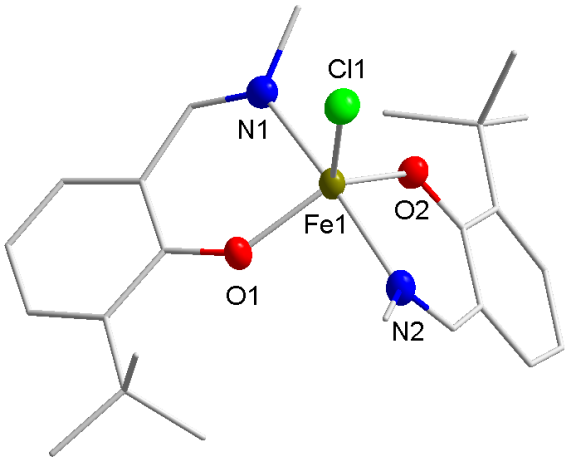

*Figure 17: Molecular structure of **C3** with ellipsoids set at the 50% probability level. Hydrogen atoms and co-crystallised solvent have been omitted for clarity. Selected bond lengths (Å): Fe1-Cl1 2.245(2), Fe1-O1 1.880(5), Fe1-O2 1.881(4), Fe1-N1 2.103(6), Fe1-N2 2.108(6). Selected bond angles (°): O1-Fe1-Cl1 116.1(2), O2-Fe1-Cl1 119.4(2), O2-Fe1-O1 124.6(2), N1-Fe1-Cl1 93.6(2), N1-Fe1-O1 87.5(2), N1-Fe1-O2 87.5(2), N2-Fe1-Cl1 96.8(2), N2-Fe1-O1 88.5(2), N2-Fe1-O2 86.9(2), N2-Fe1-N1 169.7(2).*

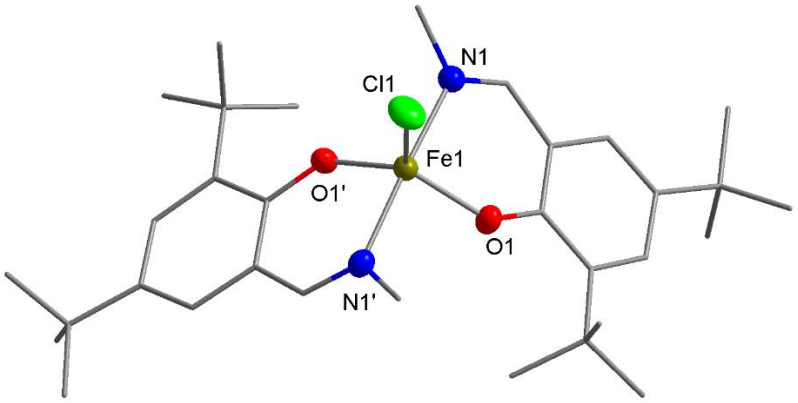

*Figure 18: Molecular structure of **C5** with ellipsoids set at the 50% probability level. Hydrogen atoms have been omitted for clarity. Selected bond lengths (Å): Fe1 - Cl1 2.2713(5), Fe1 - O1 1.8758(9), Fe1 - N1 2.111(1). Selected bond angles (°): O1- Fe1 - Cl1 119.50(3), O1'- Fe1 - O1 121.00(6), O1 - Fe1 - N1' 88.46(4), O1 - Fe1 - N1 90.28(4), N1 - Fe1 - Cl1 91.28(3), N1 - Fe1 - N1' 177.44(5).*

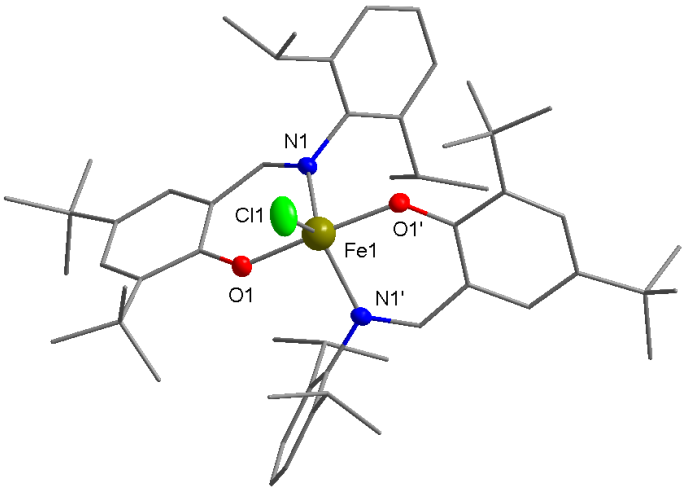

*Figure 19: Molecular structure of **C6** with ellipsoids set at the 50% probability level. Hydrogen atoms have been omitted for clarity. Selected bond lengths (Å): Fe1 - Cl1 2.215(2), Fe1 - O1 1.921(3), Fe1 - N1 2.080(3). Selected bond angles (°): O1 - Fe1 - Cl1 93.2(1), O1 - Fe1 – O1'173.7(2), O1 - Fe1 - N1 86.2(1), O1 - Fe1 – N1' 90.7(1), O1' - Fe1 – N1' 86.2(1), N1 - Fe1 - Cl1 119.4(1), N1 - Fe1 – N1' 121.1(2).*

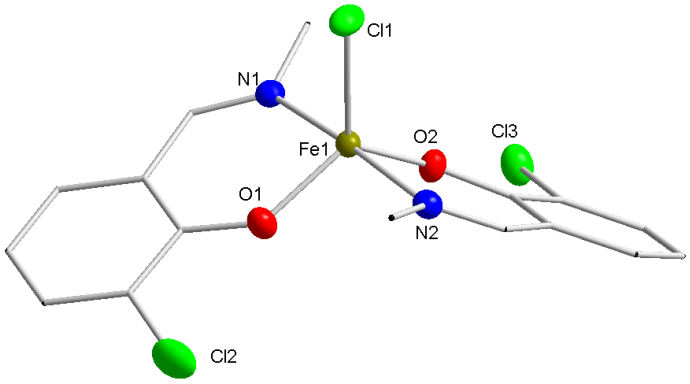

*Figure 20: Molecular structure of **C7** with ellipsoids set at the 50% probability level. Hydrogen atoms have been omitted for clarity. Selected bond lengths (Å): Fe1-Cl1 2.2517(6), Fe1-O1 1.871(2), Fe1-N1 2.092(2), Fe1-O2 1.889(2), Fe1-N2 2.104(2). Selected bond angles (°): O1-Fe1-N1 88.64(7), O1-Fe1-Cl1 117.12(5), O1-Fe1-O2 121.78(7), O1-Fe1-N2 89.43(7), N1-Fe1-Cl1 92.25(5), N1-Fe1-N2 174.92(7), O2-Fe1-N1 89.00(7), O2-Fe1-Cl1 121.11(5), O2-Fe1-N2 88.02(7), N2-Fe1-Cl1 92.81(5).*

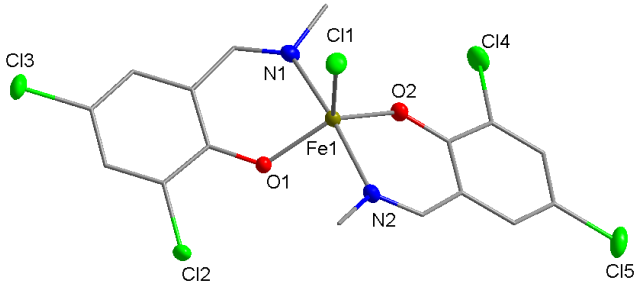

*Figure 21: Molecular structure of **C8** with ellipsoids set at the 50% probability level. Hydrogen atoms have been omitted for clarity. Selected bond lengths (Å): Fe1 - Cl1 2.2271(5), Fe1 - O1 1.881(1), Fe1 - O2 1.911(1), Fe1 - N1 2.101(1), Fe1 - N2 2.104(2). Selected bond angles (°): O1 - Fe1 - Cl1 114.06(4), O1 - Fe1 - O2 130.30(5), O1 - Fe1 - N1 87.91(5), O1 - Fe1 - N2 90.12(5), O2 - Fe1 - Cl1 115.64(4), O2 - Fe1 - N1 87.02(5), O2 - Fe1 - N2 86.78(5), N1 - Fe1 - Cl1 96.19(4), N1 - Fe1 - N2 169.98(6), N2 - Fe1 - Cl1 93.58(4).*

The X-ray diffraction studies of the complexes revealed mononuclear structures with pentacoordinate Fe centres. While **C1**, **C5** and **C6** contain a C_2 symmetry axis that runs through the Fe-Cl bond, the structure of the other three complexes (**C3**, **C7** and **C8**) featured two crystallographically independent halves.

In all six of the Fe^{III} half salen structures the ligands are arranged such, that both nitrogen and both oxygen atoms are in mutually *trans* positions. This significantly differs from Fe^{III} salen and salalen complexes, which typically possess a square pyramidal geometry with mutually *cis* N and O coordinations.[74, 83] This difference in geometry arises from the lack of a bridge connecting the two Schiff bases, with this greater ligand flexibility enabling the two bidentate ligands to minimise the

steric repulsion. The complexes bear similar structural motifs to other half salen Fe^{III}-chloride derivatives described in the literature.[22, 84-89]

The bond metrics are comparable to reported examples, with Fe-N bond lengths ranging from 2.080(3) Å to 2.111(1) Å and Fe-O bond lengths ranging from 1.871(2) Å to 1.921(3) Å.[86, 87, 90] The longest Fe-O bonds were observed in **C6** (Figure 18) suggesting stronger steric repulsion between the two bulky ^{t}Bu and N-DIPP substituted ligands. The C–O bond lengths vary from 1.318(8) Å to 1.328(3) Å and are shorter than the value reported for a related half salen pro-ligand [C–O, 1.354(2) Å],[91] indicating the resonance delocalisation of the anionic charge in the metalated complexes. Furthermore, the C-C bond lengths of the (O-)*C*=*C*-*C*(=N) scaffolds lie between the expected bond lengths for $C_{(aromatic)}$=$C_{(aromatic)}$ double bonds and $C_{(aromatic)}$-C single bonds (1.40 and 1.52 Å, respectively),[92] suggestive of a resonance delocalisation through the imine moiety (Figure 22).

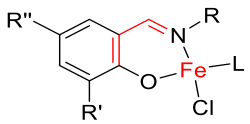

Figure 22: Partial structure of half salen Fe complexes highlighting the resonance delocalisation.

In line with related complexes described in the literature, the Fe-Cl bond lengths range from 2.215(2) Å to 2.2713(5) Å. Upon the introduction of electronegative chloro substituents to the ligand scaffold, a clear trend can be observed: as the Lewis acidity of the metal centre is increased, the Fe-Cl bond length is significantly shortened, from 2.2713(5) Å for unsubstituted **C1**, to 2.2517(6) Å for *mono*-chloro substituted **C7** and to 2.2271(5) Å for the *ortho, para*-dichloro substituted **C8**. The N-DIPP substituted **C6** features the shortest Fe-Cl bond of 2.215(2) Å, which may be attributed to this complex featuring the most sterically crowded coordination sphere.

To evaluate the geometries of the Fe^{III} half salen complexes, the τ factor developed by Addison *et al.* was calculated (Figure 23). This factor describes the geometry of a pentacoordinate complexes which falls between perfectly square pyramidal (τ = 0) and perfectly trigonal bipyramidal (τ = 1) coordination modes.[93]

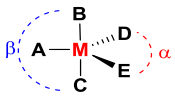

$$\tau = \frac{\beta - \alpha}{60}$$

Figure 23: Equation to calculate the τ value developed by Addison et al.

All six structurally characterised complexes displayed high τ values (τ > 0.5) indicating that they are closer to a trigonal bipyramidal than to a square pyramidal geometry (Table 3). While **C1** and **C5** were shown to be almost perfectly trigonal bipyramidal (τ = 0.94), dichloro substituted **C8** displayed the lowest τ value of 0.66 referring to a significant amount of square pyramidal distortion possibly due to electronic effects of the *para* chloro substituent. Several studies, including a report from Repo *et al.*,

described related Fe^{III} half salen complexes featuring more square-pyramidal configurations with the Fe bound chloride occupying the axial position.[18]

*Table 3: τ and μ_{eff} values of half salen Fe^{III} complexes **C1**-**C8**.*

Complex	C1	C2	C3	C4	C5	C6	C7	C8
τ	0.94	-[a]	0.75	-[a]	0.94	0.87	0.89	0.66
μ_{eff} (B.M.)	4.8	5.5	5	4.5	4.9	4.6	5.1	4.6

[a] *Complexes were not characterised via X-ray diffraction to enable calculation of τ value.*

In all five N-methyl substituted complexes, the nitrogens comprise the main axis of the trigonal bipyramid with nearly linear [169.7(2) – 177.44(5)°] N-Fe-N angles. Consequently, the chloride and the two oxygens occupy the equatorial positions. In contrast, the N-DIPP substituted complex **C6** displays an O-Fe-O main axis [173.7(2)°]. This switch in axial and equatorial occupants may arise from the significant increase in the steric bulk of the DIPP substituents in comparison to the methyl groups.

Much like **C1**-**C8**, most other Fe^{III} half salen complexes in the literature were reported to be monomeric on the basis of X-ray crystallographic analysis.[18, 22, 84, 88] However, two types of dimeric assemblies have also been observed. In the first type, two half salen complexes form 'loose dimers' in which the Fe atoms are bridged by the alkoxide oxygens constructing a four membered ring (Figure 24, left).[90] Although these dimers were not detected in the single crystals of any of the six characterised complexes (**C1**, **C3**, **C5**-**C8**), their existence in the bulk material or in the solution state cannot be unequivocally excluded. In the presence of a base, the hydrolysis of half salen Fe^{III} chloride complexes was reported to form the corresponding μ-oxo bridged dimers (Figure 24, right).[19, 23, 86, 94] While these species were not directly observed in the solid state structures either, their presence in the bulk material may be possible as a strong base (NaH) was used during their preparation. However, this seems unlikely based on the elemental analysis and HRMS results. The influence of these two types of Fe^{III} half salen dimers on the catalytic activity in CO_2/epoxide coupling reactions (compared to monomeric forms) remains unexplored. Similar dimers were investigated in catalysis by the research groups of Kleij (Fe^{III} amino triphenolate 'loose dimers') and North (μ-oxo bridged Al salen species).[51, 69]

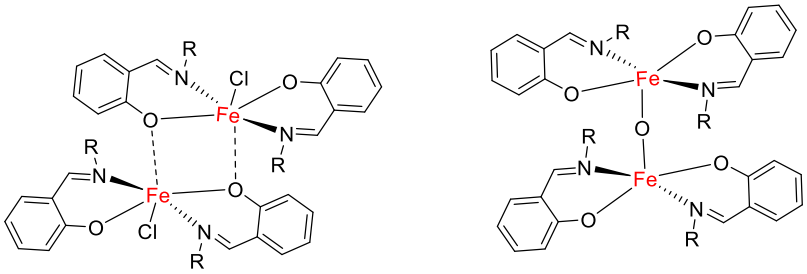

Figure 24: General structures of 'loose dimer' and μ oxo-bridged dimer Fe^{III} half salen complexes.

The solution magnetic moments of the complexes were determined *via* Evan's method in reference to the CH_3 toluene ^{1}H NMR peak shift in C_6D_6 at room temperature.[95] The obtained μ_{eff} values of 4.6-5.5 μ_B (Table 3) fall slightly below the theoretical value of 5.9 μ_B for a pentacoordinate high spin Fe^{III} complex, which suggests that this type of complex predominates. The difference can be tentatively attributed to the presence of a relatively small amount of the aforementioned dimers (Figure 24) in the bulk material of the complexes. The 'loose dimer' structure - representing an intermediate between five coordinate and six coordinate Fe species - was investigated by Bertrand and co-workers, who associated the measured μ_{eff} values of 4.52 μ_B to an antiferromagnetic coupling through the bridging oxygens.[90] The μ-oxo bridged dimers were also shown to display low μ_{eff} values (around 1.9 μ_B) by Murray *et al.*, which was attributed to a spin exchange process.[94]

CO_2/epoxide coupling reactions

To test the catalytic activity of the Fe^{III} half salen complexes (**C1**-**C8**) in CO_2/epoxide coupling reactions, propylene oxide (PO) was selected as a standard benchmark substrate.[30] Initial optimisation reactions were carried out with the mono ^{t}Bu substituted complex **C3** and tetrabutylammonium halide co-catalysts (Scheme 7).

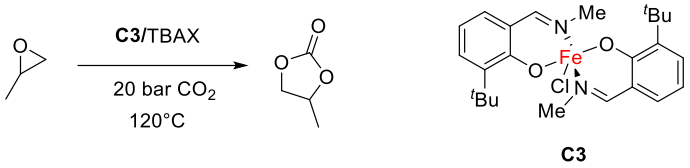

Scheme 7: Coupling of CO_2 and propylene oxide.

In line with commonly reported protocols, the reactions were performed neat, with PO acting as both solvent and substrate. As other Fe catalysts were previously shown to have moderate activity in these catalytic processes, relatively high temperature (120 °C) and CO_2 pressure (20 bar) were applied. Importantly, under these reaction conditions, cyclic carbonate products were formed selectively throughout the entire project. The presence of possible polycarbonate or polyether by-products (Scheme 3) was not observed during either of the ^{1}H NMR, ^{13}C NMR, FT-IR spectroscopy or MALDI mass spectrometry analyses (*vide infra*).

The conversions were determined through the integration of characteristic product peaks against the starting material peaks in the ^{1}H NMR spectra of crude reaction mixtures (Figure 25).[96] Before the aliquots for NMR analysis were taken, the autoclaves were thoroughly cooled to 0 °C to avoid the possible error caused by the loss of the volatile starting materials. In initial reactions hexamethylbenzene was also added as an internal standard. However, the use of an internal standard was later considered unnecessary as the conversions calculated according to the aforementioned

method were reproducible with errors below 5% (compared to the 5% error of integration using the internal standard).

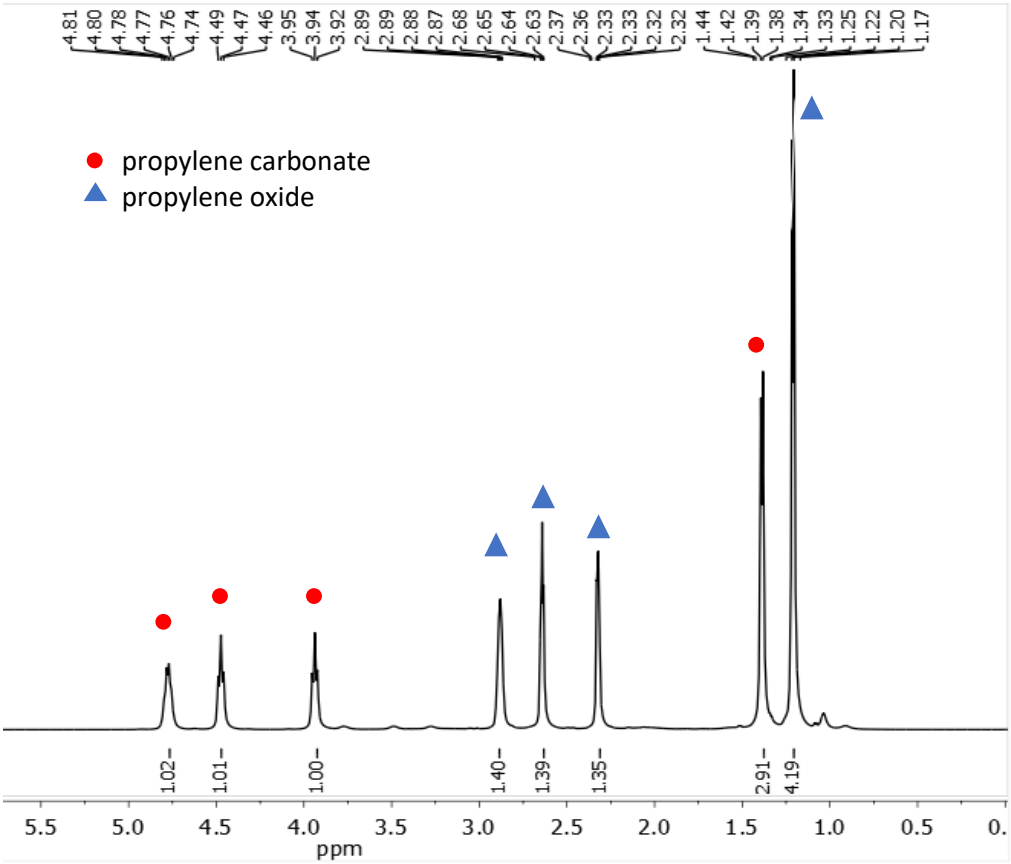

Figure 25: Typical ^{1}H NMR spectrum of a CO_2/PO coupling crude reaction mixture in $CDCl_3$ at 20 °C. Conversion was determined via integration of the CH_3 propylene carbonate (product) peak at 1.37 ppm against the CH_3 PO (starting material) peak at 1.20 ppm.

The first CO_2/propylene oxide coupling reactions were carried out in the presence of 0.1 mol % **C3** and 0.1 mol % tetrabutylammonium iodide (TBAI) as a co-catalyst (Table 4). As complete conversion was achieved after both 24 and 12 hours, the reaction time was reduced to 2 hours to reach only a moderate conversion and consequently allow study of the effects of other reaction parameters. As expected, the control reaction using only co-catalyst TBAI (Table 4, entry 4) showed some activity, in agreement with reported examples for cyclic carbonate syntheses using onium-based catalyst systems.[31] The control reaction with **C3** alone also achieved a low conversion (Table 2, entry 5), which may be attributed to the chloride (from the Fe-Cl complex) acting as a nucleophile. In conclusion, although both catalyst components individually display some activity, their combination (entry 3) clearly leads to a synergistic effect.

*Table 4: Optimisation of reaction time and control reactions with **C3** and TBAI co-catalyst.*

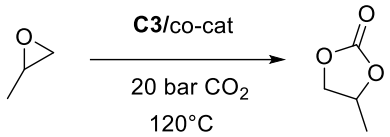

entry	t (h)	catalyst (mol %)	co-catalyst	co-cat. (mol %)	conv. (%)	TON	TOF (h^{-1})
1	24	0.1	TBAI	0.1	99	990	41
2	12	0.1	TBAI	0.1	99	990	83
3	2	0.1	TBAI	0.1	56	560	280
4	2	-	TBAI	0.1	15	-	-
5	24	0.1	-	-	13	130	5

Conditions: 0.02 mmol [Fe] and TBAI, 20.0 mmol PO, 20 bar CO_2 pressure, 120 °C, neat.

Next, the catalyst loading was reduced to 0.05 mol % (2000 eq. of PO versus Fe). Catalyst **C3** displayed tolerance towards this increased substrate ratio reaching a conversion of 40% in 2 hours (Table 5, entry 2). Following literature recommendations, doubling the co-catalyst ratio from 1 to 2 equivalents of TBAI (versus Fe) further improved the turnover frequency to 480 h^{-1} (entry 3). As the reactions were carried out on a relatively small scale, the addition of further equivalents of co-catalyst led to solubility problems and was therefore not investigated.

Table 5: Optimisation of substrate loading and co-catalyst ratio.

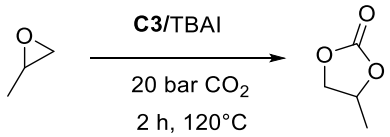

entry	catalyst (mol %)	co-catalyst	co-cat. (mol %)	conv. (%)	TON	TOF (h^{-1})
1	0.1	TBAI	0.2	91	910	455
2	0.05	TBAI	0.05	40	800	400
3	0.05	TBAI	0.1	48	960	480

Conditions: 0.02 or 0.01 mmol [Fe] and TBAI, 20.0 mmol PO, 20 bar CO_2 pressure, 120 °C, neat.

Using these partially optimised conditions, all eight Fe^{III} half salen complexes (**C1**-**C8**) were screened in the synthesis of propylene carbonate leading to good conversions (44-69%) (Table 6). In fact, the achieved TOFs (440-690 h^{-1}) were amongst the highest values reported to date for Fe catalysed CO_2/propylene oxide coupling (*vide infra*).[66, 67, 79] Remarkably, complexes bearing the ^{t}Bu or the Cl substituents (Table 6, entry 3-8) performed better compared to those with the unsubstituted ligands (entry 1-2). This can be related to the higher affinity of **C1** and **C2** complexes to form the aforementioned dimeric species (*vide supra*, Figure 24) due to their lack of steric bulk. The highest

conversion was achieved with the *ortho* chloro substituted **C7** complex (TOF 690 h^{-1}, entry 7). This falls in line with the common observation that electron withdrawing groups increase the Lewis acidity on the Fe centre and consequently facilitate epoxide coordination to promote the nucleophilic attack and ring-opening.[72, 97] A similar trend was described using Co^{III} amidoamine ligands, where complexes bearing electron withdrawing chloro or nitro substituents gave significantly enhanced catalyst activities in comparison to the methyl substituted analogues.[98] On the other hand, the *ortho, para* dichloro substituted **C8** provided slightly lower conversion, indicating that steric effects are also influential. The lower than expected activity can be related to the relatively low trigonal bipyramidal character (τ = 0.66 for **C8** compared to 0.89 for **C7**) in the solid-state structure. According to Kleij *et al.,* highly square pyramidal geometries are generally sterically congested (as there are more atoms in the plane of the metal centre) and consequently more likely to hinder the coordination of substrates to the metal centre.[30]

*Table 6: Screening of catalysts **C1**-**C8** in CO_2/propylene oxide coupling.*

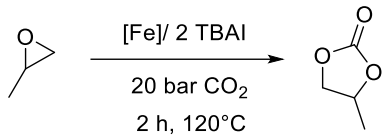

entry	complex	conv. (%)	TON	TOF (h^{-1})
1	**C1**	48	960	480
2	**C2**	44	880	440
3	**C3**	48	960	480
4	**C4**	65	1300	650
5	**C5**	56	1120	560
6	**C6**	63	1260	630
7	**C7**	69	1380	690
8	**C8**	60	1200	600

Conditions: 0.02 mmol [Fe], 0.04 mmol TBAI, 40.0 mmol PO, 20 bar CO_2 pressure, 120 °C, neat.

An alternative co-catalyst, tetrabutylammonium bromide (TBABr) was also investigated. As exchanging TBAI for TBABr resulted in a modest yet reproducible improvement in the catalytic activity (from TOF = 480 h^{-1} to 510 h^{-1}, Table 7, entry 1-2), three more catalysts (**C1**, **C7** and **C8**) were tested in combination with this co-catalyst. In all cases the conversions increased slightly using the bromide nucleophile (versus the iodide in Table 6). This is probably a result of the smaller ionic radius of bromide (185 pm) compared to iodide (206 pm), providing a less sterically hindered attack on the epoxide.[30] North *et al.* showed similar trends using different TBAX co-catalysts in combination with Cr-

salen complexes. In these studies, the conversions achieved with varying the halide anions followed the Br > I > Cl > F order.[55]

Table 7: Screening with TBABr co-catalyst in CO_2/ propylene oxide coupling.

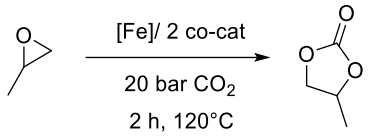

entry	complex	co-catalyst	conv. (%)	TON	TOF (h^{-1})
1	**C3**	TBAI	48	960	480
2	**C3**	TBABr	51	1020	510
3	**C1**	TBABr	53	1060	530
4	**C7**	TBABr	76	1520	760
5	**C8**	TBABr	71	1420	710

Conditions: 0.02 mmol [Fe], 0.04 mmol TBAX, 40.0 mmol PO, 20 bar CO_2 pressure, 120 °C, neat.

Kinetic studies were performed using **C3** in combination with TBABr as co-catalyst. The reactions were carried out under identical conditions in separate autoclaves for different reaction times (Table 8). These experiments confirmed a linear, first-order relationship between substrate conversion and reaction time, highlighting the catalysts stability under the reaction conditions applied (Figure 26, left). This observation falls in line with previous studies by North *et al.* who also showed first order dependence in substrate concentration when using bimetallic Al salen complexes.[51]

*Table 8: Kinetic experiments using **C3** and TBABr.*

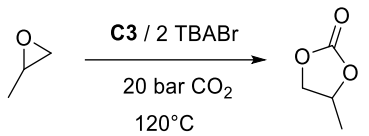

entry	t (h)	conv. (%)	TON	TOF (h^{-1})
1	1	44	880	880
2	2	51	1020	510
3	3	64	1280	427
4	4.5	74	1480	329
5	6	85	1700	283

Conditions: 0.02 mmol [Fe], 0.04 mmol TBABr, 40.0 mmol PO, 20 bar CO_2 pressure, 120 °C, neat.

After reaching a very high initial TOF of 880 h^{-1} (Table 8, entry 1), the TOF values of **C3** gradually decreased following the consumption of PO (Figure 26, right). It is important to differentiate between

initial and average TOFs when comparing catalyst systems as they are often ambiguously reported in the literature.

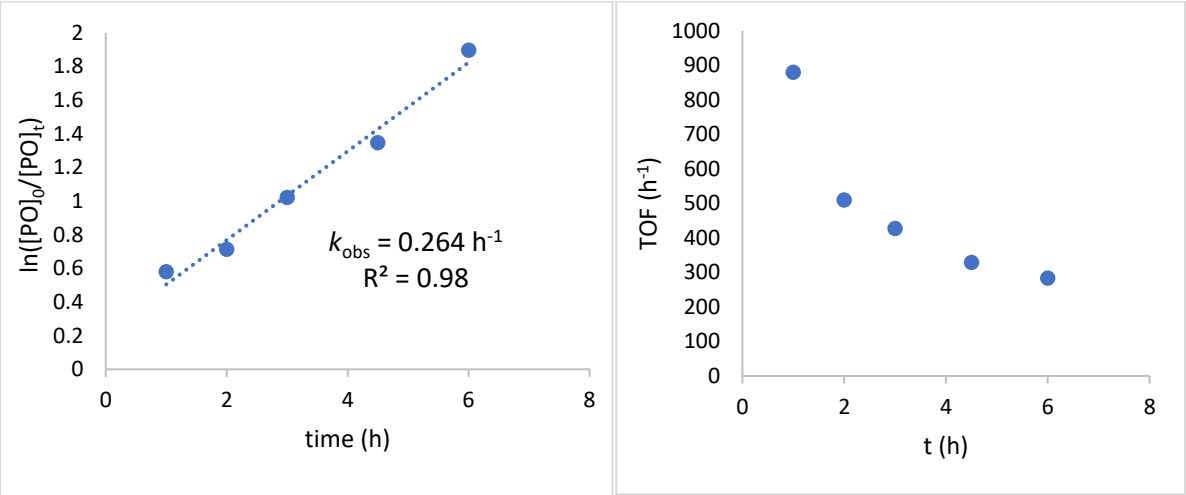

*Figure 26: Kinetic plots of CO_2/propylene oxide coupling using **C3** and TBABr.*

Several research groups have investigated the influence of reaction temperature and pressure on the turnover rates of metal catalysed CO_2/epoxide couplings.[76] While - in accordance with the Arrhenius equation - the rates were always found to proportionally increase with higher temperatures, the role of the applied CO_2 pressure seems to be more complicated and system dependent. Notably, a higher pressure can increase the solubility of the catalysts and co-catalysts. North and co-workers showed that increasing the CO_2 pressure (over the range of 1-10 bars) had a strong positive effect on the rate of cyclic carbonate synthesis using Al salen complexes. On the other hand, Capacchione *et al.* reported on Fe thioether-triphenolate catalysed CO_2/PO couplings, where reducing the CO_2 pressure from 20 bars to 5 bars did not significantly decrease the conversion (a drop from 83% to 81% was observed).[67]

In general, the comparison of the activity of Fe^{III} half salen complexes **C1**-**C8** to other Fe^{III} catalysts known for this transformation is rather complex due to the range of different reaction conditions applied. Table 9 comprises a list of Fe^{III} complexes (supported by a broad range of ligands) that achieved the best turnover values for CO_2/PO coupling to date. Remarkably, the TOF of 880 h^{-1} obtained with **C7** (entry 1) is amongst the highest values reported.

Table 9: Selected literature data of Fe^{III} catalysts reported for the synthesis of propylene carbonate.

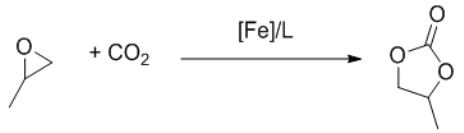

entry	Fe/co-cat/PO	T (°C)	p (bar)	t (h)	conv. (%)	TON	TOF (h^{-1})
1[a]	1/2/2000	120	20	1	44	880	880
2[68]	1/5/1000	35	1	1	10	100	100
3[67]	1/10/10000	120	20	1	52	5200	5200
4[72]	1/4/4000	100	20	6	27	1080	180
5[99]	1/1/100	100	15	1	100	100	100
6[66]	1/4/4000	100	20	6	87	3160	580
7[69]	1/5/100	25	10	18	88	88	5
8[70]	1/10/200	25	2	18	74	148	8
9[64]	1/0/200	80	35	20	69	690	34.5
10[64]	1/0/200	80	35	20	92	184	9
11[100]	1/1/1000	100	40	2	91	910	455

*[a] Results achieved with the best performing Fe^{III} half salen catalyst **C7.***

Screening a wider range of parameters such as solvents, temperature and CO_2 pressure as well as co-catalyst type and ratio was beyond the scope of our study. However, to allow a direct comparison with one of the most active Fe-based catalyst systems, reactions were carried out under identical conditions to those reported by Rieger *et al.* (100°, 20 bars of CO_2, 2 eq. of TBABr, 4000 eq. of PO versus catalyst). Table 10 shows that the Fe^{III} half salen complex (**C7**) achieved turnover rates comparable to the aforementioned Fe dithioether-triphenolate systems (Figure 12), especially when considering the TOF per Fe centre for the dimeric complex.

*Table 10: Direct comparison of **C7** to Fe^{III} dithioether triphenolate catalyst developed by Rieger et al.*

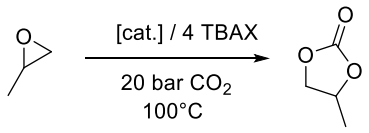

entry	catalyst	co-cat	Conv. (%)	TON	TOF (h^{-1})	TOF/[Fe] (h^{-1})
1	**Fe dithioether triphenolate**	TBABr	87	3480	580	290
2	**C7**	TBAI	34	1360	227	227
3	**C7**	TBABr	47	1880	313	313

Conditions: 0.02 mmol catalyst, 0.08 mmol TBAX, 80.0 mmol PO, 6 h, 20 bar CO_2 pressure, 100 °C, neat.

Using the most active **C7** complex, the substrate loading was further increased to 10,000 equivalents of PO versus Fe. The turnover rates stayed high, indicating the stability of the catalyst (Table 11). The kinetic plot (Figure 27) shows that although the TOF values gradually decreased, the catalyst was still active after 26 hours of reaction time.

*Table 11: Low catalyst loading kinetic experiments using **C7** catalyst.*

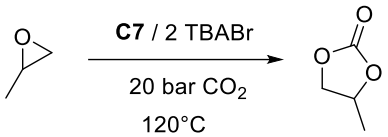

entry	substrate loading	t (h)	Conv. (%)	TON	TOF (h^{-1})
1	2000	2	76	1520	760
2	10000	2	11	1100	550
3	10000	4	20	2000	500
4	10000	8	41	4100	513
5	10000	16	53	5300	331
6	10000	20	55	5500	275
7	10000	26	63	6300	242

*Conditions: 0.02 mmol **C7**, 0.04 mmol TBABr, 200.0 mmol PO, 20 bar CO_2 pressure, 120 °C, neat.*

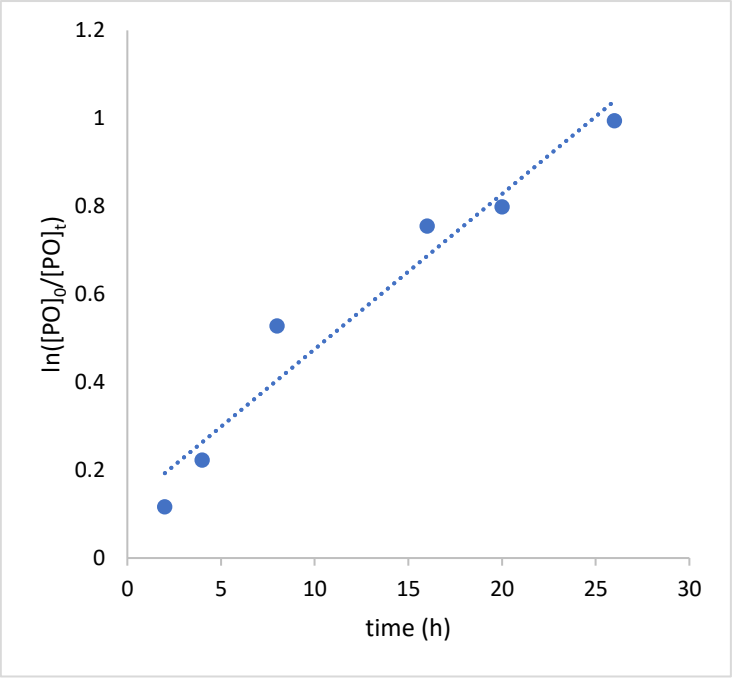

Figure 27: Kinetic plot of CO_2/epoxide coupling reaction with large (10 000 eq.) substrate loading.

To test the tolerance of our catalytic system towards common impurities, further CO_2/PO couplings were carried out with **C7** as the catalyst (Table 12). When the reaction was set up under air (without purging with CO_2 or performing vacuum/argon cycles on the autoclave prior to the reaction), **C7** still displayed high activity towards propylene carbonate formation, with only a minor reduction in the

TOF value observed (entry 1-2, from TOF = 760 h^{-1} to TOF = 650 h^{-1}). Furthermore, the addition of 100 equivalents of water (versus catalyst **C7**) afforded a relatively high TOF of 430 h^{-1}. The robustness in the presence of this significant quantity of water is remarkable, as most of the high-performing catalyst systems reported for cyclic carbonate synthesis are moisture sensitive even on a trace level. The water tolerance was further supported by FT-IR spectroscopic studies; no change was observed in the IR spectra of complex **C7** after stirring the catalyst in water. The robustness of **C7** was also demonstrated when a large-scale, low catalyst loading (0.01 mol %) reaction was repeated using unpurified PO (as received from *Sigma-Aldrich* stating 99.9% purity). Remarkably, the TOF only slightly decreased in comparison to the reaction carried out with dried and distilled substrate (Table 12, entry 4 and 5). These results suggest that the Fe^{III} half salen complexes (**C1**-**C8**) are extremely robust catalysts and could be potential candidates for a more sustainable industrial CO_2/epoxide coupling process. Their stability towards unpurified epoxides is an important feature if the utilisation of naturally derived substrates is considered. Moreover, the water tolerance may also enable the recycling of unpurified waste gases (such as flue gas) as a green CO_2 source. Consequently, the cost of energy saved on these purifications could mitigate the energy needed to maintain the relatively high reaction temperatures.

*Table 12: Investigation of the tolerance of **C7** against air, water and unpurified substrate.*

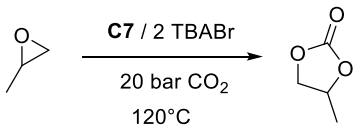

entry	substrate loading	t (h)	conv. (%)	TON	TOF (h^{-1})	impurity
1	2000	2	76	1520	760	-
2	2000	2	65	1300	650	air
3	2000	2	43	860	430	100 eq. water
4	10000	26	63	6300	242	-
5	10000	24	51	5100	213	unpurified PO

*Conditions: 0.02 mmol **C7**, 0.04 mmol TBABr, 200.0 mmol PO, 20 bar CO_2 pressure, 120 °C, neat.*

The substrate scope of the Fe^{III} half salen catalysed CO_2/epoxide couplings was extended. Three more terminal epoxides (butylene oxide, epichlorohydrin and 1,2-epoxy-3-phenoxypropane) were successfully converted to the corresponding cyclic carbonates with high conversions (50-90%) (Table 13). The turnover rates followed the nature of the substituents on the epoxides, with the presence of an electron withdrawing substituent (chloride) facilitating the epoxide ring opening. Accordingly, the highest conversion was achieved for epichlorohydrin (TOF = 900 h^{-1}) while the lowest turnover rates were observed for butylene oxide, containing a slightly electron donating alkyl group (TOF = 500 h^{-1}).

These trends fall in line with previously reported studies, such as CO_2/terminal epoxide coupling reactions catalysed by Al salen complexes.[101]

Table 13: CO_2 coupling with an extended substrate scope.

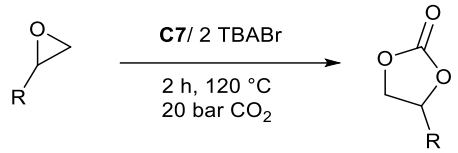

substrate	substrate loading	conv. (%)	TON	TOF (h^{-1})
	2000	76	1520	760
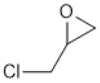	2000	90	1800	900
	2000	50	1000	500
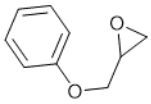	1500	69	1035	518

*Conditions: 0.02 mmol **C7**, 0.04 mmol TBABr, 40.0 mmol epoxide, 20 bar CO_2 pressure, 120 °C, neat.*

Finally, to test the catalysts' reactivity towards internal epoxides, cyclohexene oxide (CHO) was used as a benchmark substrate. In agreement with previous reports,[30] the turnover rates of CHO were a magnitude lower in comparison to the terminal epoxides after 2 hours using **C7** as catalyst (Table 14). This was expected, as the formation of the strained bicyclic carbonate product is kinetically less favoured.[31] Nevertheless, the achieved TOF of 80 h^{-1} (entry 1) was amongst the highest values reported for Fe catalysed cyclohexene carbonate syntheses.[64, 70] The high conversion (74%, entry 3) achieved after 48 hours suggests that **C7** could quantitatively convert this sterically more challenging substrate. It has previously been proposed that the metal geometry is of key importance for the conversion of sterically hindered internal epoxides to the corresponding cyclic carbonates, with complexes bearing a trigonal bipyramidal geometry around the metal centre typically showing greater success.[30, 62] Complexes **C1**–**C8** all display a distorted trigonal bipyramidal geometry, in contrast to the square pyramidal geometries often observed with Fe^{III} salen complexes.[102-105] The flexible coordination modes available when using these half salen ligands may present an advantage over the well-established standard salen analogues.

Table 14: Coupling reactions of CO_2 and cyclohexene oxide.

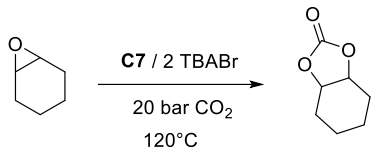

entry	t (h)	conv. (%)	TON	TOF (h^{-1})
1	2	8	160	80
2	24	56	1120	47
3	48	74	1480	31

*Conditions: 0.02 mmol **C7**, 0.04 mmol TBABr, 40.0 mmol CHO, 20 bar CO_2 pressure, 120 °C, neat.*

As internal epoxides are more prone to oligomer/polymer formation, the selectivity towards cyclic carbonates was investigated *via* ^{1}H NMR, ^{13}C NMR and FT-IR spectroscopy as well as ESI and MALDI mass spectrometry studies. The presence of polymeric by-products could not be detected with any of these analytical techniques. While the formation of CHC under the applied relatively harsh reaction condition is not unexpected, catalysts which selectively give CHC in high yields remain rare, and many catalyst systems reported in the literature yielded a mixture of poly(cyclohexene carbonate) and CHC.[30, 65, 71, 106]

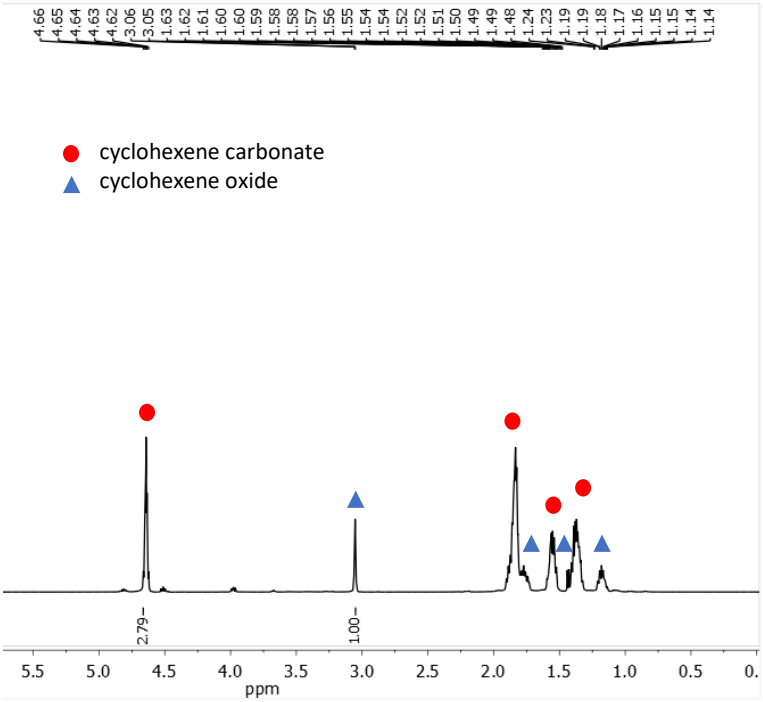

Figure 28: Typical ^{1}H NMR spectrum of a CO_2/CHO coupling crude reaction mixture in $CDCl_3$ at 20 °C. Conversion was determined via integration of the $OCHCH_2CH_2$ cyclohexene carbonate (product) peak at 4.66 ppm against the $OCHCH_2CH_2$ in CHO (starting material) peak at 3.09 ppm.[65]

Importantly, the ^{1}H NMR spectra showed that catalyst **C7** exclusively formed *cis*-CHC even at high conversions (Figure 28). This is quite unusual as the formation of the *trans*-isomer (Figure 29) often

occurs through the thermodynamically favourable back-biting of a poly(cyclohexene carbonate) chain as reported for example by Kleij *et al.* using Fe^{III} amino triphenolate catalysts.[71] However, resonances corresponding to *trans*-CHC (3.9 ppm) were absent from the ^1H NMR spectra using **C7** in combination with 2 eq. of TBABr.[30, 65] The formation of *cis*-CHC is proposed to occur through a double inversion pathway, which can be favoured through the addition of excess co-catalyst.[65, 107-110]

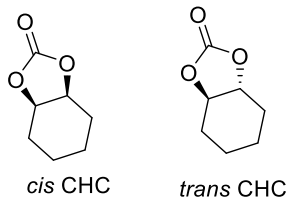

Figure 29: Structures of cis and trans cyclohexene carbonate.

The crude CO_2/CHO coupling reaction mixtures were also analysed *via* FT-IR spectroscopy (Figure 30). In all samples (regardless of the conversion) the absence of diagnostic poly(cyclohexene carbonate) peaks in the 1014 cm^{-1}, 1239-1176 cm^{-1}, and 1731-1787 cm^{-1} bands indicated the absence of polymer formation.[111]

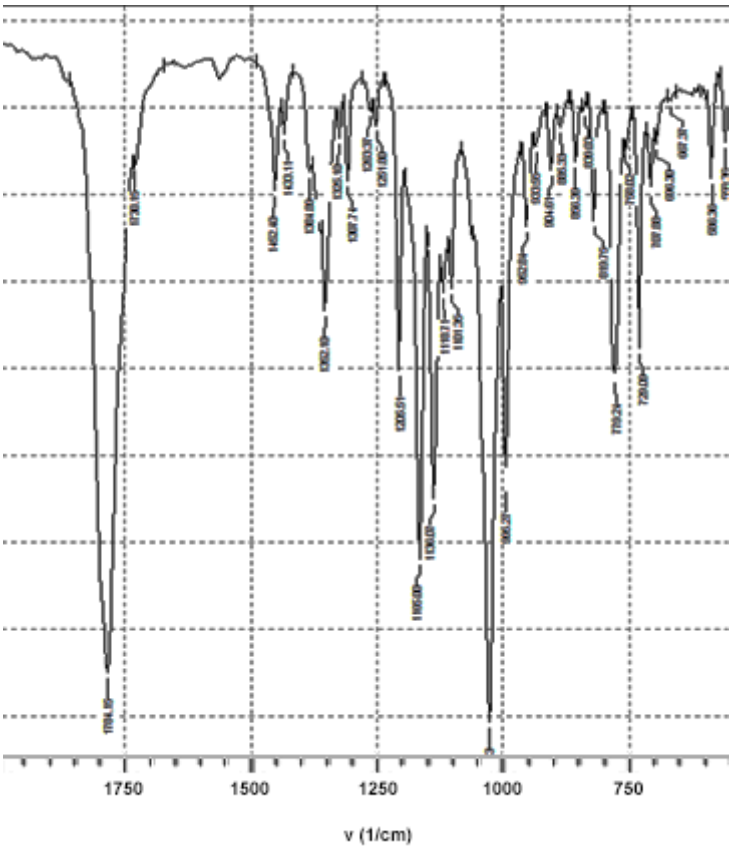

Figure 30: FT-IR spectrum of a crude CO_2/cyclohexene oxide coupling reaction mixture.

Finally, the composition of the reaction mixtures was also investigated via EI mass spectrometry (in the 1-1000 Da range) (Figure 31) and MALDI mass spectrometry (in the 1000-5000 Da range). The lack of peaks over 550 m/z further corroborated the selective cyclohexene carbonate formation.

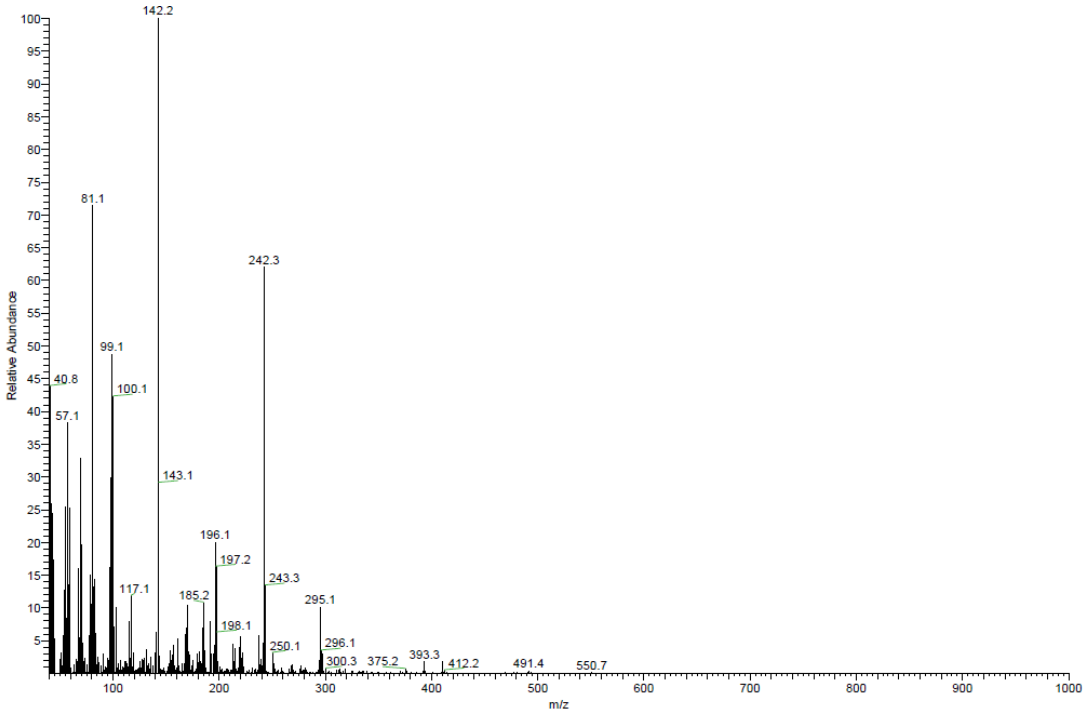

Figure 31: EI mass spectrum of a crude CO_2/cyclohexene oxide coupling reaction mixture.

The ability to convert internal epoxides is an important feature when evaluating novel catalyst systems for CO_2/epoxide coupling. To increase the sustainability of this reaction, the use of naturally derived substrates can be considered, which are most commonly produced through the oxidation of unsaturated fatty acid esters or terpenes, and consequently contain an epoxide ring substituted on both sides.[31] Catalysts that show activity towards CHO are therefore promising candidates for the production of biorenewable cyclic carbonates. While examples for the corresponding copolymers are widely reported,[112] the selective formation of bio-derived cyclic carbonates is currently emerging. For example, recent studies by Kleij and co-workers described the synthesis of cyclic carbonates from limonene derivatives (Figure 32, top),[113] while Leitner *et al.* reported on the successful conversion of methyl oleate to the corresponding cyclic carbonates (Figure 32, bottom).[108]

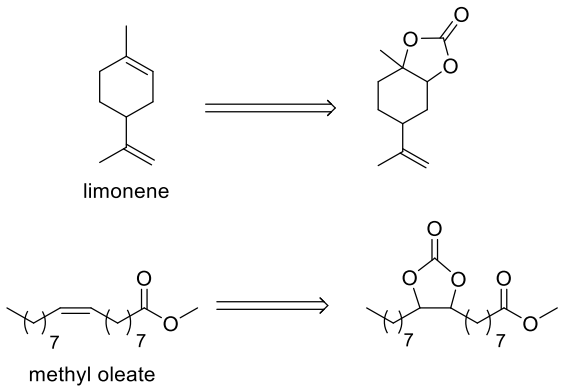

Figure 32: Structures of naturally derived cyclic carbonates.[108, 113]

Summary and future work

A series of eight bidentate half salen pro-ligands (**L1**-**L8**) bearing stereoelectronically diverse substituents were synthesised *via* simple condensation reactions. Following deprotonation with NaH, the ligands were transmetalated with $FeCl_3$ to form the corresponding novel Fe^{III} chloride complexes (**C1**-**C8**) that were characterised *via* mass spectroscopy and elemental analysis. X-ray crystallography studies of six derivatives revealed monometallic, bis-chelated complexes with distorted trigonal bipyramidal geometries. Importantly, the complexes were shown to be air- and moisture-stable.

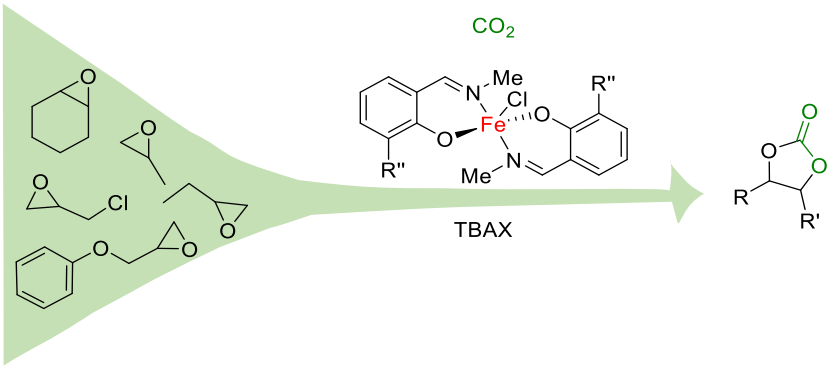

Figure 33: Structure of half salen Fe^{III} complexes and the investigated substrate scope.

The complexes were applied as catalysts in the coupling reaction of CO_2 and epoxides in the presence of TBAX co-catalysts. After initial optimisations, cyclic carbonates were selectively formed with high conversions. In the future, it would be interesting to investigate whether a significant change in reaction conditions (e. g. co-catalyst ratio, temperature, use of a solvent) could facilitate the competing copolymerisation reaction.

Notably, the catalysts were extremely robust and showed efficiency in the presence of oxygen, water and a high loading of unpurified substrate. Moreover, the thermal stability was also demonstrated as the catalyst remained active after a long reaction time (48 h) at high temperature (120 °C). The robustness of the catalysts could be further tested using flue gas from a power plant station as a green CO_2 source. In addition, the recyclability of these catalysts/co-catalyst systems may be investigated.

Structure-activity relationships were uncovered, suggesting that electron withdrawing groups on both the ligands and the substrate may further enhance the conversions. The most active mono chloro substituted **C7** complex provided turnover rates (TOF up to 880 h^{-1}) that are amongst the highest values reported for Fe-catalysed CO_2/propylene oxide coupling to date. The incorporation of chiral moieties in the ligand substituents would allow the investigation of potentially asymmetric coupling reactions starting from racemic epoxides.

The substrate scope of the reaction was investigated using four other terminal epoxides, however, this could be further extended. Remarkably, the sterically challenging internal epoxide, cyclohexene oxide could be also efficiently converted. This was attributed to the flexible, trigonal bipyramidal geometry of the half salen complexes, which may be an advantage over the standard salen backbones. As the majority of bio-derived epoxides feature similar structures, testing **C1**-**C8** in the coupling of CO_2 with renewable substrates such as terpene oxides would be worthwhile. This would further increase the sustainability of the cyclic carbonates produced.

Experimental

General considerations

All moisture- and/or air-sensitive experiments were performed under an argon atmosphere using an MBraun LABmaster glovebox and standard Schlenk techniques. Solvents were obtained from a solvent purification system (Innovative Technologies) consisting of columns of alumina and copper catalyst and were further degassed by freeze–pump–thaw cycles prior to use. Propylene oxide was dried by stirring over calcium hydride overnight followed by distillation. 2,6-Di-isopropylaniline was distilled under vacuum prior to use. N-Methylamine (33 m/m % in H_2O), salicylaldehyde, 3-chlorosalicylaldehyde, 3,5-dichlorosalicylaldehyde, 3-*tert*-butylsalicylaldehyde and 3,5-di-*tert*-butylsalicylaldehyde were all used as received. NMR spectra were obtained a 500 MHz Bruker Avance III spectrometer. Solution magnetic moments were determined *via* ^{1}H NMR spectroscopy using Evans' method in C_6D_6 with toluene as reference.[95] Mass spectra were obtained on a Bruker Daltonics micro TOF instrument operating in the positive ion electrospray mode. MALDI-ToF mass spectrometry was performed on a Bruker UltraflexExtreme MALDI-ToF spectrometer, samples were prepared using dithranol as the matrix and sodium or potassium iodide as the ionisation source. Elemental analyses were performed by Stephen Boyer at London Metropolitan University.

Synthetic procedures

General procedure for ligand precursors L1 - L8

Equimolar amounts of salicylaldehyde [salicylaldehyde, 3-*tert*-butylsalicylaldehyde, 3,5-di-*tert*-butylsalicylaldehyde, 3-chlorosalicylaldehyde or 3,5-dichlorosalicylaldehyde] and primary amine [2,6-diisopropylaniline or methylamine (40% w/w solution in water)] were dissolved in ethanol. Reaction mixtures with 2,6-diisopropylaniline were heated at reflux for 6 hours in the presence of a few drops of formic acid catalyst, then stirred at room temperature for 16 hours. Reaction mixtures with

methylamine were stirred at room temperature for 16 hours. The resulting yellow solutions were dried over $MgSO_4$ then solvents were evaporated *in vacuo*. **L1** was obtained as an orange oil while all other pro-ligands were further purified *via* recrystallisation from ethanol to produce **L2** as green crystals and **L3**-**L8** as yellow crystals. Characterisation data for **L1**[81], **L2**[78], **L4**[80], **L5**[82] and **L6**[78] was in agreement with reported values in the literature.

Data for L3: (1.86 g, 97%) ^{1}H NMR (500 MHz, $CDCl_3$) δ 14.11 (s, 1H, O*H*), 8.35 (s, 1H, *H*C=N), 7.31 (d, *J* = 7.7, 1H, Ar*H*), 7.10 (d, *J* = 7.6 Hz, 1H, Ar*H*), 6.80 (t, *J* = 7.6 Hz, 1H, Ar*H*), 3.48 (d, *J* = 1.5 Hz, 3H, NCH_3), 1.44 (s, 9H, CCH_3). ^{13}C NMR (126 MHz, $CDCl_3$) δ 166.89 (*C*=N), 160.51 (*C*-OH), 137.43, 129.32, 129.13, 118.75, 117.63 (Ar-*C*), 45.72 (N-*C*H_3), 34.83 (*C*CH_3), 29.32 (C*C*H_3). HRMS (EI): *m/z* $[M]^+$ 191.1319 calculated $[M]^+$ 191.1310.

Data for L7: (1.10 g, 99%) ^{1}H NMR (500 MHz, $CDCl_3$) δ 14.51 (s, 1H, O*H*), 8.29 (s, 1H, *H*C=N), 7.39 (d, *J* = 7.9 Hz, 1H, Ar*H*), 7.14 (d, *J* = 7.7 Hz, 1H, Ar*H*), 6.77 (t, *J* = 7.8 Hz, 1H, Ar*H*), 3.49 (d, *J* = 1.5 Hz, 3H, CH_3). ^{13}C NMR (126 MHz, $CDCl_3$) δ 165.8 (*C*=N), 158.8 (*C*-OH), 132.7, 129.6, 122.2, 119.3, 118.1 (Ar-*C*) 44.9 (*C*H_3). HRMS (EI): *m/z* $[M]^+$ 169.0315 calculated $[M]^+$ 169.0294. Elemental Analysis Calculated for C_8H_8ClNO: C, 56.65; H, 4.75; N, 8.3. Found: C, 56.5; H, 4.7; N, 8.3.

Data for L8: (2.90 g, 91%) ^{1}H NMR (500 MHz $CDCl_3$) δ 14.49 (s, 1H, O*H*), 8.23 (s, 1H, *H*C=N), 7.39 (d, *J* = 2.5 Hz, 1H, Ar*H*), 7.12 (d, *J* = 2.5 Hz, 1H, Ar*H*), 3.51 (d, *J* = 1.5 Hz, , 3H, CH_3) ^{13}C NMR (126 MHz, $CDCl_3$) δ 164.9 (*C*=N), 157.8 (*C*-OH), 132.4, 128.9, 123.3, 122.2, 119.4 (Ar-*C*), 44.9 (*C*H_3). HRMS (EI): *m/z* $[M]^+$ 202.9906 calculated $[M]^+$ 202.9905. Elemental Analysis Calculated for $C_8H_7Cl_2NO$: C, 47.1; H, 3.5; N, 6.9. Found: C, 47.3; H, 3.35; N, 7.0.

General procedure for complexes C1 - C8

To a solution of pro-ligand (**L1-L8**) in THF, 1.1 equivalents of NaH was gradually added and the mixture was stirred at ambient temperature for 1 hour. A solution of anhydrous $FeCl_3$ (0.5 equivalents) in THF was added dropwise to afford a dark coloured mixture that was stirred for a further 16 hours at room temperature. Solvents were evaporated *in vacuo* and the crude product was taken up in toluene. The NaCl by-product was removed by filtration through celite and the filtrate was dried *in vacuo*. The crude products were washed three times with hexane to afford dark purple-brown powders. Single crystals suitable for X-ray diffraction analysis were obtained *via* slow evaporation of DCM or toluene, or with the diffusion of hexane in a saturated THF solution.

Data for C1 (0.42 g, 81%) HRMS (EI): *m/z* $[M]^+$ 359.0205 calculated $[M]^+$ 359.0250 Elemental Analysis Calculated for $C_{16}H_{16}ClFeN_2O_2$: C, 53.4; H, 4.5; N, 7.8. Found: C, 53.3; H, 4.65; N, 7.6. CCDC 1855808

Data for C2 (1.10 g, 52%) HRMS (EI): *m/z* $[M]^+$ 651.2441 calculated $[M]^+$ 651.2441 Elemental Analysis Calculated for $C_{38}H_{44}ClFeN_2O_2$: C, 70.0; H, 6.8; N, 4.3. Found: C, 70.2; H, 6.8; N, 4.4.

Data for C3 (2.11 g, 98%) HRMS (EI): *m/z* $[M]^+$ 471.1523 calculated $[M]^+$ 471.1502 Elemental Analysis Calculated for $C_{24}H_{32}FeN_2O_2$: C, 61.1; H, 6.84; N, 5.9. Found: C, 60.2; H, 6.2; N, 6.0. CCDC 1855809

Data for C4 (1.1 g, 49%) HRMS (EI): *m/z* $[M]^+$ 763.3718 calculated $[M]^+$ 763.3693 Elemental Analysis Calculated for $C_{46}H_{60}ClFeN_2O_2$: C, 72.3; H, 7.9; N, 3.7. Found: C, 70.1; H, 7.8; N, 4.0.

Data for C5 (1.4 g, 89%) HRMS (EI): *m/z* $[M]^+$ 583.2790 calculated $[M]^+$ 583.2754 Elemental Analysis Calculated for $C_{32}H_{48}ClFeN_2O_2$: C, 65.8; H, 8.3; N, 4.8. Found: C, 65.9; H, 8.4; N, 4.9. CCDC 1868412

Data for C6 (1.0 g, 49%) HRMS (EI): *m/z* $[M]^+$ 875.5019 calculated $[M]^+$ 875.4945 Elemental Analysis Calculated for $C_{54}H_{76}ClFeN_2O_2$: C, 74.0; H, 8.7; N, 3.2. Found: C, 74.1; H, 8.8; N, 3.2. CCDC 1868413

Data for C7 (0.49 g, 74%) HRMS (EI): *m/z* $[M]^+$ 426.9474 calculated $[M]^+$ 426.9470 Elemental Analysis Calculated for $C_{16}H_{14}Cl_3FeN_2O_2$: C, 44.85; H, 3.3; N, 6.5. Found: C, 44.7; H, 3.35; N, 6.5. CCDC 1855810

Data for C8 (0.6 g, 45%) HRMS (EI): *m/z* $[M]^+$ 494.8716 calculated $[M]^+$ 494.8691 Elemental Analysis Calculated for $C_{16}H_{12}Cl_5FeN_2O_2$: C, 38.6; H, 2.4; N, 5.6. Found: C, 38.8; H, 2.5; N, 5.6. CCDC 1868414

General procedure for the synthesis of cyclic carbonates from CO_2 and epoxides

Reactions were carried out in 100 mL stainless steel autoclaves equipped with a magnetic stirrer, heating mantle (controlled by a thermocouple) and a pressure gauge. Complex **C1**-**C8** (10.0 µmol) and co-catalyst (TBAI or TBABr) were placed into the autoclave and purged with argon. Epoxides (1000 equivalents of propylene oxide or cyclohexene oxide) were added and the autoclave was pressurised with 20 bars of CO_2. The autoclave was heated to 120 °C for 24 hours then rapidly cooled using an ice bath and slowly vented. An aliquot of the crude reaction mixture was taken up in $CDCl_3$ and analysed *via* ^{1}H NMR spectroscopy to determine epoxide conversion.

Crystallography

X-Ray diffraction data was collected by Dr. Gary Nichol on an Agilent SuperNova diffractometer fitted with an Atlas CCD detector with Mo-Kα radiation (λ = 0.7107 Å) or Cu-Kα radiation (λ = 1.5418 Å). Crystals were mounted under paratone on MiTeGen loops. The structures were solved by direct methods using SHELXS or SHELXT interfaced through Olex2 and refined by full-matrix least-squares on F2 using SHELXL, interfaced through Olex2. Molecular graphics for all structures were generated using Diamond.

References

1. P. G. Cozzi, *Chem. Soc. Rev.*, **2004**, *33*, 410-421.
2. K. C. Gupta and A. K. Sutar, *Coord. Chem. Rev.*, **2008**, *252*, 1420-1450.
3. D. J. Darensbourg, *Chem. Rev.*, **2007**, *107*, 2388-2410.
4. A. Avdeef and W. P. Schaefer, *J. Am. Chem. Soc.*, **1976**, *98*, 5153-5159.
5. C. J. Whiteoak, G. Salassa and A. W. Kleij, *Chem. Soc. Rev.*, **2012**, *41*, 622-631.
6. A. W. Kleij, *Eur. J. Inorg. Chem.*, **2009**, 193-205.
7. P. Pfeiffer, E. Buchholz and O. Bauer, *J. Prakt. Chem.*, **1931**, *129*, 163-177.
8. G. Bácskai, *Magyar Chem. F.*, **1940**, *46*, 125-136.
9. H. Nozaki, H. Takaya, S. Moriuti and R. Noyori, *Tetrahedron*, **1968**, *24*, 3655-3669.
10. M. Ma, X. Shen, W. Wang, J. Li, W. Yao and L. Zhu, *Eur. J. Inorg. Chem.*, **2016**, *2016*, 5057-5062.
11. J. Ternel, P. Roussel, F. Agbossou-Niedercorn and R. M. Gauvin, *Cat. Sci. Technol.*, **2013**, *3*, 580-583.
12. T. Chakraborty, S. Dasgupta, E. Zangrando and D. Das, *New J. Chem.*, **2018**, *42*, 14933-14942.
13. T. A. Tshabalala and S. O. Ojwach, *J. Organomet. Chem.*, **2018**, *873*, 35-42.
14. L. F. Groux, T. Weiss, D. N. Reddy, P. A. Chase, W. E. Piers, T. Ziegler, M. Parvez and J. Benet-Buchholz, *J. Am. Chem. Soc.*, **2005**, *127*, 1854-1869.
15. K. Dey, *Z. Anorg. Allg. Chem.*, **1970**, *376*, 209-213.
16. A. C. Silvino, A. L. C. Rodrigues and J. A. L. C. Resende, *Inorg. Chem. Comm.*, **2015**, *55*, 39-42.
17. K. S. Murray, A. van den Bergen, M. J. O'Connor, N. Rehak and B. O. West, *Inorg. Nucl. Chem. Lett.*, **1968**, *4*, 87-89.
18. F. A. Al-Qaisi, N. Genjang, M. Nieger and T. Repo, *Inorg. Chim. Acta*, **2016**, *442*, 81-85.
19. A. van den Bergen, K. S. Murray, M. J. O'Connor, N. Rehak and B. O. West, *Aust. J. Chem.*, **1968**, *21*, 1505-1515.
20. M. A. Torzilli, S. Colquhoun, J. Kim and R. H. Beer, *Polyhedron*, **2002**, *21*, 705-713.
21. T. Feng, D. Bu and H. Lei, *Polyhedron*, **2018**, *148*, 109-117.
22. M. Amini, A. Arab, P. G. Derakhshandeh, M. Bagherzadeh, A. Ellern and L. K. Woo, *Spectrochim. Acta A*, **2014**, *133*, 432-438.
23. G. Markiewicz, A. Walczak, F. Perlitius, M. Piasecka, J. M. Harrowfield and A. R. Stefankiewicz, *Dalton Trans.*, **2018**, *47*, 4254-14262.
24. A. Djouhra, O. Ali, R.-R. Ramiro and M. Emilia, *Spectrochim. Acta A*, **2017**, *184*, 299-307.
25. M. Sunjuk, A. S. Abu-Surrah, E. Al-Ramahi, A. K. Qaroush and A. Saleh, *Trans. Metal Chem.*, **2013**, *38*, 253-257.

26. M. Aresta, A. Dibenedetto and A. Angelini, *Chem. Rev.*, **2014**, *114*, 1709-1742.
27. M. Cokoja, C. Bruckmeier, B. Rieger, W. A. Herrmann and F. E. Kühn, *Angew. Chem. Int. Ed.*, **2011**, *50*, 8510-8537.
28. N. Takeda and S. Inoue, *Bull. Chem. Soc. Japan*, **1978**, *51*, 3564-3567.
29. T. Sakakura and K. Kohno, *Chem. Comm.*, **2009**, 1312-1330.
30. C. Martín, G. Fiorani and A. W. Kleij, *ACS Catal.*, **2015**, *5*, 1353-1370.
31. H. Büttner, L. Longwitz, J. Steinbauer, C. Wulf and T. Werner, *Top. Curr. Chem.*, **2017**, *375*, 50.
32. D. C. Webster and A. L. Crain, *Prog. Org. Coat.*, **2000**, *40*, 275-282.
33. H. Zhang, H. B. Liu and J. M. Yue, *Chem. Rev.*, **2014**, *114*, 883-898.
34. B. Schäffner, F. Schäffner, S. P. Verevkin and A. Börner, *Chem. Rev.*, **2010**, *110*, 4554-4581.
35. A. Duval and L. Avérous, *ACS Sustain. Chem. Eng.*, **2017**, *5*, 7334-7343.
36. D. J. Darensbourg and M. W. Holtcamp, *Coord. Chem. Rev.*, **1996**, *153*, 155-174.
37. J. Datta and M. Włoch, *Polym. Bull.*, **2016**, *73*, 1459-1496.
38. H. Sun and D. Zhang, *J. Phys. Chem. A*, **2007**, *111*, 8036-8043.
39. C. H. Guo, H. S. Wu, X. M. Zhang, J. Y. Song and X. Zhang, *J. Phys. Chem. A*, **2009**, *113*, 6710-6723.
40. W. L. Dai, S. L. Luo, S. F. Yin and C. T. Au, *Appl. Catal. A.*, **2009**, *366*, 2-12.
41. K. Vierling, *I. Farbenindustrie Patent,* DE740366, **1943**.
42. M. L. J. Cooper, *J. Chem. Patent,* US2773070, **1956**.
43. T. Nishikubo, A. Kameyama, J. Yamashita, M. Tomoi and W. Fukuda, *J. Polym. Sci. A*, **1993**, *31*, 939-947.
44. V. Caló, A. Nacci, A. Monopoli and A. Fanizzi, *Org. Lett.*, **2002**, *4*, 2561-2563.
45. G. J. Harmsen, E. van der Heide and C. L. Vrouwenvelder, *Shell Patent,* WO2004089866 **2004**.
46. T. M. Nisbet and G. G. Vaporciyan, *Shell Patent,* WO2008128956, 2008.
47. M. Chihiro, T. Tomoya, O. Kanae and E. Tadashi, *Angew. Chem. Int. Ed.*, **2015**, *54*, 134-138.
48. C. Maeda, S. Sasaki and T. Ema, *ChemCatChem*, **2017**, *9*, 946-949.
49. D. Bai, S. Duan, L. Hai and H. Jing, *ChemCatChem*, **2012**, *4*, 1752-1758.
50. X. B. Lu and D. J. Darensbourg, *Chem. Soc. Rev.*, **2012**, *41*, 1462-1484.
51. W. Clegg, R. W. Harrington, M. North and R. Pasquale, *Chem. Eur. J.*, **2010**, *16*, 6828-6843.
52. D. Zhao, X. H. Liu, Z. Z. Shi, C. D. Zhu, Y. Zhao, P. Wang and W.-Y. Sun, *Dalton Trans.*, **2016**, *45*, 14184-14190.
53. N. Tenhumberg, H. Büttner, B. Schäffner, D. Kruse, M. Blumenstein and T. Werner, *Green Chem.*, **2016**, *18*, 3775-3788.

54. T. Sakakura, J.-C. Choi and H. Yasuda, *Chem. Rev.*, **2007**, *107*, 2365-2387.
55. J. A. Castro-Osma, K. J. Lamb and M. North, *ACS Catalysis*, **2016**, *6*, 5012-5025.
56. X. Zhang, Y.-B. Jia, X.-B. Lu, B. Li, H. Wang and L.-C. Sun, *Tetrahedron Lett.*, **2008**, *49*, 6589-6592.
57. M. Taherimehr, A. Decortes, S. M. Al-Amsyar, W. Lueangchaichaweng, C. J. Whiteoak, E. C. Escudero-Adán, A. W. Kleij and P. P. Pescarmona, *Catal. Sci. Technol.*, **2012**, *2*, 2231-2237.
58. D. Tian, B. Liu, Q. Gan, H. Li and D. J. Darensbourg, *ACS Catalysis*, **2012**, *2*, 2029-2035.
59. X.-B. Lu, Y.-J. Zhang, B. Liang, X. Li and H. Wang, *J. Mol. Cat. A*, **2004**, *210*, 31-34.
60. M. North and R. Pasquale, *Angew. Chem. Int. Ed.*, **2009**, *48*, 2946-2948.
61. J. A. Castro-Osma, A. Lara-Sánchez, M. North, A. Otero and P. Villuendas, *Cat. Sci. Technol.*, **2012**, *2*, 1021-1026.
62. C. J. Whiteoak, N. Kielland, V. Laserna, E. C. Escudero-Adán, E. Martin and A. W. Kleij, *J. Am. Chem. Soc.*, **2013**, *135*, 1228-1231.
63. J. Qin, P. Wang, Q. Li, Y. Zhang, D. Yuan and Y. Yao, *Chem. Comm.*, **2014**, *50*, 10952-10955.
64. M. A. Fuchs, T. A. Zevaco, E. Ember, O. Walter, I. Held, E. Dinjus and M. Doring, *Dalton Trans.*, **2013**, *42*, 5322-5329.
65. A. Buchard, M. R. Kember, K. G. Sandeman and C. K. Williams, *Chem. Comm.*, **2011**, *47*, 212-214.
66. A. Buonerba, A. De Nisi, A. Grassi, S. Milione, C. Capacchione, S. Vagin and B. Rieger, *Cat. Sci. Tech.*, **2015**, *5*, 118-123.
67. F. Della Monica, S. V. C. Vummaleti, A. Buonerba, A. D. Nisi, M. Monari, S. Milione, A. Grassi, L. Cavallo and C. Capacchione, *Adv. Synth. Cat.*, **2016**, *358*, 3231-3243.
68. F. Della Monica, B. Maity, T. Pehl, A. Buonerba, A. De Nisi, M. Monari, A. Grassi, B. Rieger, L. Cavallo and C. Capacchione, *ACS Catalysis*, **2018**, *8*, 6882-6893.
69. C. J. Whiteoak, B. Gjoka, E. Martin, M. M. Belmonte, E. C. Escudero-Adán, C. Zonta, G. Licini and A. W. Kleij, *Inorg. Chem.*, **2012**, *51*, 10639-10649.
70. C. J. Whiteoak, E. Martin, M. M. Belmonte, J. Benet-Buchholz and A. W. Kleij, *Adv. Synth. Catal.*, **2012**, *354*, 469-476.
71. M. Taherimehr, S. M. Al-Amsyar, C. J. Whiteoak, A. W. Kleij and P. P. Pescarmona, *Green Chem.*, **2013**, *15*, 3083-3090.
72. D. Alhashmialameer, J. Collins, K. Hattenhauer and F. M. Kerton, *Cat. Sci. Technol.*, **2016**, *6*, 5364-5373.
73. A. Abu-Surrah, H. Abdel-Halim, H. A. N. Abu-Shehab and E. Al-Ramahi, *Transit. Met. Chem.*, **2016**, *42*, 117-122.

74. M. Cozzolino, V. Leo, C. Tedesco, M. Mazzeo and M. Lamberti, *Dalton Trans.*, **2018**, *47*, 13229-13238.
75. Q. Han, B. Qi, W. Ren, C. He, J. Niu and C. Duan, *Nature Comm.*, **2015**, *6*, 10007.
76. C. Beattie, M. North, P. Villuendas and C. Young, *J. Org. Chem.*, **2013**, *78*, 419-426.
77. M. North, B. Wang and C. Young, *Energy Environ. Sci.*, **2011**, *4*, 4163-4170.
78. F. M. García-Valle, R. Estivill, C. Gallegos, T. Cuenca, M. E. G. Mosquera, V. Tabernero and J. Cano, *Organometallics*, **2015**, *34*, 477-487.
79. E. Fazekas, G. S. Nichol, M. P. Shaver and J. A. Garden, *Dalton Trans.*, **2018**, *47*, 13106-13112.
80. T. Opstal, K. Couchez and F. Verpoort, *Adv. Synth. Catal.*, **2003**, *345*, 393-401.
81. P. A. Nikitina, A. S. Peregudov, T. Y. Koldaeva, L. G. Kuz'mina, E. I. Adiulin, I. I. Tkach and V. P. Perevalov, *Tetrahedron*, **2015**, *71*, 5217-5228.
82. E. Safaei, M. M. Kabir, A. Wojtczak, Z. Jagličić, A. Kozakiewicz and Y. I. Lee, *Inorg. Chim. Acta*, **2011**, *366*, 275-282.
83. R. Duan, C. Hu, X. Li, X. Pang, Z. Sun, X. Chen and X. Wang, *Macromolecules*, **2017**, *50*, 9188–9195.
84. J. E. Davies and B. M. Gatehouse, *Acta Crystallogr. B*, **1972**, *28*, 3641-3645.
85. C. J. Magurany and C. E. Strouse, *Inorg. Chem.*, **1982**, *21*, 2348-2350.
86. J. M. Becker, J. Barker, G. J. Clarkson, R. van Gorkum, G. K. Johal, R. I. Walton and P. Scott, *Dalton Trans.*, **2010**, *39*, 2309-2326.
87. M. Amini, M. M. Haghdoost, M. Bagherzadeh, A. Ellern and L. Keith Woo, *Polyhedron*, **2013**, *61*, 94-98.
88. Y. Elerman and H. Paulus, *Acta Crystallogr. C*, **1996**, *52*, 1971-1973.
89. M. Amini, M. Bigdeli, S. Delsouz-Hafshejani, A. Ellern and L. K. Woo, *Z. Anorg. Allg. Chem.*, **2014**, *640*, 385-389.
90. J. A. Bertrand, J. L. Breece and P. G. Eller, *Inorg. Chem.*, **1974**, *13*, 125-131.
91. R. Jamjah, M. Nekoomanesh, R. Zahedi, G. Zohuri, F. Afshar Taromi and B. Notash, *Acta Crystallogr. E*, **2012**, *68*, 522.
92. G. S. Manku, *Theoretical Principles of Inorganic Chemistry*, Tata McGraw-Hill, New Delhi, **1980**.
93. A. W. Addison, T. N. Rao, J. Reedijk, J. van Rijn and G. C. Verschoor, *Dalton Trans.*, **1984**, *1*, 1349-1356.
94. K. S. Murray, *Coord. Chem. Rev.*, **1974**, *12*, 1-35.
95. D. F. Evans, *Chem. Commun.*, **1959**, 2003-2005.
96. L. Hongchun and N. Yongsheng, *Polym. Adv. Technol.*, **2016**, *27*, 1191-1194.

97. D. R. Moore, M. Cheng, E. B. Lobkovsky and G. W. Coates, *J. Am. Chem. Soc.*, **2003**, *125*, 11911-11924.

98. P. Ramidi, N. Gerasimchuk, Y. Gartia, C. M. Felton and A. Ghosh, *Dalton Trans.*, **2013**, *42*, 13151-13160.

99. J. E. Dengler, M. W. Lehenmeier, S. Klaus, C. E. Anderson, E. Herdtweck and B. Rieger, *Eur. J. Inorg. Chem.*, **2011**, *2011*, 336-343.

100. X. Sheng, L. Qiao, Y. Qin, X. Wang and F. Wang, *Polyhedron*, **2014**, *74*, 129-133.

101. L. Cuesta-Aluja, J. Castilla and A. M. Masdeu-Bultó, *Dalton Trans.*, **2016**, *45*, 14658-14667.

102. L. D. Wickramasinghe, S. Mazumder, K. K. Kpogo, R. J. Staples, H. B. Schlegel and C. N. Verani, *Chem. Eur. J.*, **2016**, *22*, 10786-10790.

103. Z. Chu, W. Huang, L. Wang and S. Gou, *Polyhedron*, **2008**, *27*, 1079-1092.

104. A. Karahan, R. Kurtaran, Y. Yahsi, E. Gungor and H. Kara, *J. Struct. Chem.*, **2016**, *57*, 731-736.

105. B. Chen, D. S. Contreras, Y. L. Clancy and F. R. Fronczek, *Acta Crystallogr. E*, **2004**, *60*, 732-734.

106. D. J. Darensbourg and A. D. Yeung, *Macromolecules*, **2013**, *46*, 83-95.

107. V. Laserna, G. Fiorani, C. J. Whiteoak, E. Martin, E. Escudero-Adán and A. W. Kleij, *Angew. Chem. Int. Ed.*, **2014**, *53*, 10416-10419.

108. J. Langanke, L. Greiner and W. Leitner, *Green Chem.*, **2013**, *15*, 1173-1182.

109. C. J. Whiteoak, E. Martin, E. Escudero-Adán and A. W. Kleij, *Adv. Synth. Catal.*, **2013**, *355*, 2233-2239.

110. F. Castro-Gómez, G. Salassa, A. W. Kleij and C. Bo, *Chem. Eur. J.*, **2013**, *19*, 6289-6298.

111. J. A. Garden, P. K. Saini and C. K. Williams, *J. Am. Chem. Soc.*, **2015**, *137*, 15078-15081.

112. C. M. Byrne, S. D. Allen, E. B. Lobkovsky and G. W. Coates, *J. Am. Chem. Soc.*, **2004**, *126*, 11404-11405.

113. G. Fiorani, M. Stuck, C. Martín, M. M. Belmonte, E. Martin, E. C. Escudero-Adán and A. W. Kleij, *ChemSusChem*, **2016**, *9*, 1304-1311.

Chapter 4

Iron half salen complexes in radical and ring opening polymerisations

Introduction

Half salen complexes as polymerisation catalysts

Complexes of half salen ligands (Figure 1) have been underexplored in comparison to the ubiquitous tetradentate salen analogues. Examples using half salen catalysts are especially scarce in small molecule transformation reactions (Chapter 3), however, they have been more frequently investigated in polymer chemistry.

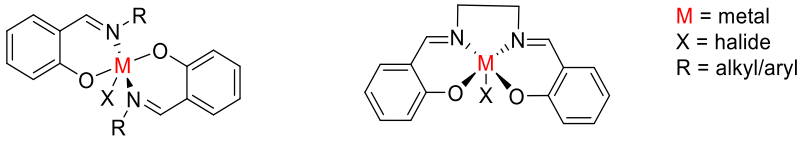

Figure 1: General structures of a half salen complex versus a salen complex.

One of the major applications of half salen complexes was established in the 1990s, when Ti, Zr and Hf derivatives played an important role in the post-metallocene era of polyolefin production. Following the pioneering work of Floriani and Fujita, these Group 4 complexes (coined as 'FI catalysts' from the Japanese 'fenokishi imin' for phenoxyimine) showed extremely high ethylene polymerisation activities. Moreover, the dispersity (*Đ*) of the obtained polyethylene could be exceptionally well controlled (*Đ* = 1.05) by altering the ligand substituents, for example incorporating *ortho* fluorinated aniline moieties (Figure 2, left).[1] Later the development of polyolefin catalysts was extended to the application of Ni and V half salen complexes that showed comparably high efficiency.[2-4] Iron based half salen complexes (Figure 2, right) have been also employed in the polymerisation of ^{t}Bu-acrylate in the presence of methylaluminoxane activator reaching high conversions.[5]

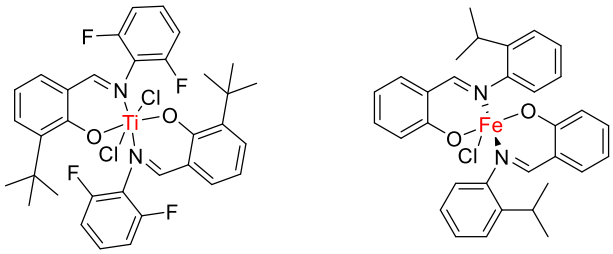

Figure 2: Structures of a Ti 'FI catalyst'[1] and a Fe^{III} half salen catalyst.[5]

The bidentate nature of half salen ligands enables their employment in mixed ligand systems. Verpoort and co-workers developed [RuCl(=CHPh)(PCy_3)(half salen)] type complexes (Figure 3, left) that displayed good control over the atom transfer radical polymerisation (ATRP) of vinyl monomers in toluene-water suspension.[6, 7] Related Ru half salen complexes (Figure 3, right) have been

successfully employed as mediators in the ATRP of styrene and in the ring-opening metathesis polymerisation (ROMP) of norbornene.[8]

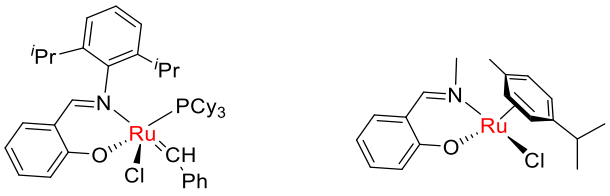

Figure 3: Structures of mixed ligand Ru complexes for suspension ATRP reactions.[8]

Half salen derived catalysts have also shown promise for the ring opening polymerisation (ROP) of cyclic esters. Chakraborty and co-workers developed a range of related complexes containing metals such as Ti, Zr, Hf, Nb, Ta, Ga and In to polymerise lactide in a well-controlled manner.[9-12] Similarly to the standard salen analogues, the half salen catalysed ROP has been largely dominated by Al complexes.[13] For example, Nomura *et al.* applied mono-chelated Al half salens in the ROP of ε-caprolactone, showing that electron withdrawing imine substituents can significantly increase the rate of the reaction.[14] More recently, Milione and co-workers reported on the utilisation of bis-chelated, monometallic Al half salen catalysts (Figure 4, left) in the well-controlled ROP of γ-butyrolactone.[15] Moreover, a series of related Al and In derivatives bearing bulky *o*-$SiPh_3$ substituents have been applied in the stereocontrolled ROP of lactide.[16] For the latter reaction, half salen catalysts with alternative main group metals have been also intensely researched, including Mg derivatives that provided good control over the PLA tacticity (P_i > 0.7).[17] Tabernero *et al.* reported on extremely active dimeric Li, Na and K half salen complexes (Figure 4, middle) that could achieve complete conversion of lactide in less than one minute, however, the polymerisations using these catalyst systems were less controlled giving relatively broad dispersities (*Đ* >1.5).[18] Mono-chelated Al derivatives (Figure 4, right) have also been employed as catalysts for the random copolymerisation of lactide and caprolactone.[19] Recently, Mazzeo and co-workers observed high activity using half salen catalysts for the ring opening copolymerisation (ROCOP) of cyclic esters and epoxides.[20]

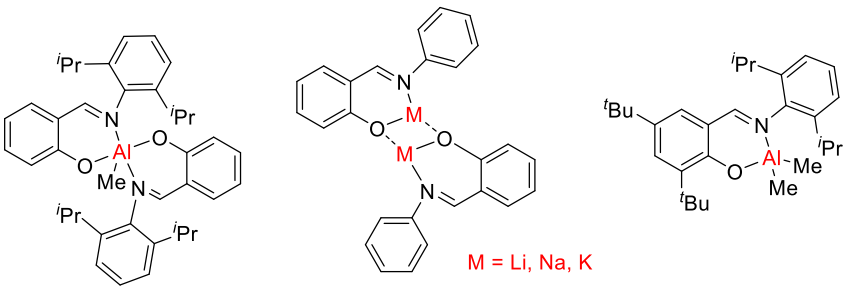

Figure 4: Structures of mono- and bimetallic half salen catalysts for ROP of cyclic esters.[15, 18, 19]

Atom transfer radical polymerisation

Synthetic polymers are used everywhere in the modern world; thus, they are annually produced on a multi-million-ton scale. A large part of this is carried out *via* free radical polymerisation methods that are uncontrolled due to the fast propagation and termination reactions caused by the reactive radical centres.[21] Importantly, radical polymerisations are typically tolerant towards many functional groups and can convert a broad scope of monomers into macromolecules.[22] While these processes are indispensable in the manufacture of several commodity plastics including low density polyethylene, free radical polymerisations do not provide adequate control over the molecular structure of the products. High value applications require more sophisticated, well-defined polymers that were traditionally only accessible through living/ionic polymerisation methods. However, since the 1980s controlled radical polymerisation (CRP) techniques have also been developed. By limiting the rate of termination reactions, CRPs are able to control the molecular weight, dispersity and macromolecular architecture of the obtained polymers and consequently enable the fine-tuning of their mechanical and thermal properties. Exploiting this idea, a range of different CRP methods, including stable free radical polymerisation (SFRP) and reversible addition-fragmentation chain transfer (RAFT) polymerisation were established.

Pioneered by the groups of Matyjaszewski and Sawamoto in the mid-1990s, atom transfer radical polymerisation (ATRP) has emerged as one of the most successful versions of CRP.[23, 24] Since its discovery, the design of novel ATRP catalyst systems for homo- and copolymerisations as well as surface- and star-initiated polymerisations has been an area of intense research.[21] Exploiting the precisely controllable polymer composition and properties, the first industrial applications of ATRP have recently appeared.[25] These initial, large-scale examples all target specialty polymers, such as acrylate derivatives for the production of adhesives, surfactants, resins and coating materials.[26, 27]

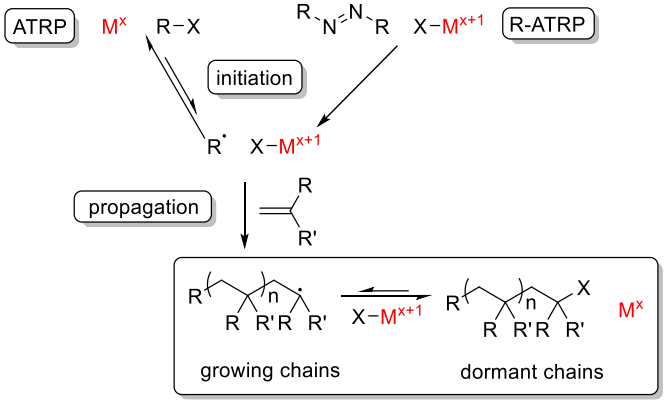

Scheme 1: Proposed mechanism of ATRP and R-ATRP.[22]

ATRP is based on a dynamic equilibrium between the propagating radicals and the (reversibly deactivated) dormant polymer chains, using a metal-mediated halogen-exchange process (Scheme 1). The initiation can be approached *via* two methods: standard ATRP starts from a low-oxidation-state metal complex (M^x) and an alkyl halide (R-X) initiator, while 'reverse ATRP' (R-ATRP) features the metal in its more stable, oxidised from (M^{x+1}) in combination with a conventional radical source such as 2,2'-azobisisobutyronitrile (AIBN). Rather than forming a direct metal-carbon bond, the oxidised metal halide complex (X-M^{x+1}) transfers the halogen atom to a growing polymer chain and yields a halogen-terminated dormant species as well as a reduced metal complex (M^x). The key to control the process during propagation is to lower the concentration of the active (radical) chains and as such, minimise the chance of bimolecular termination reactions. The ATRP mechanism can interplay with organometallic mediated radical polymerisation (OMRP) side-reactions, where direct metal-carbon bonds are formed (Scheme 2).[28]

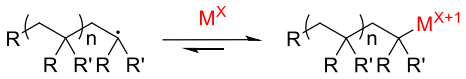

Scheme 2: Formation of M-C bonds in OMRP.

The initial reports on ATRP described the use of catalyst systems based on Ru^{II}/Ru^{III} and Cu^{I}/Cu^{II} halide complexes supported by phosphine and bipyridine ligands, respectively.[23, 24] In the following decades, copper-based complexes bearing a broad scope of ligands became the predominant mediators in the field of ATRP. It was shown that tailoring the steric and electronic properties of the ligands strongly influences the activity and control during the polymerisation.[29] The development of novel catalysts enabled the synthesis of precisely designed macromolecular compositions such as linear (Figure 5),[30] comb and star-shaped block copolymers as well as hyperbranched structures.[31]

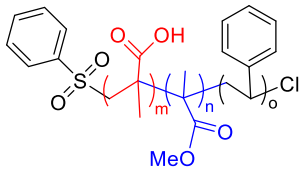

Figure 5: Structure of a linear triblock copolymer synthesised via ATRP.[30]

A general drawback of ATRP systems is the relatively high catalyst loading required, typically in the order of 0.1-1 mol % versus monomer.[31] Traces of the conventional Cu catalysts remaining in the polymer products have led to issues with toxicity and an undesired dark colour. Consequently, the development of processes with lower catalyst loading or efficient catalyst removal gained primary importance, as well as the employment of other redox-active metals including Ti,[32] Mo,[33] Re,[34] Rh[35] Pd,[36] Co,[37] Os[38] and Ni.[39] Nevertheless, the development of Cu catalyst systems remains relevant. For example, a recent report by Matyjaszewski *et al.* described the synthesis of Cu tris[(4-dimethylaminopyridyl)methyl]amine complexes (Figure 6) that showed the highest activities reported

to date for the well-controlled ATRP of methyl methacrylate.[40] This observation was attributed to the increased redox potential of these complexes in comparison to Cu complexes featuring other nitrogen-based ligands.

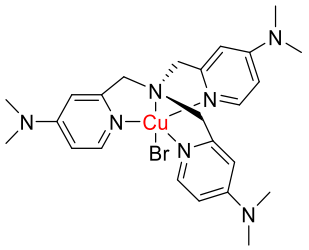

Figure 6: Structure of a Cu-based ATRP mediator.[40]

In the search for greener, non-toxic ATRP catalysts, abundant and inexpensive iron is an ideal candidate, especially considering that it also has a lesser impact on the colour of the polymer products. The first Fe-based ATRP systems were developed by the groups of Matyjaszewski and Sawamoto, originally using simple $Fe^{II}X_2(PR_3)_2$ -type complexes (X = Cl, Br, R = Me, Ph).[41, 42] Since these pioneering studies, Fe catalysts with a variety of other ligands such as phosphines, imines and amines have been explored.[43] Some of the most efficient examples for standard ATRP include Fe^{II} chloride mediators supported by bidentate α-diimine and tridentate salicylaldiminato ligands (Figure 7).[44, 45] Although these complexes showed excellent reactivity and control in the polymerisation of a broad scope of vinyl monomers, they were often extremely air- and moisture-sensitive.

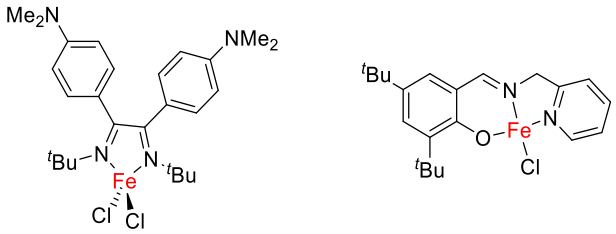

Figure 7: Structures of Fe^{II} α-diimine and salicylaldiminato catalysts for ATRP.[44, 45]

Catalysts containing Fe^{III} have the benefit of an increased stability towards oxygen and water, allowing a simple, user-friendly synthesis and ease of handling. Importantly, regardless of the catalysts' sensitivity, radical polymerisations need to be carried out under an inert atmosphere to prevent the trapping of the active radicals by triplet oxygen. Fe^{III} catalyst systems operate *via* the R-ATRP mechanism (Scheme 1). The first examples of Fe-mediated R-ATRP of MMA were reported by Teyssié *et al.* using $FeCl_3$ in the presence of triphenylphosphine ligands, achieving moderate conversions and low dispersities.[46] As an outstanding example, tetradentate amine bisphenolate (ABP) complexes (Figure 8, left) of Fe^{III} showed high activity and good control in the polymerisation of styrene and acrylate monomers.[47-51] Mechanistic studies of these Fe ABP catalysed polymerisations revealed multi-mechanism systems with the interplay of both ATRP and OMRP pathways.[28, 52]

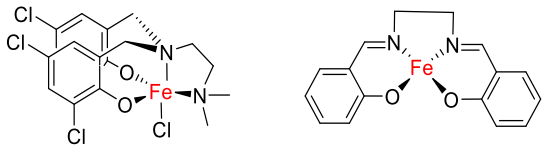

Figure 8: Structures of Fe^{III} ABP and Fe^{II} salen complexes. [47, 53]

Interestingly, the ubiquitous salen-type ligands have been scarcely studied in Fe-catalysed ATRP reactions. During the early stages of ATRP development, Claverie *et al.* reported on the application of Fe^{II} salen complexes (Figure 8, right) in combination with AIBN initiator in the polymerisation of styrene. Although only low conversions and broad dispersities were achieved, these complexes were promising traps for organic radicals and were shown to operate through an OMRP-type mechanism.[53] In another example, Fe^{II}/Fe^{III} salen complexes were investigated in an electrochemically-triggered ATRP process with alkyl-halide initiators, showing that the dispersity of the polymer strongly depends on the initial Fe^{II}/Fe^{III} ratio.[54]

Ring opening polymerisation of lactide

The ring opening polymerisation (ROP) of lactide is one of the most widely studied methods for sustainable polymer production as it offers several advantages over the conventional, petrochemical-based plastic manufacturing.[55] The monomer, lactide, is a cyclic diester that can be derived from annually renewable natural sources such as corn starch or sugar beet. The polymer product, poly(lactic acid) (PLA), is biodegradable *via* the hydrolysis of the ester bonds in the backbone.[56] Importantly, as the polymer and its metabolites are non-toxic for the human body, PLA is also considered to be biocompatible and therefore it is an excellent choice for food packaging and implants.[57] The ROP of lactide is now commercialised in the production of a broad range of sustainable plastics, from textiles, fibres, packaging materials to the more sophisticated biomedical devices.[58] Similarly to polymers obtained *via* ATRP, the molecular weight and dispersity of the PLA can strongly influence its mechanical and thermal properties. In addition, lactide has three distinct diastereomers: *L*-, *D*- and *meso*-lactide, and the 1:1 racemic mixture of *L*- and *D*-lactide is termed '*rac*-lactide' (Figure 9).[56] Depending on the catalyst and reaction conditions of the polymerisation, the obtained PLA may feature isotactic, heterotactic and syndiotactic linkages in different ratios. The control over this tacticity also significantly impacts the characteristics (such as melting point or brittleness) of the polymer.[55] Alternatively, PLA can also be obtained *via* the step-growth polycondensation of lactic acid, however, this method generally provides lower control compared to the ROP of lactide.[55]

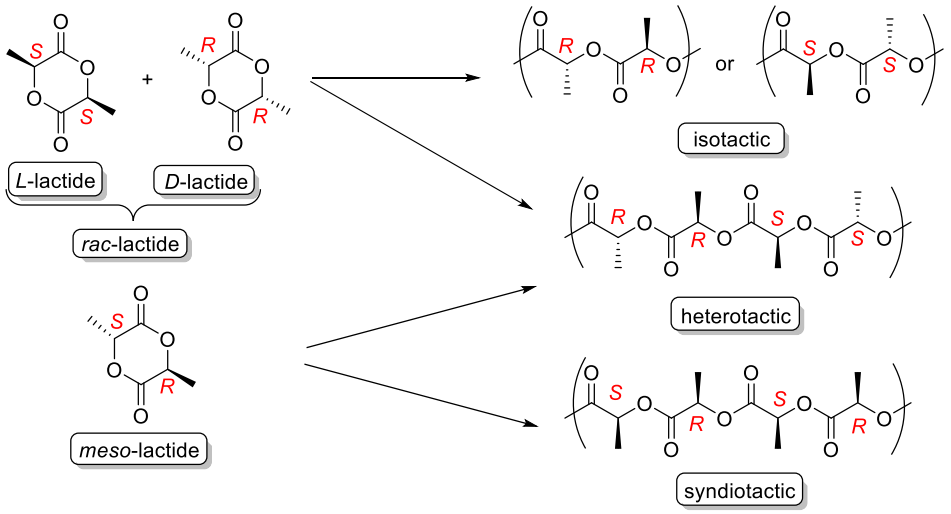

Figure 9: Structures of different lactide stereoisomers and different PLA tacticities.

While anionic, nucleophilic and cationic polymerisation strategies also exist, the ROP process most commonly occurs through a coordination-insertion pathway catalysed by Lewis acidic metal-alkoxide species (Scheme 3).[55] The mechanism – first proposed by Dittrich and Schulz in 1971 – starts with the coordination of the lactide carboxyl group to the metal centre.[59] During propagation, the alkoxide (M-*OR*) attacks the activated carbonyl, and a subsequent ring-opening results in the formation of a new, chain-extended metal alkoxide species. The driving force behind the opening of the six-membered lactide ring is the relief of the increased strain resulting from the presence of two connected planar ester groups.[60] Upon termination, the hydrolysis of the active metal-alkoxide bond leads to the formation of hydroxyl end groups.

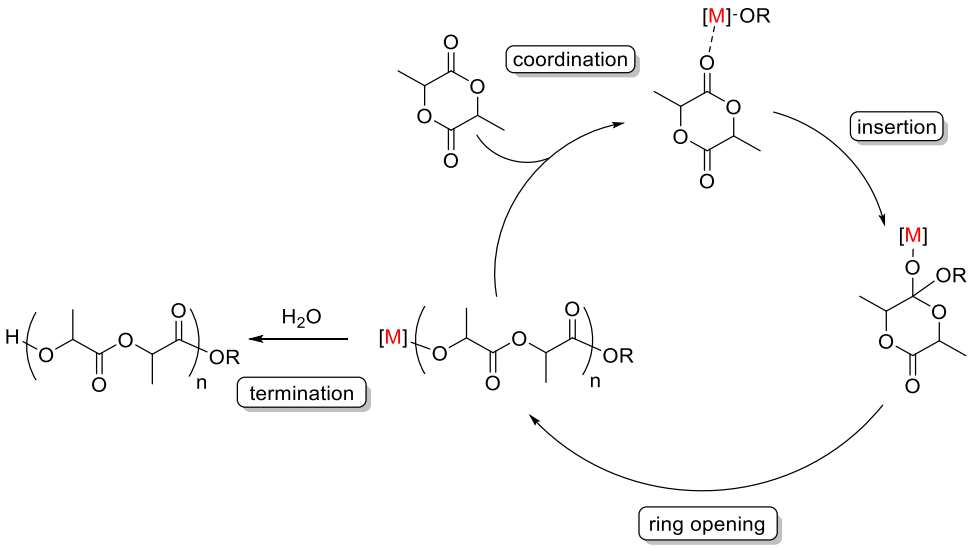

Scheme 3: Proposed coordination-insertion mechanism of the ROP of lactide.[55]

Following the pioneering work of Kleine *et al.* in the 1950s,[61] the metal-catalysed method became predominant in lactide ROP. Notably, organocatalysts have been also successfully applied, but their

detailed introduction is outside of the scope of this summary.[55] As a Lewis acidic metal promotor for ROP, tin octanoate [Sn^{II} bis(2-ethylhexanoate), Figure 10, left] was traditionally employed, which remains the catalyst of choice in most of the current industrial procedures.[62] This catalyst provides excellent activity, however, the requisite relatively harsh reaction conditions often lead to undesired side-reactions and consequently reduce the control over the polymerisation.[55] While tin octanoate is FDA approved, its potential toxicity is often problematic, especially when the PLA is used for biomedical applications.[63] Alternatively, Al-alkoxide catalysts (especially Al isopropoxide, Figure 10, right) have been extensively studied in the ROP of lactide, achieving moderate conversions.[55] It was shown that these complexes were prone to aggregate (most commonly tetramer) formation, which led to the growth of multiple polymer chains per catalyst, complicating the catalyst characterisation and the mechanistic understanding.[64]

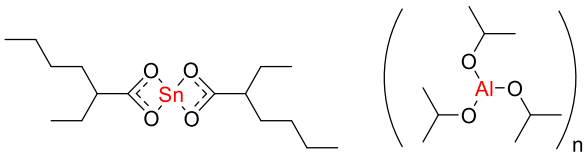

Figure 10: Structures of Sn octanoate and Al isopropoxide catalysts.

From the 1980s an intensive effort to develop selective ROP catalysts has led to a plethora of new metal-alkoxide complexes.[58] These well-defined, single-site complexes enabled a deeper mechanistic insight into the reaction, with just one polymer chain growing per metal centre. Consequently, catalysts based on a range of metals, including Ti, Sn and Zn, as well as rare-earth metals have been investigated.[65-67] Al-based complexes supported by various N- and O-donor ligands showed exceptionally high activities and became popular catalysts for controlled lactide ROP.[13] In the early 1990s, Spassky *et al.* described the use of chiral Al salen complexes (Figure 11, left) that provided high control over the tacticity of the obtained PLA.[68] Following these early studies, salen-type complexes with a broad scope of metals have been designed for stereoselective ROP catalysis.[69] Thakur and co-workers developed a method based on homonuclear decoupled ^{1}H NMR spectroscopy to determine and quantify the degree of control over the tacticity of the obtained PLA, introducing the isotactic bias (P_i) values.[70] In the following years, another significant catalyst family was developed by Coates *et al.*: β-diketiminato (BDI) Zn alkoxide complexes (Figure 11, right) demonstrated high activity and selectivity towards heterotactic PLA at ambient temperatures.[71]

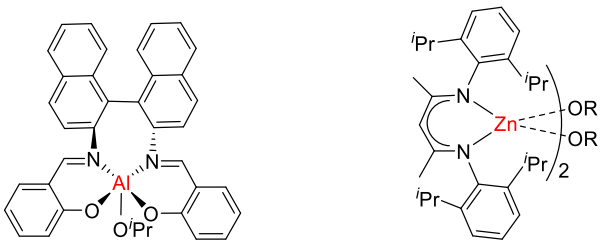

Figure 11: Structures of Al salen [68] and Zn BDI alkoxide complexes.[71]

Iron catalysts are especially attractive candidates for lactide polymerisation considering the aforementioned *in vivo* applications of PLA, where residual traces of a toxic metal in the polymer may be problematic. However, surprisingly few papers describe efficient Fe-based catalyst systems.[55, 72-76] In the early stages of ROP catalyst development, Kricheldorf and co-workers employed simple Fe oxides and Fe salts such as carboxylates. These catalysts showed relatively low activity, requiring harsh reaction conditions and long reaction times (often days) to polymerise lactide.[76, 77] Consequently, the large proportion of transesterification and epimerisation side-reactions eliminated the possibility of well-controlled molecular weights or tacticities. In search for more defined and structurally characterised catalysts, Hillmyer and Tolman applied $Fe_5(\mu_5\text{-}O)(OEt)_{13}$ clusters that achieved high conversions and relatively narrow dispersities ($Đ$ = 1.1-1.2).[72] Through the introduction of bulkier alkoxide groups, the catalyst structures could be further simplified to form dimers, which included heterobimetallic Na-Fe^{II} species.[78] Later, the same group also reported on the use of single-site Fe amidinate complexes (Figure 12, left), but surprisingly these were poorer catalysts than the aforementioned alkoxide clusters.[73] In 2002 Gibson *et al.* developed a series of Fe^{II} BDI complexes (Figure 12, middle) as one of the first examples of efficient, well-defined, single-site Fe catalysts for the ROP of lactide.[74] More recently, Byers and co-workers designed a range of bis(imino)pyridine Fe alkoxide catalysts (Figure 12, right) and showed that the polymerisation was sensitive to both the oxidation state and the electron density of the metal.[79, 80] Complexes of the ubiquitous salen ligand with Fe^{II} have been investigated by Idage *et al*. in the ROP of L-lactide.[81]

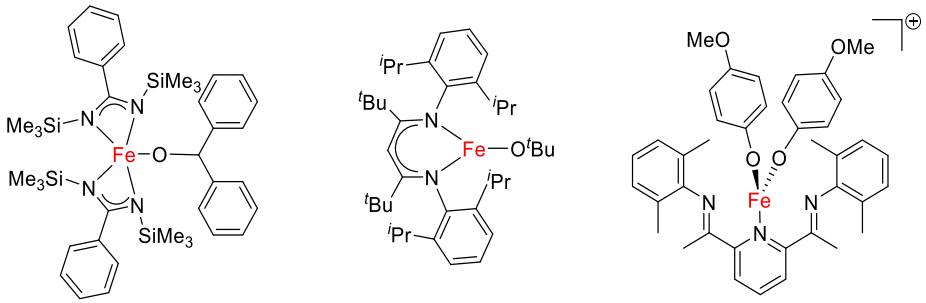

Figure 12: Structures of Fe amidinate,[73] Fe BDI [74] and Fe bis(imino)pyridine catalysts for the ROP of lactide. [83]

The synthesis, purification and handling of most of these metal-alkoxide catalysts is relatively difficult due to their high air- and moisture-sensitivity, which is a significant drawback for potential industrial applications. On a laboratory scale, the alkoxides are typically formed *via* the *in situ* conversion of an equally or more labile metal-alkyl group through the addition of an alcohol.[58] To circumvent issues with the sensitivity, metal alkoxides can be generated *in situ* from the more robust metal-chlorides, *via* the addition of an epoxide, such as propylene oxide (PO). This method was first described by Maron *et al.* using Al-based catalyst systems,[82] and was later successfully extended to Fe-based catalysts.[83-85] The proposed mechanism starts with the insertion of ring-opened PO into the Fe-Cl bond to form the catalytically active Fe-alkoxide (Scheme 4).

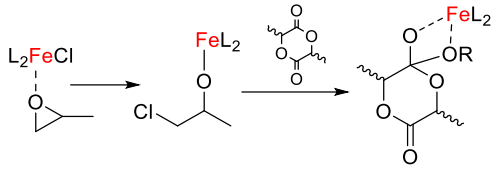

Scheme 4: Proposed initiation mechanism of in situ Fe-alkoxide catalysed lactide polymerisation.[83]

Exploiting this PO-triggered initiation strategy, Duan and co-workers employed salen-based Fe^{III} catalysts (Figure 13, left),[83] while Lamberti *et al.* used related salen, salan and salalen Fe^{III} derivatives (Figure 13, right) in the ROP of lactide.[84] In all cases, the addition of a massive excess (>2000 equivalents) of the carcinogenic PO was required to achieve good conversions, hence greatly reducing the atom efficiency and biocompatibility of these reactions.

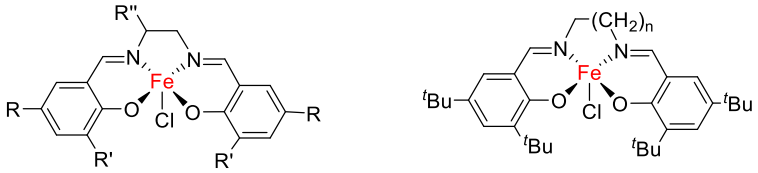

Figure 13: Structures of salen-type Fe^{III} chloride complexes for the PO-triggered initiation of ROP. [83, 84]

Critical evaluation

Although their current industrial volume does not reach the capacity of the highest-scale polymerisation methods, both ATRP and lactide ROP are among the most rapidly developing areas of polymer science. Both techniques have been already commercialised for the production of specialty polymers and materials for advanced technologies,[86] moreover, continuously appearing patents and publications indicate further interest to expand their applications. In particular, the production of the biodegradable PLA is expected to rapidly increase in the following years, as it may offer an attractive replacement for petrochemical-based single-use plastics that are currently being phased out of the

western world. Consequently, the development of active and selective catalyst systems for these processes is of crucial importance.

In the field of ATRP, significant improvements have been achieved in the past decades, which include lowering the catalyst concentration and/or implementing efficient catalyst removal to avoid the toxicity and discolouration problems associated with the dominating Cu-based catalyst systems.[87] Among the novel catalysts featuring alternative metals, the non-toxic iron is an ideal choice to circumvent these issues. While scarcely studied, the oxidatively stable Fe^{III} mediators offer the advantage of facile synthesis and application in reverse ATRP processes.

Despite the ROP of lactide has been receiving increasing attention, the continuous research towards more active and stereoselective catalysts remains important. Moreover, the practical aspects of finding air-stable systems, preferably featuring a non-toxic metal pose further challenges. The recently emerging idea of *in situ* Fe-alkoxide generation is an elegant way to bypass the air- and moisture-sensitivity issues of conventional ROP catalysts, however, the large excess of carcinogenic epoxide used can compromise the otherwise green reaction.

Aims

The presence of the Fe-Cl bond in the half salen complexes **C1**-**C8** (described in Chapter 3) provided the possibility of their application as catalysts in R-ATRP and ROP processes. As the pro-ligands (**L1**-**L8**) feature stereoelectronically diverse properties, we aimed to explore their structure-activity relationships with consideration of the polymerisation control.

Initially, the plan was to screen the Fe^{III} half salen complexes as non-toxic mediators in R-ATRP reactions using styrene and methyl methacrylate as benchmark monomers. We also wished to investigate the role of reaction temperature, therefore two different initiators were tested.

Moreover, we aimed to exploit half salen Fe^{III} chloride complexes for the ROP of *rac*-lactide, initiated by the *in situ* ring-opening of PO. To improve the sustainability of the reaction, our goal was to minimise the amount of propylene oxide and to understand whether the polymerisation could still be efficient.

Results and discussion

A series of eight novel half salen Fe^{III} chloride complexes **C1**-**C8** (Figure 14) first described in Chapter 3 were employed as catalysts in radical and ring opening polymerisation reactions.

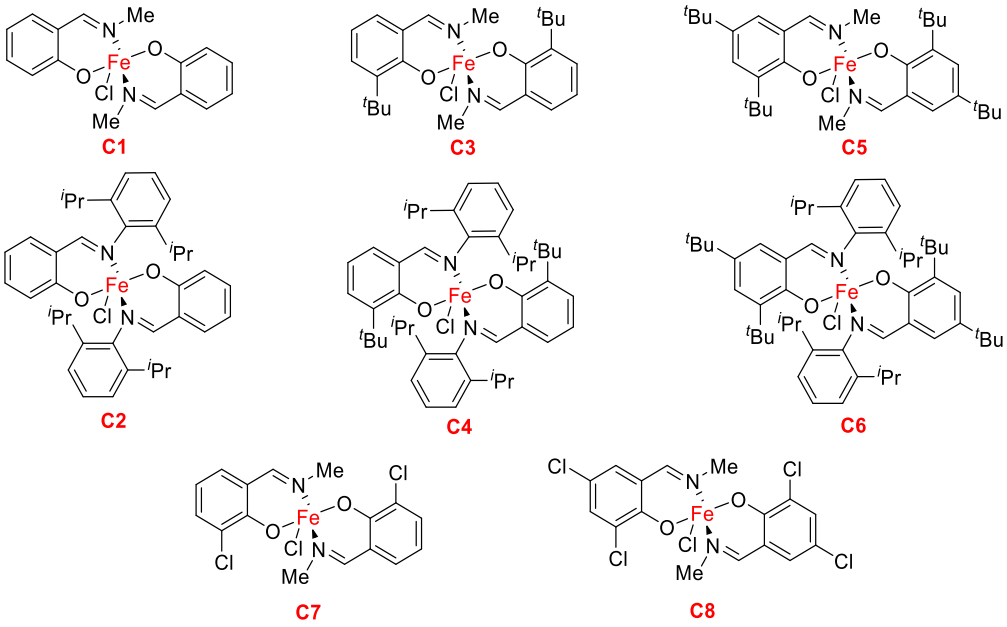

*Figure 14: Structures of Fe^{III} half salen complexes **C1**-**C8**.*

Atom transfer radical polymerisation

Reverse ATRP of styrene

Complexes **C1**-**C8** were screened as mediators in the R-ATRP of styrene. Reaction conditions were selected following standard protocols developed by the Shaver group, with 100 equivalents of monomer versus catalyst and an equivolume amount of toluene solvent.[47, 49] Conventional azo-initiators were applied as the radical source, in a slight excess of 0.6 equivalents (versus catalyst), as each of these initiators generates two alkyl radicals upon thermal decomposition. To allow the investigation at different temperatures, two different initiators were employed: reactions with 2,2'-azobisisobutyronitrile (AIBN, Figure 15, left) were carried out at 120 °C, while reactions with 2,2'-azobis(4-methoxy-2,4-dimethylvaleronitrile) (V-70, Figure 15, right) were performed at 75 °C to ensure instantaneous, quantitative radical formation.

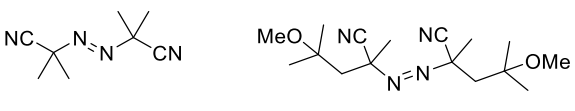

Figure 15: Structures of AIBN and V-70 radical initiators.

The monomer conversions were determined *via* ^{1}H NMR spectroscopy by integrating characteristic polymer peaks against the residual styrene peaks in the spectra of the crude reaction mixtures (Figure 16). To ensure reproducibility, the polymerisation reactions were carried out multiple (2-3) times, affording less than 5% experimental error in conversions. However, the precipitation of the polymers in acidified methanol was not always successful (especially at low conversions), which made the GPC analysis of certain products unfeasible. The tables below contain selected representative data from reactions, where molecular weight and dispersity values were available.

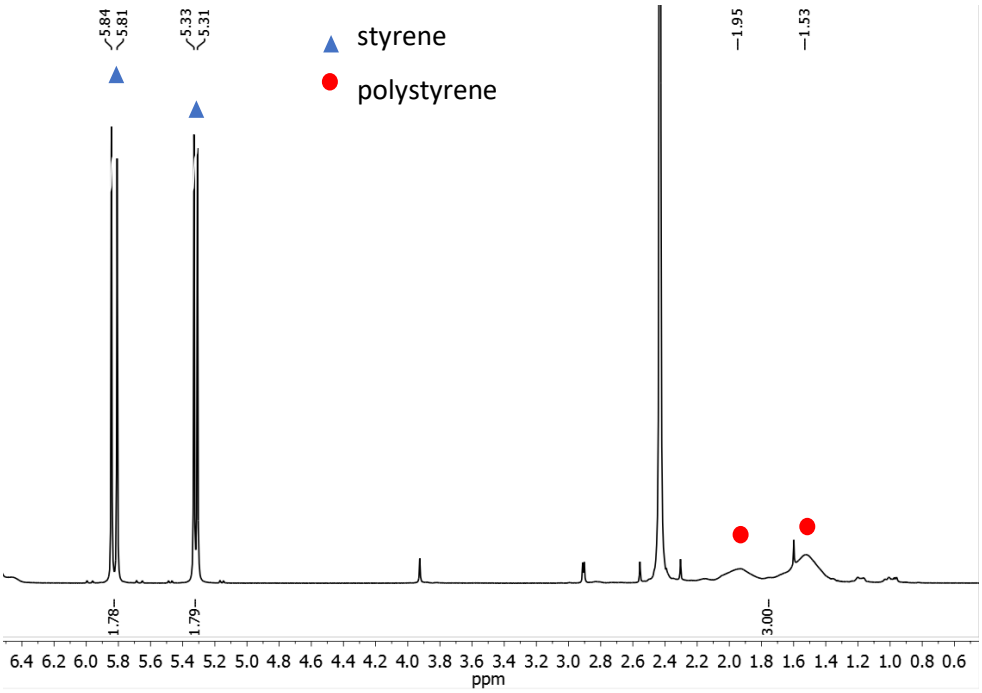

Figure 16: Typical ^{1}H NMR spectrum of a styrene ATRP crude reaction mixture in $CDCl_3$ at 20 °C. Conversion was determined via integration of the multiplet polymer peaks 2.2-1.2 ppm against the $=CH_2$ styrene (starting material) peaks at 5.31 and 5.81 ppm.

After 2 hours, modest to high (23-79%) conversions were achieved using **C1**-**C8** in the R-ATRP of styrene (Table 1). Following the trend of increasing Lewis acidity of the Fe centre (by introducing electron withdrawing chloro substituents on the ligand) the conversion using complexes **C1**, **C7** and **C8** (entry 1, 7 and 8) gradually increased. The obtained polystyrene samples were purified, dried and examined *via* gel permeation chromatography (GPC) with triple-detection to determine the average molecular weight and dispersity values. Complexes **C3** and **C6** provided a moderate degree of control ($Đ$ = 1.40 to 1.48), while **C1**, **C2**, **C5** and **C7** were relatively poor mediators providing broad dispersities ($Đ$ > 1.5). The observed conversions and dispersities fall in line with results using Fe^{III} ABP mediators (Figure 8) under similar conditions.[88] Along with providing one of the highest conversions (56%) the dichloro substituted **C8** also displayed the lowest dispersity ($Đ$ = 1.19, entry 8), which is comparable to the best values reported for Fe^{III} R-ATRP systems.[49, 89] This also corresponds to previous findings by Shaver *et al.* who achieved lower dispersities using ABP complexes substituted with electron

withdrawing (Cl) groups in comparison to alkyl substituted analogues.[88] However, in most cases (entries 2, 5-8), the number average molecular weights (M_n) were in excess of the theoretical values ($M_{n,th}$) predicted using the initial concentration of the mediator. This may indicate a limited number of growing polymer chains, potentially due to inefficient initiation or rapid radical termination reactions.[47]

Table 1: R-ATRP of styrene with AIBN initiator.

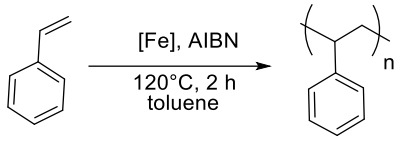

entry	complex	conversion (%)	$M_{n,th}$ (Da)	M_n (Da)	$Đ$
1	**C1**	29	3000	3800	1.65
2	**C2**	61	6400	11600	1.71
3	**C3**	34	3500	4000	1.48
4	**C4**	40	4200	4200	1.43
5	**C5**	79	8200	15500	2.21
6	**C6**	23	2400	4200	1.40
7	**C7**	45	4700	14200	1.63
8	**C8**	56	5800	10900	1.19

Conditions: [styrene]:[Fe^{III}]:[AIBN] = 100:1:0.6, styrene : toluene = 1:1 (v/v), 120 °C, 2 hours. $M_{n,th\ [Fe]}$ = $[styrene]_0/[Fe]$ x M(styrene) x conversion.

As expected, the lower temperature reactions using V-70 initiator featured lower propagation rates and consequently led to lower conversions and slightly narrower molecular weight distributions (Table 2). Most of the Fe^{III} half salen complexes showed moderate control under these reaction conditions. Of particular interest is catalyst **C6**, which was an excellent mediator affording polystyrene with very narrow dispersity ($Đ$ = 1.05, entry 6) and good agreement between the theoretical and experimental molecular weights. This may suggest that the electron donating ^{t}Bu substituents can stabilise the reduced Fe^{II} species during the R-ATRP process by decreasing its Lewis acidity and therefore efficiently limiting the concentration of active chains. On the contrary, when the corresponding ligand **L6** was investigated by Gibson *et al.* in a mono-chelated $LFeCl_2$ complex, poor control was achieved in the polymerisation of styrene, attributed to the relative instability of the reduced tricoordinate Fe^{II} species.[45] Interestingly, mediator **C5** with identical ^{t}Bu substituents on the phenol moiety displayed significantly lower control, which can be tentatively linked to the lack of steric hindrance and thus protection of the coordination sphere by the DIPP group on the imine.

Table 2: R-ATRP of styrene with V-70 initiator.

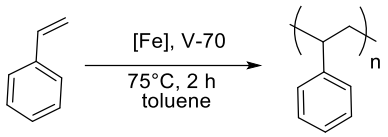

entry	complex	conversion (%)	$M_{n,th}$ (Da)	M_n (Da)	$Đ$
1[a]	**C1**	18	1900	3600	1.43
2	**C2**	36	3800	6800	1.46
3	**C3**	24	2700	4000	1.46
4	**C4**	31	3200	3300	1.45
5	**C5**	33	6800	13800	1.77
6	**C6**	25	2600	2600	1.05
7	**C7**	23	2400	6000	1.40
8[a]	**C8**	14	1500	5700	1.23

Conditions: [styrene]:[Fe^{III}]:[V-70] = 100:1:0.6, styrene : toluene = 1:1 (v/v), 75 °C, 2 hours. [a] Insufficient polymer was precipitated after 2 hours to allow analysis, therefore a sample precipitated after 4 hours reaction time was used.

Considering the catalytic efficiency of **C1**-**C8** at both reaction temperatures, kinetic experiments were performed using complex **C8** as the top-performing representative in combination with AIBN initiator. The reaction kinetics deviated slightly from the expected first-order dependence on monomer concentration (Figure 17, left), which indicated the presence of competing side-reactions (*vide infra*). The molecular weights increased linearly with conversion (Figure 17, right), suggesting a controlled polymerisation process. Notably, this trendline does not go through the origin, but would cross the axis around the 1100 Da value. Due to issues with the precipitation at low conversions (below 20%), GPC analysis of the polymer products in this region was not possible. As the experimental molecular weights (M_n) in Table 1 were consistently higher than the theoretical values ($M_{n,th}$), this phenomenon was tentatively attributed to inefficient initiation.

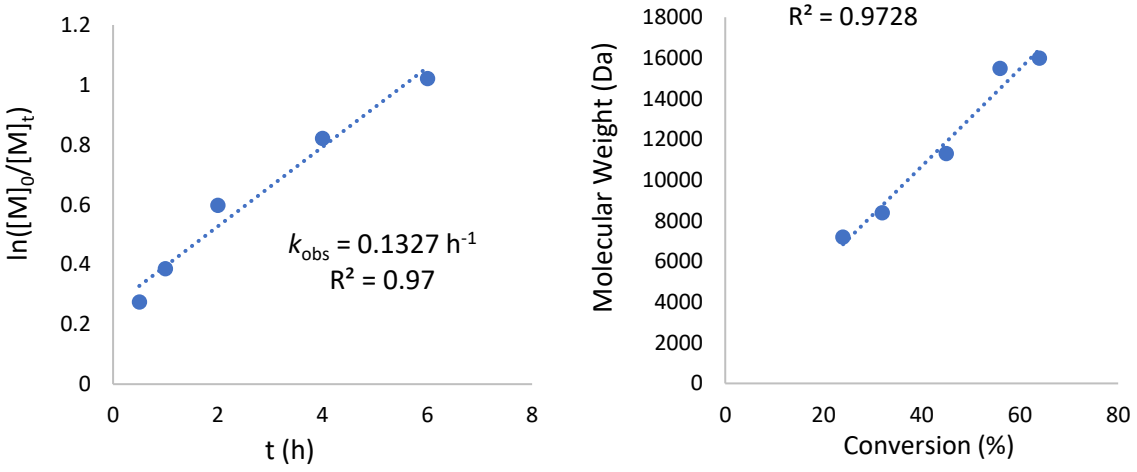

*Figure 17: Kinetic plots of styrene ATRP using AIBN initiator and **C8** as mediator.*

To provide insight into the nature of the polymer end groups, the purified polystyrene samples were further investigated by ^{1}H NMR spectroscopy (Figure 18). Besides the expected broad resonance for the halide capping group (ClC*H*(Ph)CH_2 at 4.4 ppm), the strong presence of olefin terminated polymer chains was also observed, as indicated by diagnostic doublets at 5.27 and 5.78 ppm. These peaks have been also detected in the spectra of crude, unpurified reaction mixtures using all eight half salen complexes (**C1**-**C8**), indicating that the unsaturated chain ends are formed during the polymerisation and not during the purification procedure. To quantify the proportion of olefin terminated chains, the integration of these peaks was attempted. Unfortunately, this led to extreme variability and irreproducible results due to the large error when integrating against the olefin resonances against the relatively very large and broad peaks arising from the aliphatic polymer backbone (0.8-2.2 ppm).

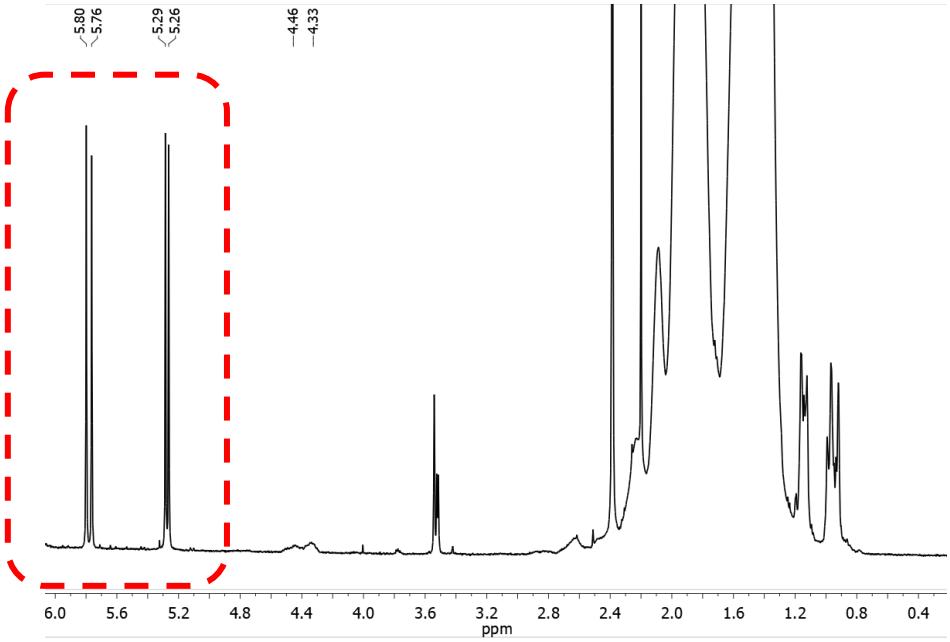

Figure 18: ^{1}H NMR spectrum of a purified polystyrene sample showing doublet peaks of olefin terminated polymer chains formed via CCT ($CDCl_3$, 20 °C).

The deviation from first order kinetics and the presence of olefin terminated polymer chains strongly suggested that catalytic chain transfer (CCT) side-reactions occur, which is a commonly observed competing mechanism in ATRP and OMRP systems. CCT is proposed to proceed through a H-atom transfer from the β carbon atom of an active radical chain to the reduced M^x complex, resulting in a terminated polymer chain with an unsaturated end-group and a metal-hydride complex, M^{x+1}-H (Scheme 5). The latter can subsequently transfer the H-atom to a new monomer, starting the growth of a new polymer chain.[90, 91] Alternatively, the olefin terminated chains can also form through β hydrogen elimination from the organometallic species that may arise *via* the OMRP mechanism. CCT is often shown to compete with ATRP and OMRP mechanisms, especially in Fe mediated systems.[47, 48]

As CCT typically leads to the formation of shorter polymer chains, lower molecular weights and broader dispersities are expected in the final product. While the M_n values were lower than expected, GPC analysis of the polystyrene samples obtained from the kinetic experiments (using **C8** and AIBN) showed that the molecular weights increased linearly with the conversion (Figure 17). This may suggest only a small contribution of the CCT mechanism when using **C8** as mediator in the R-ATRP of styrene.

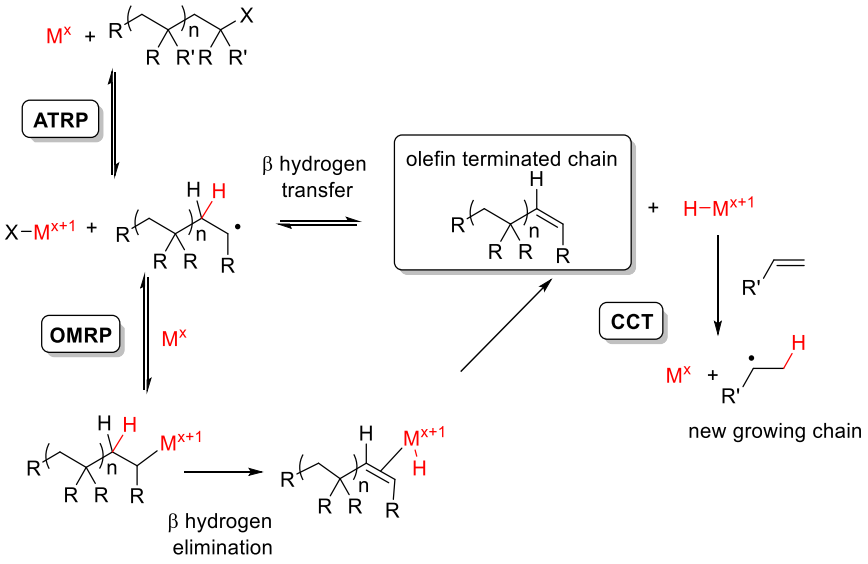

Scheme 5: Proposed mechanisms of catalytic chain transfer (CCT).[43]

Reverse ATRP of methyl methacrylate

The R-ATRP of methyl methacrylate (MMA) using **C1**-**C8** as mediators and AIBN initiator afforded moderate to good conversions (28-85%, Table 3). GPC analysis showed that the molecular weights of the polymers (M_n) were significantly in excess of the theoretical values ($M_{n,th}$), which is a common phenomenon when using MMA with azo initiators.[47] Similarly to styrene reactions, this may indicate the loss of a significant number of radicals before the ATRP equilibrium is established. The complexes were found to be moderate to poor mediators achieving relatively broad dispersities ($Đ$ = 1.43-2.23). The exception was the unsubstituted half salen complex **C1**, which exerted a good control ($Đ$ = 1.14) at the low conversion of 28%. This observation is consistent with the general principle in normal ATRP, where the mediator must be fine-tuned so that the polymerisation rate is sufficiently rapid, but not so active that radical termination dominates the reaction.[92] Moreover, the aforementioned affinity of **C1** to form dimeric species (*vide supra*) with increased steric crowding around the metal centres might have also contributed to the increased selectivity.

Table 3: R-ATRP of methyl methacrylate with AIBN initiator.

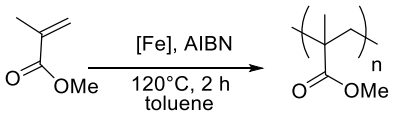

entry	complex	conversion (%)	$M_{n,th}$	M_n	$Đ$
1	**C1**	28	2800	8400	1.14
2	**C2**	76	7600	17000	1.81
3	**C3**	47	4700	12700	1.56
4	**C4**	85	8500	18400	1.43
5	**C5**	61	6100	16700	2.23
6	**C6**	65	6500	22800	1.43
7	**C7**	68	6800	18900	1.73
8	**C8**	64	6400	16100	1.76

Conditions: [MMA]:[Fe^{III}]:[AIBN] = 100:1:0.6, MMA : toluene = 1 : 1 (v/v), 120 °C, 2 hours. Conversion was determined using ^{1}H NMR spectra of crude reaction mixtures

Unlike the styrene experiments, the R-ATRP of MMA using the lower temperature initiator (V-70) did not lead to significantly lower conversions (24-68%, Table 4). This may indicate that the reactions have been limited by the rate of initiation. With the exception of **C1**, the relatively broad dispersities ($Đ$ = 1.39- 2.29) suggest that under these conditions the steric bulk at the imine position of the ligands does not have a significant effect upon the degree of control.

Table 4: R-ATRP of methyl methacrylate with V-70 initiator.

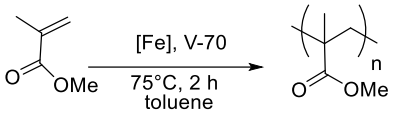

entry	complex	conversion (%)	$M_{n,th}$	M_n	$Đ$
1	**C1**	30	3000	13000	1.24
2	**C2**	66	6600	18900	2.29
3	**C3**	24	2400	18800	1.49
4	**C4**	68	6800	15700	1.43
5	**C5**	54	5400	16500	1.89
6	**C6**	62	6200	14900	1.39
7	**C7**	62	6200	19400	1.56
8	**C8**	63	6300	16400	1.43

Conditions: [MMA]:[Fe^{III}]:[V-70] = 100:1:0.6, MMA : toluene = 1 : 1 (v/v), 75 °C, 2 hours. Conversion was determined using ^{1}H NMR spectra of crude reaction mixtures.

Kinetic experiments were carried out using the top representative, **C1,** as mediator and AIBN as initiator. As Figure 19 shows, the reaction slowed down considerably in comparison to first order behaviour reaching a plateau at moderate conversions (28% after 2 hours). This deviation was more significant than that observed with styrene, suggesting that along with CCT other mechanisms such as OMRP may more intensely interplay.[43, 91] A light purple colour of some of the polymer samples indicated the presence of chains capped with the metal mediator, which may also suggest a competing OMRP mechanism (Scheme 5). This ATRP-OMRP-CCT interplay has been previously reported for several Fe mediated systems.[28, 88] Similarly to the reactions carried out with styrene, the molecular weights increased linearly with conversion (Figure 19, right), featuring a trendline that did not cross the origin. This observation, along with the higher than expected experimental molecular weights indicates a slow rate of initiation in comparison to the rate of propagation.[88] Shaver *et al.* observed similar trends using Fe^{III} ABP complexes in the R-ATRP of styrene, where the reaction rate was significantly higher in the first 20 minutes.[88]

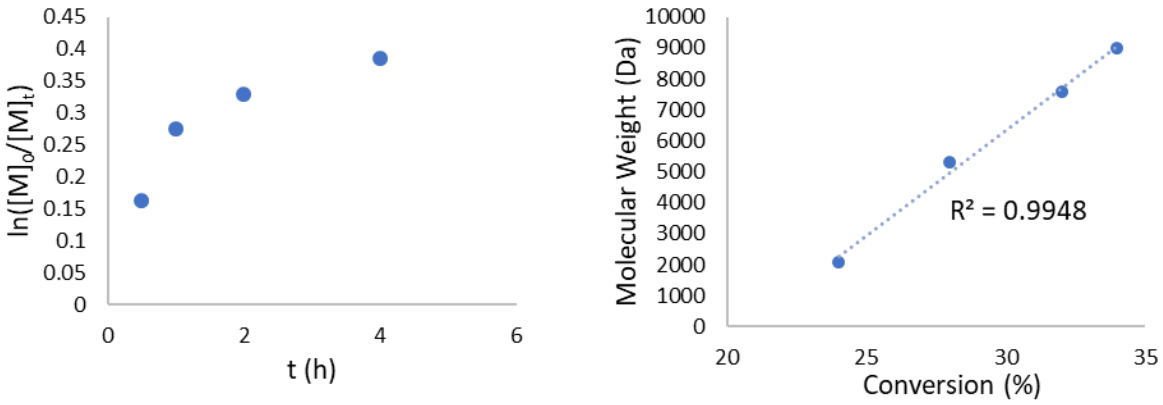

*Figure 19: Kinetic plots of MMA ATRP using AIBN initiator and **C1** as mediator.*

The ^{1}H NMR analysis of the purified pMMA samples also revealed the presence of olefin terminated polymer chains (Figure 20). The integrals of these peaks were relatively small compared to the polymer peaks, which suggested that the CCT mechanism was less prevalent than in the ATRP of styrene. In addition, on the basis of ^{1}H NMR signals, the proportion of halogen capped chains ends was lower than expected, which also corroborates the possible involvement of OMRP mechanisms.

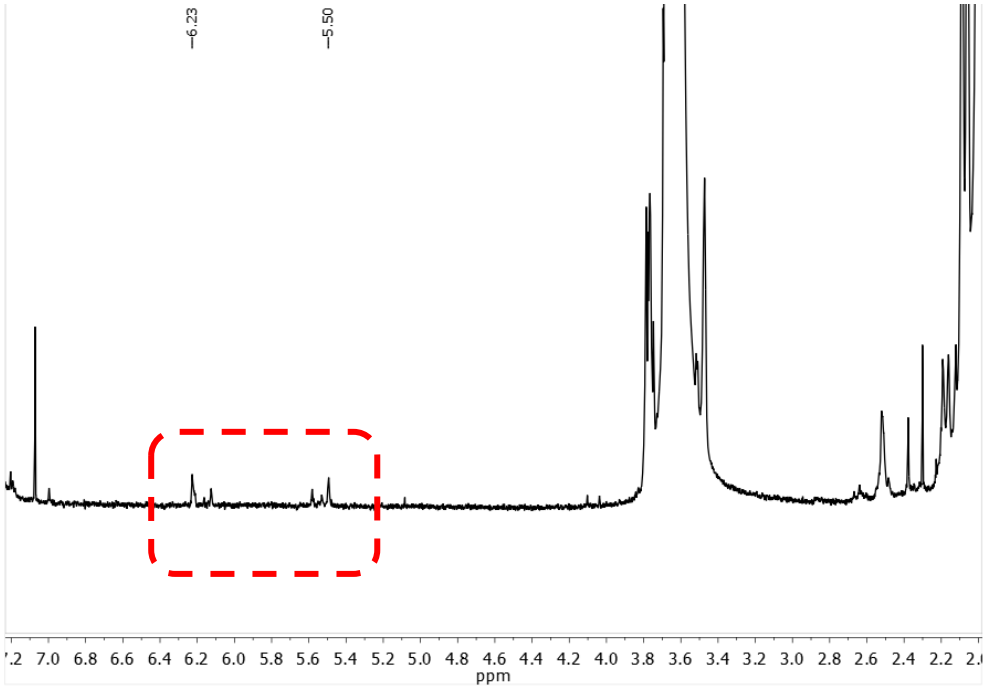

Figure 20: Typical ^{1}H NMR spectrum of a purified pMMA sample, showing olefin terminated polymer chains formed via CCT.

As our main goal was to test the activity and control of the Fe^{III} half salen complexes under standard R-ATRP conditions, further mechanistic investigation of these systems was outside the scope of this work. Concluding the results, **C1**-**C8** were moderately active and selective mediators in the R-ATRP of both styrene and MMA. The observed first order rate constants (k_{obs} ≈ 0.13 h^{-1} for styrene, and k_{obs} ≈ 0.22 h^{-1} for the linear stage of MMA polymerisation) fall below the activity of other Fe mediated R-ATRP systems.[45, 49, 88] The significant contribution of competing mechanisms such as CCT and possibly OMRP may have reduced the differences in structure-activity relationship of the diversely substituted individual complexes.

Ring opening polymerisation of lactide

The eight half salen Fe^{III} chloride complexes, **C1**-**C8**, were also tested as catalysts for the ROP of *rac*-lactide following the aforementioned technique using propylene oxide (PO) to *in situ* generate the active Fe-alkoxide species. The monomer conversions were determined *via* ^{1}H NMR spectroscopy by integrating characteristic polymer peaks against the residual monomer peaks in the spectra of the crude reaction mixtures (Figure 21). The lack of characteristic polyether peaks in the ^{1}H NMR spectra indicated that the propylene oxide was not incorporated into the polymer chains under the applied reaction conditions.[93] This observation is in contrast with reports using Al chloride complexes that formed block copolymers in the presence of a larger ratio of PO.[94]

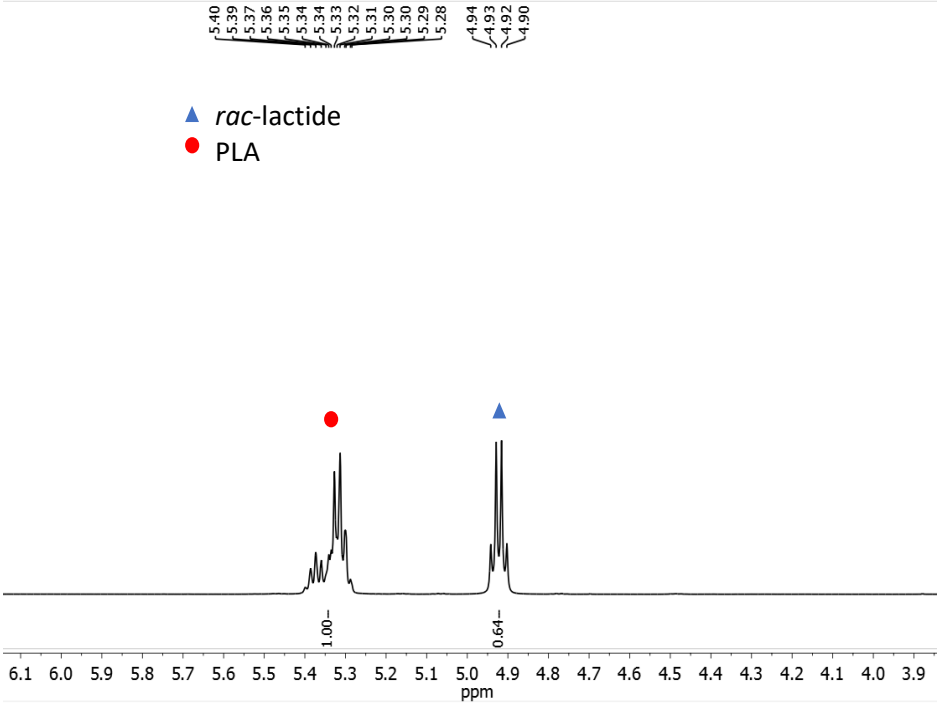

Figure 21: Typical ^{1}H NMR spectrum of a rac-lactide ROP crude reaction mixture in $CDCl_3$ at 20 °C. Conversion was determined via integration of the CH-CH_3 polymer (product) peak 5.28-5.40 ppm against the CH-CH_3 lactide (starting material) peak at 4.90-4.92 ppm.

The polymerisations were carried out with 1 mol % Fe catalyst (versus lactide) in toluene as solvent. Contrary to the previously reported procedures, we aimed to avoid the excessive use of PO (as both reagent and solvent), which would compromise the benefits of the relatively 'green' Fe/lactide system due to its high toxicity. Optimisation of the PO/Fe ratio using catalyst **C8** showed that a high conversion of lactide can be achieved with as low as 50 equivalents of PO when the reaction was carried out at 120 °C for 24 hours (Table 5, entry 1). This modification enabled the polymerisations to be performed in airtight vials instead of the autoclaves reported in the literature procedures, as the partial pressure of PO upon heating became negligible. Notably, further reduction of the PO ratio (1-20 equivalents,

entry 2-4) only afforded traces of PLA. These findings fall in line with previous reports from Duan *et al.* who investigated the effect of PO concentration on the activity of salen Fe^{III} chloride complexes. They reported that upon reducing the PO/Fe ratio from 500 to 100 equivalents (and substituting the missing PO volume with toluene as solvent), the conversion dramatically dropped from 60% to 15%.[83] Control reactions using catalyst **C8** without the PO additive (entry 5) or the PO activator alone (entry 6) led to no conversion, indicating that both catalyst components are essential for the efficient initiation.

*Table 5: ROP of rac-lactide with **C8** catalyst and PO activator.*

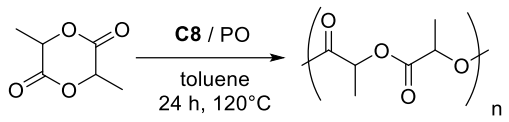

entry	complex	PO (eq./Fe)	conversion (%)
1	**C8**	50	89
2	**C8**	1	3
3	**C8**	5	4
4	**C8**	20	5
5	**C8**	-	0
6	-	50	0

*Conditions: 0.01 mmol **C8**, 1 mmol rac-lactide, 0.5 mmol PO, 1 ml toluene, 24 h, 120 °C.*

In the presence of 50 equivalents of PO activator, all eight Fe^{III} half salen complexes **C1**-**C8** polymerised *rac*-lactide with nearly complete conversions (89-95%, Table 6). GPC analysis of the purified PLA samples using a triple-detection system showed inconsistent molecular weights (ranging from 1.5 to 40.6 kg/mol) and relatively broad dispersities (*Đ* = 1.40-1.81), indicating poor control over the polymerisation. These features are commonly observed in lactide ROP at high conversions and are often attributed to the presence of transesterification side-reactions, which generally lead to a broader molecular weight distribution. For example, Gibson *et al.* reported that transesterification becomes competitive at low monomer concentrations using Fe^{II} alkoxide catalysts.[74] The relatively long reaction time (24 h) and a high reaction temperature (120 °C) are also known to give rise to such side-reactions.[55] The few previously reported examples using the *in situ* PO-triggered initiation method all describe polymers with broad dispersities, including a recent study from Chen and co-workers who obtained PLA with *Đ* values up to 2.1 using Fe^{III} salen complexes under similar reaction conditions.[85] This may be linked to the relatively slow ring opening of the epoxide by the metal halides that leads to variable initiation rates (*vide infra*).

*Table 6: ROP of rac-lactide using catalysts **C1**- **C8**.*

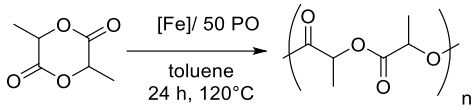

entry	complex	conversion (%)	$M_{n,th}$ (Da)	M_n (Da)	$Đ$
1	**C1**	95	13700	8800	1.40
2	**C2**	95	13700	1500	1.70
3	**C3**	95	13700	3300	1.41
4	**C4**	95	13700	9000	1.59
5	**C5**	93	13400	40600	1.61
6 [a]	**C6**	95	13700	2100	-
7	**C7**	93	13400	12600	1.81
8	**C8**	89	12800	17200	1.48

Conditions: 0.01 mmol [Fe], 1 mmol rac-lactide, 0.5 mmol PO, 1 ml toluene, 24 h, 120 °C. [a] GPC analysis of the polymer sample showed a bimodal polymer with ambiguity determining the Đ.

The obtained PLA samples were also analysed with MALDI-ToF mass spectrometry to investigate the nature of the polymers' repeating units and chain end groups. In addition to the expected lactide repeating units (144.1 Da), equally intense intervals corresponding to a half lactide (72.05 Da) could be detected (Figure 22). This observation further corroborates the strong prevalence of transesterification reactions, as starting from a dimeric monomer (lactide), PLA chains with an odd number of lactic acid units can only form *via* the cleavage of an even-numbered poly(lactide) chain. In accordance with insertion of the PO activator into the Fe-Cl bond (Scheme 4), the spectra showed a series of chains terminated by -OCH(Me)CH_2Cl groups (Figure 23). Notably, upon initiation the ring opening of the asymmetric PO can occur *via* nucleophilic attack of either α-C, giving rise to two possible end groups with identical molecular weights (93 Da). The ^{1}H NMR spectra of the quenched polymer products did not provide conclusive information regarding this question. As the paramagnetic nature of the Fe^{III} complexes limited the opportunity to study the intermediates by ^{1}H NMR spectroscopy, the site of attack was not investigated in further detail. Consequently, the ring opening was assumed to occur on the less substituted side of PO, affording the aforementioned -OCH(Me)CH_2Cl terminated PLA chains, as has previously been reported in studies with related salen Fe^{III} chloride complexes.[84, 85] An additional polymer series with molecular weights corresponding to -OCH(Me)CH_2OH end groups was also observed (Figure 24), which may be explained by the hydrolysis of the C-Cl terminus due to the presence of trace water. Alternatively, some catalysts can convert epoxides to diols through reaction with trace water.[95] If present, propylene diol could act as a chain transfer agent (CTA), which would account for the presence of the propylene diol end group. It is worthy of note that propylene diol contains a primary and a secondary alcohol, both of which may act as a CTA. The potential growth of one or two polymer chains from a propylene diol unit is difficult to

unequivocally distinguish from the MALDI-ToF analysis, as the end groups of two polymers only differ by one m/z unit. This feature may have contributed to the broad dispersities observed. Furthermore, a third set of peaks with significantly lower intensity was detected, also containing lactide repeating units (144.1 Da). This series was tentatively assigned to OH end groups (144.1n + 57 Da with K as cation) that may form *via* hydrolysis or initiation from a metal-hydroxide species that formed due to the presence of trace water. However, due to the low signal-to-noise ratio and the systematic error in the calibration (+/- 3 Da), the determination of this third end group was less accurate. It is worth noting that in line with the NMR studies, peaks corresponding to poly(propylene oxide) were absent from the MALDI-ToF spectra of all products, further confirming that no epoxide (co)polymerisation occurred.

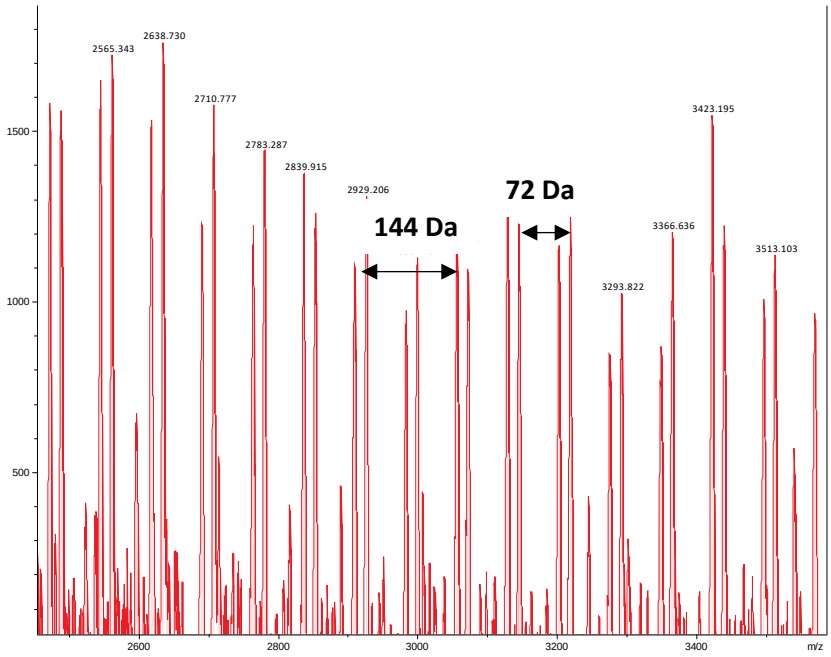

Figure 22: Typical MALDI spectrum of a PLA sample showing three series of peaks with lactide (144.1 Da) and lactic acid (72 Da) repeat units.

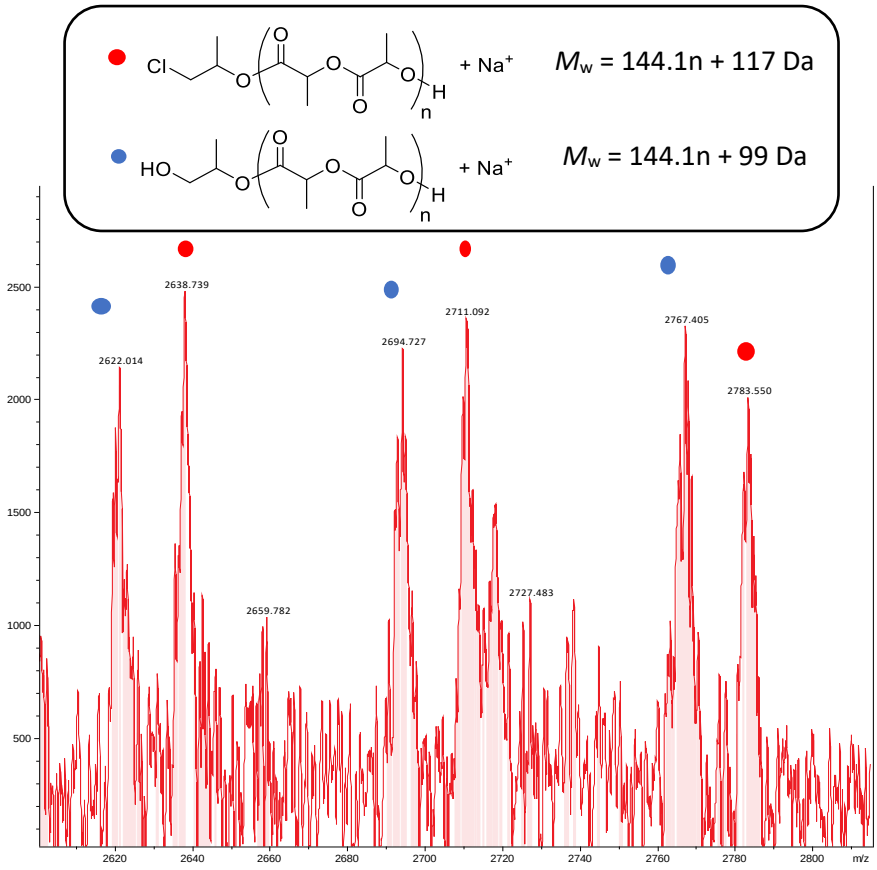

Figure 23: Detailed MALDI spectrum of a PLA sample showing the series of peaks corresponding to the α-OCH(Me)CH₂Cl/ω-H end groups (red) and the α-OCH(Me)CH₂OH/ω-H end groups (blue), with Na⁺ as the cation.

Transesterification reactions can occur both intermolecularly, leading to chain redistribution and intramolecularly, leading to macrocyclic structures (Figure 24).[55] Both processes significantly broaden the molecular weight distribution of the PLA chains, causing a divergence from the desired molecular weights. The presence of low molecular weight cyclic oligomers was not detected in the MALDI-ToF spectra of polymers obtained using catalysts **C1**-**C8**, however, these smaller species may have been lost during the sample preparation (precipitation and filtration of PLA). Consequently, the occurrence of intramolecular transesterifications cannot be unequivocally excluded. The extent of these undesired side-reactions has been reported to strongly depend on the nature of the metal in the catalyst: with Sn octanoate transesterification is usually prevalent from the very beginning of the polymerisation, whereas with Al alkoxide catalysts, it only starts at higher conversions.[55] It has previously been shown that iron complexes can limit transesterification and provide narrow dispersities ($Đ$ < 1.2) in lactide ROP, especially when isolated Fe^{II} alkoxide species were applied.[74, 79] However, the broad dispersities observed using catalysts **C1**-**C8** fall in line with previous reports employing the PO-triggered initiation method with salen Fe^{III} chloride complexes.[83, 85]

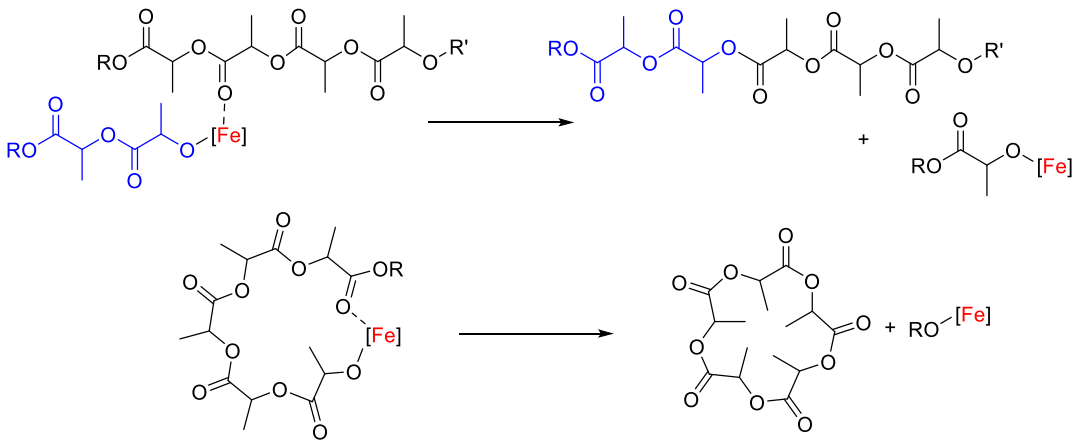

Figure 24: Mechanisms of intermolecular and intramolecular transesterification reactions.[55]

The stereochemical microstructure (tacticity) of the purified polymers was investigated *via* homonuclear decoupled ^{1}H NMR spectroscopy following the method proposed by Coates and Ovitt.[96] These calculations are based on the relative ratio of integrals in the methine region (5.16-5.26 ppm) of the ^{1}H NMR spectra. The proportion of different peaks corresponds to the proportion of different tetrads in the PLA chain (consisting of three *iso* or *syndio* linkages between adjacent stereocenters, Figure 25). For the PLA samples obtained using the Fe^{III} half salen catalysts (**C1**-**C8**), the studies revealed a lack of control over the tacticity, with P_i (isotactic bias) values near 0.5, indicating atactic polymers. These results match previous observations by Duan *et al.* who showed that for Fe^{III} salen catalysts, the PLA stereoselectivity was strongly dependent on the reaction temperature: lower P_i values around 0.68 were achieved at 120 °C, while higher control (P_i = 0.78) was exerted when the temperature was reduced to 60 °C, when using PO as both activator and solvent.[83]

As an attempt to reduce the rate of side-reactions and achieve higher control over the tacticity, control reactions were carried out under milder conditions (85 °C) with **C8**. These experiments afforded only traces of PLA indicating that the *in situ* initiation is not sufficient at this temperature. When the **C8**-alkoxide complex was pre-formed *via* stirring with PO prior to the reaction, high conversions were achieved at 85 °C (*vide infra*). However, similarly atactic PLA chains were obtained even at this lower reaction temperature, indicating a lack of control over the polymerisation and possibly the retention of high rates of transesterification reactions (as confirmed by MALDI-ToF analysis). It is worth noting that the polarity of the solvent can also influence the activity and selectivity of the system. Using toluene as solvent (instead of a large excess of PO) led to a more limited window of applicable reaction temperatures (85 °C <) as the solubility of *rac*-lactide in toluene is relatively low at milder temperatures. On the other hand, replacing PO with toluene solvent improved the applicability of the reaction by removing the need for high pressure equipment.

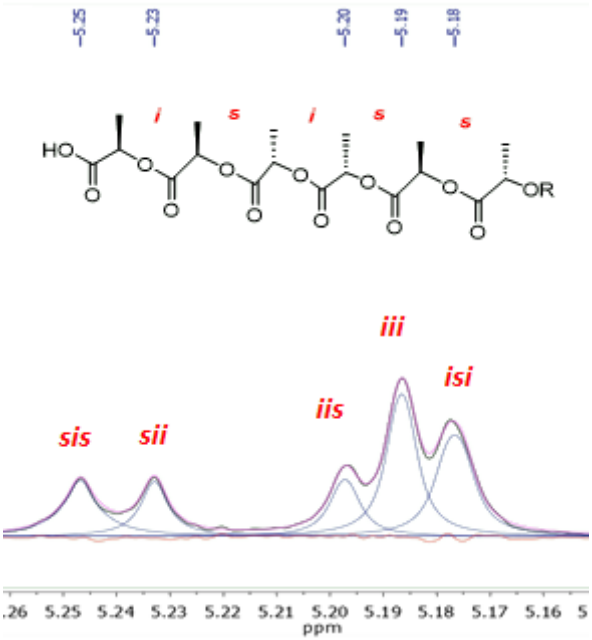

*Figure 25: Methine region of a typical homonuclear decoupled ^{1}H NMR spectrum of a purified PLA sample obtained using catalyst **C5**.*

Attempts to reduce the reaction time from 24 hours to 2 hours using **C5** led to variable conversions with significant errors in reproducibility (Table 7, entry 1-4) suggesting that the rate limiting step is the *in situ* formation of the active Fe-alkoxide catalyst. The extremely variable average conversions achieved with complexes **C1**-**C8** (entry 5-11) may also be linked to the presence of an induction period for the epoxide ring opening by the metal-halide. This phenomenon has previously been observed in epoxide/CO_2 copolymerisation reactions, but may have been overlooked in the *in situ* formation of metal-alkoxide catalysts for ROP. [97-99] The inefficient initiation observed after 2 hours of reaction time using **C2**, **C5**, **C7** and **C8** (Table 7, entry 1-4, 6, 10-11) may arise from the increased strength of the Fe-Cl bond in these complexes. For example, the molecular structures of **C1**, **C7** and **C8** suggest that the presence of electronegative chloro- substituents shortens and strengthens the Fe-Cl bond (*vide supra* in Chapter 3). This falls in line with the conversions obtained with **C1** (78%, entry 5), **C7**, (49%, entry 10) and **C8**, (1%, entry 11).

*Table 7: ROP of rac-lactide using **C1**- **C8** catalyst.*

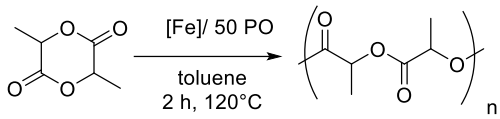

entry	complex	conversion (%)	$M_{n,th}$ (Da)	M_n (Da)	Đ
1	**C5**	15	-	-	-
2	**C5**	28	-	-	-
3	**C5**	28	-	-	-
4	**C5**	49	-	-	-
5	**C1**	78	-	-	-
6	**C2**	2	-	-	-
7	**C3**	89	12900	5500	1.1
8	**C4**	90	13000	45900	1.7
9	**C6**	91	13100	42200	1.5
10	**C7**	49	7100	22000	1.4
11	**C8**	1	-	-	-

Conditions: 0.01 mmol [Fe], 1 mmol rac-lactide, 0.5 mmol PO, 1 ml toluene, 2 h, 120 °C.

Efforts to minimise the observed variability through the use of a PO stock solution in toluene were unsuccessful (Table 8, entry 1-3). Suspecting the partial loss of the volatile PO activator, a higher-boiling alternative activator, butylene oxide (BO, b.p. 63 °C) was also tested, however, the reproducibility problems persisted (Table 8, entry 4-6).

Table 8: ROP of rac-lactide using propylene or butylene oxide activator stock solutions.

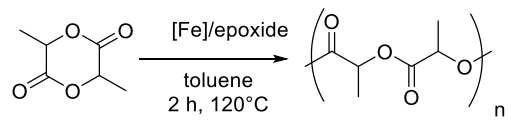

entry	complex	epoxide/ Fe	conversion (%)
1	**C5**	50 PO	15
2	**C5**	50 PO	28
3	**C5**	50 PO	28
4	**C1**	50 BO	40
5	**C1**	50 BO	39
6	**C1**	50 BO	22

Conditions: 0.01 mmol [Fe], 1 mmol rac-lactide, 0.5 mmol PO or BO in stock solution of 1 ml toluene, 2 h, 120 °C.

It is known that *in situ* initiation can lead to greater experimental variation in comparison to the use of isolated metal alkoxide complexes. Indeed, pre-forming the active Fe-alkoxide species by stirring the Fe^{III}-Cl complex **C8** with excess PO for 16 hours, prior to the addition of lactide, drastically

increased the conversion from 1% to 90% (Table 9, entry 1 and 2). While the dispersity remained broad, the experimental molecular weight was close to the expected value indicating a better control. Moreover, using the pre-formed catalyst the reaction temperature could be lowered to 85 °C while maintaining the high activity (89%, entry 3).

Table 9: ROP of rac-lactide catalysed by in situ or pre-formed Fe-alkoxides.

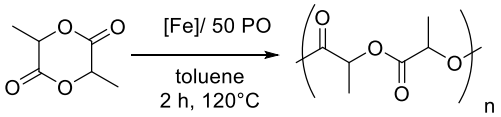

entry	complex	T (°C)	alkoxide formation	conversion (%)	$M_{n,th}$ (Da)	M_n (Da)	$Đ$
1	**C8**	120	*in situ*	1	-	-	-
2	**C8**	120	pre-formed	90	13000	15900	2.1
3	**C8**	85	pre-formed	89	12800	17200	1.5

Conditions: 0.01 mmol [Fe], 1 mmol rac-lactide, 0.5 mmol PO, 1 ml toluene, 2 h, 120 °C

As our main goal was to test whether the half salen Fe^{III} Cl complexes (**C1**-**C8**) could catalyse the ROP of *rac*-lactide in the presence of a small amount of PO, the investigation of pre-formed complexes was not continued. The obtained results show that further optimisation of the PO-activated *in situ* catalysis would be clearly necessary to match the efficiency of isolated metal-alkoxide catalysts. Due to time constraints, this fell outside of the scope of this work. Under the reaction conditions applied, the control exerted by the differently substituted complexes is likely masked by the relatively high rate of side-reactions. Further fine-tuning to minimise transesterification reactions would potentially allow a better investigation of these structure-activity relationships.

Summary and future work

A series of eight half salen Fe^{III} chloride complexes (**C1**-**C8**) were applied as mediators in the reverse atom transfer radical polymerisation (R-ATRP) of styrene and methyl methacrylate. In combination with azo-initiators, the complexes generally displayed moderate rates and moderate to good control over the molecular weights and dispersities of the polymers. As the top performing representatives, **C8** provided high control over the polymerisation of styrene achieving dispersities as low as 1.19, while **C6** achieved a very low *Đ* value of 1.05 in combination with V-70 initiator. In the polymerisation of MMA, **C1** exerted the best control with a low *Đ* of 1.14 using V-70 as the initiator. Kinetic experiments with these best-performing systems showed a deviation from first order behaviour, indicating the presence of competing processes besides the ATRP. NMR analysis of the polymers revealed the presence of unsaturated chain ends that are likely formed *via* catalytic chain transfer (CCT) reactions. Moreover, the interplay of organometallic mediated radical polymerisation (OMRP) was also suspected as indicated by some purple coloured products and a lower than expected proportion of halogen capped chains. To conclude, these results suggest that a significant contribution of competing mechanisms such as CCT and possibly OMRP may have strongly influenced the efficiency of **C1**-**C8** as ATRP mediators. Further kinetic studies and optimisation of reaction conditions (such as temperature, initiator ratio, solvent, bulk polymerisation) would be useful to separate out the mechanisms. This would allow the more precise investigation of structure-activity relationships and further comparisons to be drawn between the diversely substituted individual catalysts.

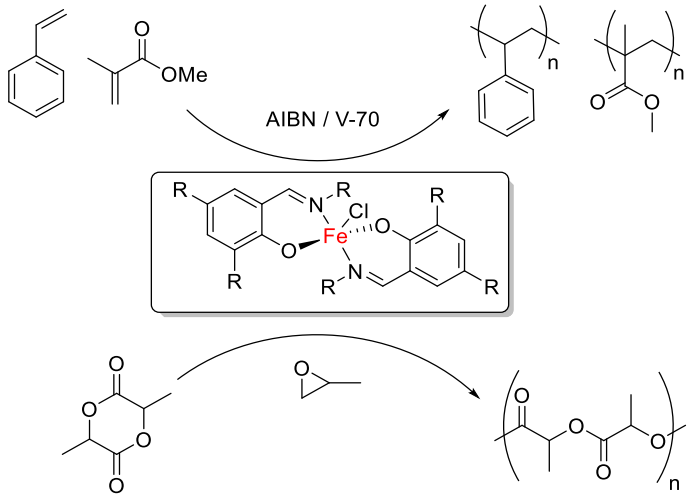

Scheme 6: Application of Fe^{III} half salen complexes in R-ATRP and ROP.

Complexes **C1**-**C8** were also tested as catalysts in the ring opening polymerisation of *rac*-lactide using a recently discovered propylene oxide-triggered *in situ* initiation technique. Initial optimisation of the PO ratio has shown that these catalysts can provide high conversions even with the addition of as few as 50 equivalents of PO (in comparison to the initial reports using an excess of 2000

equivalents). This modification has greatly improved the sustainability and atom efficiency of the literature method by reducing the amount of carcinogenic PO used by 97%. Moreover, it allowed the reactions to be carried out in small vials instead of specialist autoclave reactors. However, the relatively harsh conditions and long reaction times applied gave rise to transesterification side-reactions. This has significantly reduced the controllability of the polymerisation leading to atactic PLA chains with typically broad dispersities as established *via* GPC, MALDI-ToF and NMR studies. Reducing the temperature and reaction time has led to variable results with a lower reproducibility, suggesting that some of the complexes **C1**-**C8** require an initiation period to form the active alkoxide species before the polymerisation can start. Similar to the ATRP reactions, further optimisation would clearly be necessary to minimise side-reactions and allow the more precise determination of structure-activity relationships of the individual complexes, as these may have been masked by the strong presence of transesterification mechanisms.

Experimental

General considerations

All air- and/or moisture-sensitive experiments were performed under an argon atmosphere using an MBraun LABmaster glovebox and standard Schlenk techniques. Solvents were obtained from a solvent purification system (Innovative Technologies) consisting of columns of alumina and copper catalyst, and were further degassed by freeze–pump–thaw cycles prior to use. Styrene and methyl methacrylate (MMA) were dried by stirring over calcium hydride, vacuum transferred and stored at −35 °C. *Rac*-lactide was sublimed three times and stored at −35 °C. 2,2'-Azobis(4-methoxy-2,4-dimethylvaleronitrile (V-70) was washed with methanol, dried under vacuum and stored at −35 °C. 2,2’-Azobis(2-methylpropionitrile) (AIBN) was recrystallised from methanol, dried under vacuum and stored at −35 °C. Gel permeation chromatography (GPC) was carried out in HPLC grade THF solvent at a flow rate of 1 mL /min at 35 °C on a Malvern Instruments Viscotek 270 GPC Max triple-detection system with 2× mixed bed styrene/ DVB columns (300 × 7.5 mm). Absolute molar masses were obtained using the refractive index increment (dn/dc values) for this sample/solvent combination of 0.185 mL/g for poly(styrene)[100], 0.088 mL/g for poly(methyl methacrylate)[101] and 0.05 mL/g for poly(lactic acid).[102] NMR spectra were obtained a 500 MHz Bruker Avance III spectrometer. EI mass spectra were obtained on a Bruker Daltonics micro TOF instrument operating in the positive ion electrospray mode. MALDI mass spectrometry was performed on a Bruker UltraflexExtreme MALDI-ToF spectrometer, samples were prepared dithranol ad matrix and sodium or potassium iodide as the ionisation source.

General procedure for the R-ATRP of styrene and methyl methacrylate

In a glovebox, the complex (**C1**-**C8**) (24.0 µmol), monomer (100 equivalents, 2.40 mmol, 250.0 mg of styrene or 240.0 mg of MMA), toluene (toluene : monomer, 1 : 1, v/v) and initiator (0.6 equivalents, 14.4 µmol, 2.4 mg of AIBN or 4.4 mg of V-70) were sequentially added to an airtight screwcap vial equipped with a magnetic stirrer bar. The vial was sealed with a cap and PTFE film, removed from the glovebox and heated in an oil bath to 75 °C or 120 °C for 2 hours. The vial was subsequently quickly cooled to room temperature under running water, and an aliquot of the crude mixture was analysed in $CDCl_3$ *via* ^1H NMR spectroscopy to determine the monomer conversion. The remainder of the reaction mixture was quenched with chloroform (approximately 1 mL) and the polymer was purified by precipitation in acidified methanol (MeOH : HCl(aq), approximately 75 ml : 1 ml). The polymer was isolated by filtration and was subsequently dried *in vacuo* until constant weight was achieved. Samples

for GPC analysis were prepared in HPLC grade THF (in approx. 5 mg/ml concentration) and filtered through a 0.20 μm pore sized syringe filter.

General procedure for the ROP of *rac*-lactide

In a glovebox, complex (**C1-C8**) (10.0 μmol), *rac*-lactide (100 equivalents, 1.0 mmol, 0.144 g), toluene (1 ml) and propylene oxide (50 equivalents, 0.5 mmol, 35 μl), were added sequentially to a screwcap vial equipped with a magnetic stirrer bar. The vial was sealed with a cap and PTFE film, transferred to the bench and heated to 120 °C in an oil bath for 24 hours. The vial was subsequently cooled to room temperature under running water, the reaction mixture was quenched with hexane, and an aliquot of the crude mixture was analysed in $CDCl_3$ *via* ^1H NMR spectroscopy to determine monomer conversion. The remainder of the reaction mixture was dissolved in chloroform (approximately 1 mL) and the polymer was precipitated by the addition of the solution to cold (0 °C) acidified methanol (MeOH : HCl(aq), 75 ml : 1 ml). The polymer was then isolated by filtration and dried *in vacuo* until constant weight was achieved. Samples for GPC analysis were prepared in HPLC grade THF solvent (in approx. 15 mg/ml concentration) and filtered through a 0.20 μm pore sized syringe filter prior to analysis.

References

1. M. Mitani, J. I. Mohri, Y. Yoshida, J. Saito, S. Ishii, K. Tsuru, S. Matsui, R. Furuyama, T. Nakano, H. Tanaka, S. I. Kojoh, T. Matsugi, N. Kashiwa and T. Fujita, *J. Am. Chem. Soc.*, **2002**, *124*, 3327-3336.
2. C. Wang, S. Friedrich, T. R. Younkin, R. T. Li, R. H. Grubbs, D. A. Bansleben and M. W. Day, *Organometallics*, **1998**, *17*, 3149-3151.
3. L. J. Jian, D. D. Zhang, X. B. Zhou, M. J. Lin, H. P. Li and Z. C. Zhang, *Chinese J. Struct. Chem.*, **2017**, *36*, 1511-1517.
4. J. Ma, K.-Q. Zhao, M. J. Walton, J. A. Wright, J. W. A. Frese, M. R. J. Elsegood, Q. Xing, W. H. Sun and C. Redshaw, *Dalton Trans.*, **2014**, *43*, 8300-8310.
5. A. Abu-Surrah, H. Abdel-Halim, H. A. N. Abu-Shehab and E. Al-Ramahi, *Transit. Met. Chem.*, **2016**, *42*, 117-122.
6. B. De Clercq and F. Verpoort, *Macromolecules*, **2002**, *35*, 8943-8947.
7. T. Opstal, K. Couchez and F. Verpoort, *Adv. Synth. Catal.*, **2003**, *345*, 393-401.
8. B. De Clercq and F. Verpoort, *J. Mol. Catal. A*, **2002**, *180*, 67-76.
9. T. K. Saha, M. Mandal, M. Thunga, D. Chakraborty and V. Ramkumar, *Dalton Trans.*, **2013**, *42*, 10304-10314.
10. T. K. Saha, M. Mandal, D. Chakraborty and V. Ramkumar, *New J. Chem.*, **2013**, *37*, 949-960.
11. M. Mandal, U. Monkowius and D. Chakraborty, *New J. Chem.*, **2016**, *40*, 9824-9839.
12. S. Ghosh, R. R. Gowda, R. Jagan and D. Chakraborty, *Dalton Trans.*, **2015**, *44*, 10410-10422.
13. R. Jianming, X. Anguo, W. Hongwei and Y. Hailin, *Des. Monomers Polym.*, **2014**, *17*, 345-355.
14. N. Iwasa, J. Liu and K. Nomura, *Catal. Commun.*, **2008**, *9*, 1148-1152.
15. F. M. García-Valle, V. Tabernero, T. Cuenca, M. E. G. Mosquera, J. Cano and S. Milione, *Organometallics*, **2018**.
16. M. Normand, V. Dorcet, E. Kirillov and J.-F. Carpentier, *Organometallics*, **2013**, *32*, 1694-1709.
17. S. Ghosh, D. Chakraborty and V. Ramkumar, *J. Polym. Sci. Part A*, **2015**, *53*, 1474-1491.
18. F. M. García-Valle, R. Estivill, C. Gallegos, T. Cuenca, M. E. G. Mosquera, V. Tabernero and J. Cano, *Organometallics*, **2015**, *34*, 477-487.
19. T. Shi, W. Luo, S. Liu and Z. Li, *J. Polym. Sci. Part A*, **2018**, *56*, 611-617.
20. F. Isnard, M. Lamberti, C. Pellecchia and M. Mazzeo, *ChemCatChem*, **2017**, *9*, 2972-2979.
21. K. Matyjaszewski and N. V. Tsarevsky, *Nat. Chem.*, **2009**, *1*, 276.
22. K. Matyjaszewski and J. Xia, *Chem. Rev.*, **2001**, *101*, 2921-2990.
23. J. S. Wang and K. Matyjaszewski, *J. Am. Chem. Soc.*, **1995**, *117*, 5614-5615.

24. M. Kato, M. Kamigaito, M. Sawamoto and T. Higashimura, *Macromolecules*, **1995**, *28*, 1721-1723.
25. K. Matyjaszewski and J. Spanswick, *Mater. Today*, **2005**, *8*, 26-33.
26. W. Jakubowski, in *Progress in Controlled Radical Polymerization: Mechanisms and Techniques*, eds. K. Matyjaszewski, B. S. Sumerlin and N. V. Tsarevsky, ACS, **2012**, 203-216.
27. M. Destarac, *Macromol. React. Eng.*, **2010**, *4*, 165-179.
28. B. R. M. Lake and M. P. Shaver, in *Controlled Radical Polymerization: Mechanisms*, ACS, **2015**, 311-326.
29. M. Kamigaito, Y. Watanabe, T. Ando and M. Sawamoto, *J. Am. Chem. Soc.*, **2002**, *124*, 9994-9995.
30. N. Saleh, K. Sirk, Y. Liu, T. Phenrat, B. Dufour, K. Matyjaszewski, R. D. Tilton and G. V. Lowry, *Environ. Eng. Sci.*, **2007**, *24*, 45-57.
31. N. V. Tsarevsky and K. Matyjaszewski, *Chem. Rev.*, **2007**, *107*, 2270-2299.
32. Y. A. Kabachii, S. Y. Kochev, L. M. Bronstein, I. B. Blagodatskikh and P. M. Valetsky, *Polymer Bull.*, **2003**, *50*, 271-278.
33. E. Le Grognec, J. Claverie and R. Poli, *J. Am. Chem. Soc.*, **2001**, *123*, 9513-9524.
34. Y. Kotani, M. Kamigaito and M. Sawamoto, *Macromolecules*, **2000**, *33*, 6746-6751.
35. G. Moineau, C. Granel, P. Dubois, R. Jérôme and P. Teyssié, *Macromolecules*, **1998**, *31*, 542-544.
36. P. Lecomte, I. Drapier, P. Dubois, P. Teyssié and R. Jérôme, *Macromolecules*, **1997**, *30*, 7631-7633.
37. B. Wang, Y. Zhuang, X. Luo, S. Xu and X. Zhou, *Macromolecules*, **2003**, *36*, 9684-9686.
38. W. A. Braunecker, Y. Itami and K. Matyjaszewski, *Macromolecules*, **2005**, *38*, 9402-9404.
39. H. Uegaki, Y. Kotani, M. Kamigaito and M. Sawamoto, *Macromolecules*, **1998**, *31*, 6756-6761.
40. T. G. Ribelli, M. Fantin, J.-C. Daran, K. F. Augustine, R. Poli and K. Matyjaszewski, *J. Am. Chem. Soc.*, **2018**, *140*, 1525-1534.
41. T. Ando, M. Kamigaito and M. Sawamoto, *Macromolecules*, **1997**, *30*, 4507-4510.
42. K. Matyjaszewski, M. Wei, J. Xia and N. E. McDermott, *Macromolecules*, **1997**, *30*, 8161-8164.
43. R. Poli, L. E. N. Allan and M. P. Shaver, *Prog. Polym. Sci.*, **2014**, *39*, 1827-1845.
44. M. P. Shaver, L. E. N. Allan, H. S. Rzepa and V. C. Gibson, *Angew. Chem. Int. Ed.*, **2006**, *45*, 1241-1244.
45. R. K. O'Reilly, V. C. Gibson, A. J. P. White and D. J. Williams, *J. Am. Chem. Soc.*, **2003**, *125*, 8450-8451.

46. G. Moineau, P. Dubois, R. Jérôme, T. Senninger and P. Teyssié, *Macromolecules*, **1998**, *31*, 545-547.
47. B. R. M. Lake and M. P. Shaver, *Dalton Trans.*, **2016**, *45*, 15840-15849.
48. D. L. Coward, B. R. M. Lake and M. P. Shaver, *Organometallics*, **2017**, *36*, 3322-3328.
49. L. E. N. Allan, J. P. MacDonald, A. M. Reckling, C. M. Kozak and M. P. Shaver, *Macromol. Rapid Comm.*, **2012**, *33*, 414-418.
50. H. Schroeder, M. Buback and M. P. Shaver, *Macromolecules*, **2015**, *48*, 6114-6120.
51. H. Schroeder, B. R. M. Lake, S. Demeshko, M. P. Shaver and M. Buback, *Macromolecules*, **2015**, *48*, 4329-4338.
52. R. Poli and M. P. Shaver, *Inorg. Chem.*, **2014**, *53*, 7580-7590.
53. J. Claverie, *Research disc.*, **1998**, 1595-1604.
54. V. Bonometti, E. Labbé, O. Buriez, P. Mussini and C. Amatore, *J. Electroanal. Chem.*, **2009**, *633*, 99-105.
55. O. Dechy-Cabaret, B. Martin-Vaca and D. Bourissou, *Chem. Rev.*, **2004**, *104*, 6147-6176.
56. S. Inkinen, M. Hakkarainen, A. C. Albertsson and A. Södergård, *Biomacromolecules*, **2011**, *12*, 523-532.
57. J. Wu, T.-L. Yu, C. T. Chen and C. C. Lin, *Coord. Chem. Rev.*, **2006**, *250*, 602-626.
58. M. J. Stanford and A. P. Dove, *Chem. Soc. Rev.*, **2010**, *39*, 486-494.
59. V. W. Dittrich and R. C. Schulz, *Angew. Makromol. Chem.*, **1971**, *15*, 109-126.
60. A. Duda and S. Penczek, *Macromolecules*, **1990**, *23*, 1636-1639.
61. V. J. Kleine and H. H. Kleine, *Makromol. Chem.*, **1959**, *30*, 23-38.
62. P. Degée, P. Dubois, R. Jérŏme, S. Jacobsen and H. G. Fritz, *Macromol. Symp.*, **1999**, *144*, 289-302.
63. R. H. Platel, L. M. Hodgson and C. K. Williams, *Polym. Rev.*, **2008**, *48*, 11-63.
64. A. Kowalski, A. Duda and S. Penczek, *Macromolecules*, **1998**, *31*, 2114-2122.
65. Y. Nakayama, K. Watanabe, N. Ueyama, A. Nakamura, A. Harada and J. Okuda, *Organometallics*, **2000**, *19*, 2498-2503.
66. A. Dumitrescu, B. Martin-Vaca, H. Gornitzka, J. B. Cazaux, D. Bourissou and G. Bertrand, *Eur. J. Inorg. Chem.*, **2002**, *2002*, 1948-1951.
67. H. Ma, T. P. Spaniol and J. Okuda, *Dalton Trans.*, **2003**, 4770-4780.
68. A. Le Borgne, V. Vincens, M. Jouglard and N. Spassky, *Makromol. Chem.*, **1993**, *73*, 37-46.
69. J. P. MacDonald and M. P. Shaver, in *Green Polymer Chemistry: Biobased Materials and Biocatalysis*, ACS, **2015**, 147-167.

70. K. A. M. Thakur, R. T. Kean, E. S. Hall, J. J. Kolstad, T. A. Lindgren, M. A. Doscotch, J. I. Siepmann and E. J. Munson, *Macromolecules*, **1997**, *30*, 2422-2428.
71. M. Cheng, A. B. Attygalle, E. B. Lobkovsky and G. W. Coates, *J. Am. Chem. Soc.*, **1999**, *121*, 11583-11584.
72. B. J. O'Keefe, S. M. Monnier, M. A. Hillmyer and W. B. Tolman, *J. Am. Chem. Soc.*, **2001**, *123*, 339-340.
73. B. J. O'Keefe, L. E. Breyfogle, M. A. Hillmyer and W. B. Tolman, *J. Am. Chem. Soc.*, **2002**, *124*, 4384-4393.
74. V. C. Gibson, E. L. Marshall, D. Navarro-Llobet, A. J. P. White and D. J. Williams, *Dalton Trans.*, **2002**, 4321-4322.
75. X. Wang, K. Liao, D. Quan and Q. Wu, *Macromolecules*, **2005**, *38*, 4611-4617.
76. H. R. Kricheldorf and D. O. Damrau, *Macromol. Chem. Phys.*, **1997**, *198*, 1767-1774.
77. H. R. Kricheldorf and C. Boettcher, *Makromol. Chem.*, **1993**, *194*, 463-473.
78. Y. K. Gun'ko, U. Cristmann and V. G. Kessler, *Eur. J. Inorg. Chem.*, **2002**, *2002*, 1029-1031.
79. A. B. Biernesser, B. Li and J. A. Byers, *J. Am. Chem. Soc.*, **2013**, *135*, 16553-16560.
80. K. R. Delle Chiaie, A. B. Biernesser, M. A. Ortuno, B. Dereli, D. A. Iovan, M. J. T. Wilding, B. Li, C. J. Cramer and J. A. Byers, *Dalton Trans.*, **2017**, *46*, 12971-12980.
81. B. B. Idage, S. B. Idage, A. S. Kasegaonkar and R. V. Jadhav, *Mater. Sci. Eng. B*, **2010**, *168*, 193-198.
82. C. Robert, T. E. Schmid, V. Richard, P. Haquette, S. K. Raman, M. N. Rager, R. M. Gauvin, Y. Morin, X. Trivelli, V. Guérineau, I. del Rosal, L. Maron and C. M. Thomas, *J. Am. Chem. Soc.*, **2017**, *139*, 6217-6225.
83. R. Duan, C. Hu, X. Li, X. Pang, Z. Sun, X. Chen and X. Wang, *Macromolecules*, **2017**, *50*, 9188–9195.
84. M. Cozzolino, V. Leo, C. Tedesco, M. Mazzeo and M. Lamberti, *Dalton Trans.*, **2018**, *47*, 13229-13238.
85. Y. Liang, R. L. Duan, C. Y. Hu, L. L. Li, X. Pang, W. X. Zhang and X. S. Chen, *Chinese J. Polym. Sci.*, **2018**, *36*, 185-189.
86. N. Ajellal, J. F. Carpentier, C. Guillaume, S. M. Guillaume, M. Helou, V. Poirier, Y. Sarazin and A. Trifonov, *Dalton Trans.*, **2010**, *39*, 8363-8376.
87. K. Matyjaszewski, *Macromolecules*, **2012**, *45*, 4015-4039.
88. L. E. N. Allan, M. P. Shaver, A. J. P. White and V. C. Gibson, *Inorg. Chem.*, **2007**, *46*, 8963-8970.

89. L. E. N. Allan, J. P. MacDonald, G. S. Nichol and M. P. Shaver, *Macromolecules*, **2014**, *47*, 1249-1257.
90. A. A. Gridnev and S. D. Ittel, *Chem. Rev.*, **2001**, *101*, 3611-3660.
91. R. Poli, *Chem. Eur. J.*, **2015**, *21*, 6988-7001.
92. D. Konkolewicz and K. Matyjaszewski, in *Controlled Radical Polymerization: Mechanisms*, ACS, **2015**, 87-103.
93. J. Herzberger, K. Niederer, H. Pohlit, J. Seiwert, M. Worm, F. R. Wurm and H. Frey, *Chem. Rev.*, **2016**, *116*, 2170-2243.
94. M. H. Chisholm, D. Navarro-Llobet and W. J. Simonsick, *Macromolecules*, **2001**, *34*, 8851-8857.
95. G. P. Wu and D. J. Darensbourg, *Macromolecules*, **2016**, *49*, 807-814.
96. T. M. Ovitt and G. W. Coates, *J. Polym. Sci. A*, **2000**, *38*, 4686-4692.
97. J. A. Garden, P. K. Saini and C. K. Williams, *J. Am. Chem. Soc.*, **2015**, *137*, 15078-15081.
98. D. J. Darensbourg and A. I. Moncada, *Inorg. Chem.*, **2008**, *47*, 10000-10008.
99. X. B. Lu, L. Shi, Y. M. Wang, R. Zhang, Y. J. Zhang, X. J. Peng, Z. C. Zhang and B. Li, *J. Am. Chem. Soc.*, **2006**, *128*, 1664-1674.
100. S. Grcev, P. Schoenmakers and P. Iedema, *Polymer*, **2004**, *45*, 39-48.
101. K. Min, H. Gao, J. A. Yoon, W. Wu, T. Kowalewski and K. Matyjaszewski, *Macromolecules*, **2009**, *42*, 1597-1603.
102. S. A. Cairns, A. Schultheiss and M. P. Shaver, *Polym. Chem.*, **2017**, *8*, 2990-2996.

Chapter 5

Conclusions

Metal complexes play an important role as homogeneous catalysts in a wide variety of chemical processes. The aim of this thesis was to develop novel/underexplored complexes comprising earth abundant first-row transition metals, and their application as catalysts in small molecule activation or polymerisation reactions.

The work in **Chapter 2** was carried out in collaboration with an industrial partner (*Evonik*). Focusing on the phosphorus ligands, the project involved the investigation of Ni-based catalyst systems in alkene hydrocyanation reactions. The catalytic studies aimed to improve the three-stage *DuPont* adiponitrile process (hydrocyanation of butadiene, isomerisation of 2M3BN and hydrocyanation of 3PN), which is of great industrial relevance in the production of nylon 66. Firstly, the extremely air- and moisture-sensitive complex, **TP2Ni,** was synthesised and characterised *via* X-ray crystallography as a unique example of diphosphite Ni-(cod) complexes. This catalyst was shown to be moderately active in the isomerisation of 2M3BN, which was an important discovery contradicting previously reported patents. Another diphosphite ligand, **Biphephos**, was also employed in hydrocyanation catalysis. Initial studies using styrene as a model substrate helped to optimise crucial reaction parameters such as the pre-formation of the Ni complex or the continuous, slow addition of the HCN source to avoid catalyst deactivation. The Ni complex of this ligand was also active in all three steps of the *DuPont* process. As the best results were achieved in the isomerisation of 2M3BN, the reaction conditions of this process were systematically optimised. Consequently, high turnover rates (TON up to 343) were achieved that are comparable with the most active diphosphite-based systems reported.

Chapter 3 describes the design and synthesis of eight bidentate half salen ligands (**L1**-**L8**) and the corresponding novel Fe^{III}-Cl complexes (**C1**-**C8**). X-ray crystallographic studies of the air- and moisture-stable complexes revealed bis-chelated, monometallic structures with distorted trigonal bipyramidal geometries around the metal centre. The complexes were applied as catalysts in the coupling reaction of CO_2 and epoxides which has led to the selective formation of cyclic carbonates with high conversions. Notably, the catalysts were extremely robust and showed efficiency in the presence of oxygen, water and a high loading of unpurified substrate. Structure-activity relationships were uncovered, with the monochloro substituted **C7** complex reaching extremely high turnover rates (TOF up to 880 h^{-1}) which is amongst the highest values reported for Fe catalysts to date. After initial optimisations using propylene oxide, the substrate scope of the cycloadditions was extended to four other epoxides. This includes the successful conversion of the sterically challenging internal epoxide, CHO, which showed that the conformational flexibility of half salen complexes may be an advantage over the standard salen scaffolds.

The catalytic activity of the Fe^{III} half salen complexes was further explored in **Chapter 4** investigating polymerisation reactions. Firstly, **C1**-**C8** were employed as mediators in the reverse atom transfer

radical polymerisation of styrene and methyl methacrylate. Using AIBN or V-70 initiators, the complexes exerted moderate to good control over the molecular weights and dispersities of the obtained polymers. Some structure-reactivity relationships were discovered; however, the absence of clear trends suggested the interference of side-reactions under the conditions tested. ^{1}H NMR spectroscopic and kinetic studies revealed a high proportion of olefin terminated polymer chains and divergence from first order behaviour. These observations indicated the presence of competing catalytic chain transfer mechanisms as well as the possible contribution of an organometallic mediated alternative pathway.

Following a recent trend of epoxide-triggered initiation, the Fe^{III} chloride complexes (**C1**-**C8**) were also employed in the ring opening polymerisation of *rac*-lactide. Aiming to minimise the amount of the carcinogenic epoxide additive, initial optimisations have shown that all eight catalysts are highly active in the presence of just 50 equivalents of propylene oxide. However, it was necessary to conduct these reactions under increased temperatures and long reaction times to achieve reproducibly high conversions. GPC analysis of the obtained polymers revealed poor control over the molecular weights and dispersities, indicating a strong presence of transesterification side-reactions. This was confirmed *via* MALDI-ToF mass spectrometry studies. Attempts to carry out the polymerisations under milder conditions have led to variable conversions, suggesting that some of the half salen complexes require an initiation period to form the active alkoxide species *in situ* before the initiation.

To conclude, the findings in this thesis have demonstrated that intricate ligand design can help to exploit abundant, inexpensive transition metals such as Ni and Fe in a broad range of catalytic processes. The application of Ni with phosphorus ligands is already predominant in hydrocyanation reactions, however, the novel ligand systems explored in this work might offer advantages. Due to the huge scale of the *DuPont* adiponitrile process, even an incremental rise in activity or selectivity can realise significant cost-reductions. On the other hand, Fe catalysts remain underexplored in both cyclic carbonate synthesis and polymerisation reactions. The robust, easy-to-make Fe^{III} half salen complexes described herein can serve as a basis for further optimisations with an ultimate goal of replacing the unstable, expensive or toxic catalyst systems that are currently employed.